

**Electrical Instrumentation of a Contra-rotating
Propeller Drive System**

by

Matthew G. Angle

S.B. EE, M.I.T., 2007

Submitted to the Department of Electrical Engineering and Computer Science

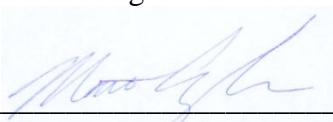
in Partial Fulfillment of the Requirements for the Degree of

Master of Engineering in Electrical Engineering and Computer Science

at the Massachusetts Institute of Technology

February, 2011

©2010 Massachusetts Institute of Technology
All rights reserved.



Author_____

Department of Electrical Engineering and Computer Science
January 31, 2011

Certified by_____

Professor James L. Kirtley, Jr.

Accepted by_____

Dr. Christopher J. Terman
Chairman, Masters of Engineering Thesis Committee

Electrical Instrumentation of a Contra-rotating
Propeller Drive System
by
Matthew G. Angle

Submitted to the
Department of Electrical Engineering and Computer Science

January 31, 2011

In Partial Fulfillment of the Requirements for the Degree of
Master of Engineering in Electrical Engineering and Computer Science

ABSTRACT

A prototype ship propulsion device based on an electric motor that spins propellers in opposite directions was constructed and tested. The device uses a single motor to spin both propellers without a gearbox. The rotor is attached to one propeller and the stator to the other. It relies on the propellers to balance rotational speeds of the two shafts. Non-intrusive Load Monitoring (NILM) techniques were used to diagnose performance of the machine. This analysis confirmed a sensor failure in testing.

Thesis Supervisor: James L. Kirtley, Jr.

Title: Professor, Department of Electrical Engineering and Computer Science

Chapter 1: Background

Non-Intrusive Load Monitoring

Non-Intrusive Load Monitoring is a method of identifying loads in a power system based on their characteristic power consumption. It was initially investigated in the 1980s at MIT by Professor Fred Scheppe and Dr. George Hart. They were interested in load monitoring for residential buildings to provide electric utilities with a monitoring tool that was minimally invasive. To identify loads, they would look for steady-state changes in real and reactive power drawn through the utility access point in the home. Each different type of load has a unique signature in this aspect. An induction motor, for instance, will draw a certain amount of real and reactive power, while a lightbulb will draw mostly real power. Positive and negative changes could be paired to establish use cycles for individual loads. See figure 1.1. [1]

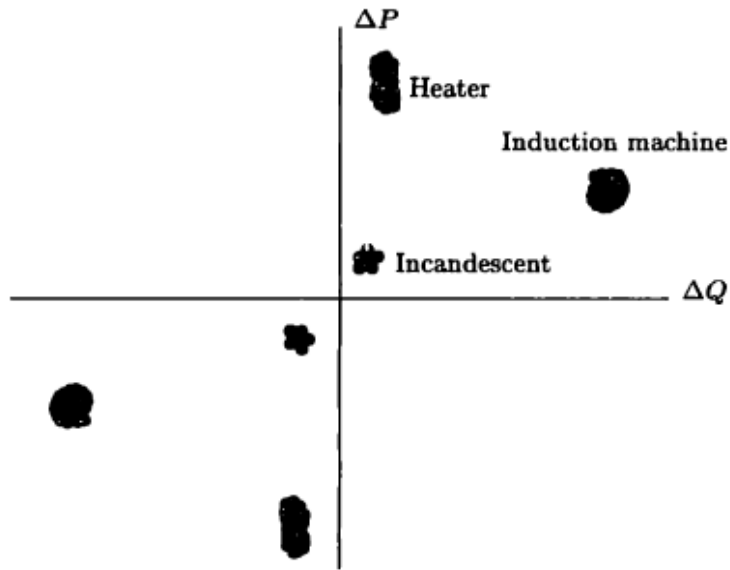


Figure 1.1 [2]

They outlined a five step process for detection of loads. First, an edge detector would detect a change in the steady state values of power and reactive power flow in to the home. Second, a cluster algorithm would identify the load in a two-dimensional space of real and reactive power. Third, positive and negative clusters of similar magnitude would be paired. This pairing

establishes turn on/turn off. Fourth, anomalies would be grouped together with a best-fit algorithm. Finally, further analysis could associate clusters with individual loads. [1,3,4]

This technique works well in residential environments where the number of devices is comparatively small and switching events are unlikely to happen simultaneously or quickly. In a commercial or industrial environment, large numbers of devices that may be switched on and off in close succession look similar. The 2-D real versus reactive power space becomes crowded. Many loads are not operated in a manner that allows them to settle in to a steady state of power consumption. Thus other methods of identifying loads are needed. [1,3,4]

Loads may also be identified by their steady-state high frequency components of current. This is performed by taking a phase-locked fourier transform to obtain magnitude coefficients for each frequency in real and reactive power. Equations are shown below. Certain loads exhibit particular harmonic power consumption. A computer power supply, for instance, draws a “signature” third harmonic. Variable speed drives, which are difficult to track (no steady state), have harmonic signatures that shift with load. This technique allows the use of steady-state detection methods, as described above, in more complicated systems. See figure 1.2. [1,4]

$$a_k = \frac{2}{T} \int_0^T i(\tau) \cos(k \frac{2\pi}{T} \tau) d\tau, \quad b_k = \frac{2}{T} \int_0^T i(\tau) \sin(k \frac{2\pi}{T} \tau) d\tau \quad k \geq 1.$$

[4]

In the early 1990s, Professor Steven Leeb began investigating the use of high-order harmonics, and a second technique to identify loads. This second technique identifies turn-on and turn-off transients. Electrical devices have unique and repeatable transient responses that allow loads to be classified. Further, they are often sufficient to identify individual loads. To perform this task, transients are matched against examples of known devices. [1,4]

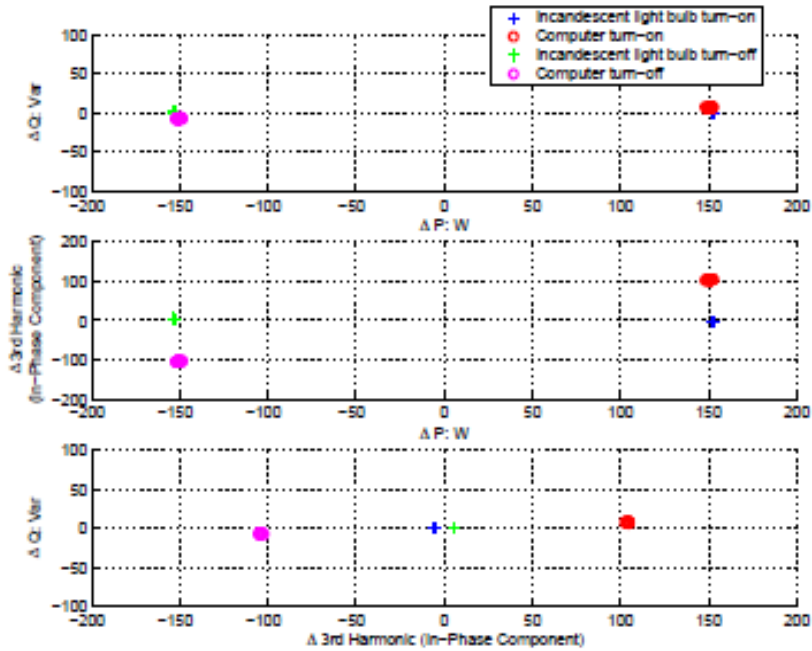


Figure 1.2 [1]

Electrical transients are often functions of the physical parameters of the load attached to the device. Because of this, these transients often contain other information that is useful for diagnostics. Specifically, conjectures may be made about the state of physical devices connected to the electrical device. Mechanical faults are often easily identifiable in startup transients. Because of this, it may be useful to attach a NILM device to the leads of one electrical device in need of monitoring, such as a motor. Diagnostics may be run on the motor while it is running. [1,4,5]

The primary advantage of NILM lies in the fact that it takes all measurements from a centralized location with small numbers of sensors. Sensors themselves are costly, as is installing and maintaining them. Installing sensors on every component requires a complicated network just to power and assemble data from each sensor. NILM can do the work of a much more complicated sensor architecture cheaper and more reliably.[1]

Permanent Magnet Motors

Permanent magnet motors may be well characterized by looking only at their electrical transients. Electrical parameters, such as internal resistances and inductances, along with mechanical shaft parameters, may be determined from unloaded tests. One particular paper [7]

demonstrated three techniques for finding the characteristic parameters of different induction motors given the unloaded transient stator current waveforms. Similar techniques may be used for PM machines.

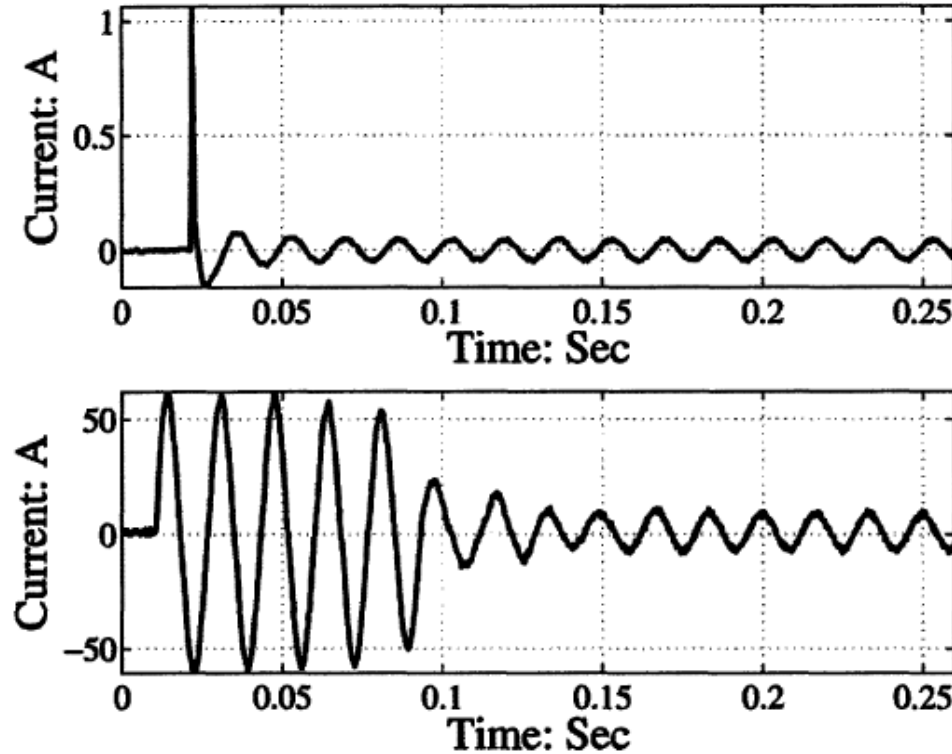


Figure 2-2: Top trace: Current drawn during the start of an incandescent lamp. Bottom trace: Stator current drawn during the start of an unloaded, fractional horsepower induction machine.

Figure 1.3 [6]

Ship Applications

In the future, the Navy anticipates much more sophisticated electrical architectures and increased electrical loads on ships. Propulsion and ship service power demands, ranging from advanced sensors such as radar to future weapon systems such as railguns and lasers, are expected to increase drastically. Figure 4 shows historic and future projected installed generation capacity aboard US Navy destroyers. [8,9]

As ships become more power-dense and increase their reliance on an electrical system, the number of sensors is expected to go up drastically. DDG-1000 is projected to have 200k+ conventional sensors. The attraction of NILM is that it minimizes number by placing only a few sensors on main power distribution points and on leads to more critical loads that must be individually instrumented, such as propulsion motors.[3]

While mass production of sensors has reduced their cost, installation and maintenance of vast sensor networks is still prohibitive. On a ship, it is desirable to have fewer sensors to maintain and possibly fail, but there is a trade that comes when the number of sensors is reduced to the point that the number of points of critical failure increases. [6,9]

The Navy has also shifted from a Preventative Maintenance System to Condition Based Maintenance System. The preventative system consisted of regularly scheduled maintenance at times well short of the expected lifetime of the component. Reliability is had at the expense of unnecessary manpower and replacement of components short of their potential life time. [6,9]

Condition Based Maintenance relies on accurate diagnostics to detect imminent failures of components. Only then are they repaired or replaced. Following the CBM schedule has the potential to drastically reduce maintenance man hours, which in turn leads to reduced vessel manning. Reduced manning leads to a larger fraction of the ship that is useful for payload.[6,9]

The concept of Condition Based Maintenance is expanded to an Integration Condition Assessment System, which consists of an engineering plant monitoring system. It continuously collects equipment status information and transmits it to a shore facility, where it is analyzed to determine maintenance needs. [6]

The shift in maintenance schedules requires increased reliance on an increased number of sensors. NILM provides a cheaper and more reliable alternative to instrumenting every parameter of interest.

Previous Work

NILM is a popular research topic inside the Lab for Electromagnetic and Electronic Systems at MIT and is an important tool for a number of research areas. In the past, several grad students have worked on related projects. A sizable number of these have been Naval Officers with access to actual data and systems.

Data from a tour on the USCGC SENECA has been used to validate the use of NILM. From the data, several diagnostic abilities have been demonstrated.

The ship uses a vacuum system for waste disposal. Vacuum is maintained by two large pumps. Researchers were able to identify leaks in the system through analysis of the use cycles of the pumps. First, the use of the system by the crew was modeled as a poisson process. Normal cycles were then calculated for the system. It was obvious when looking at the actual cycles of the pumps that there was a leak in the system that was later found. [3, 9, 10]

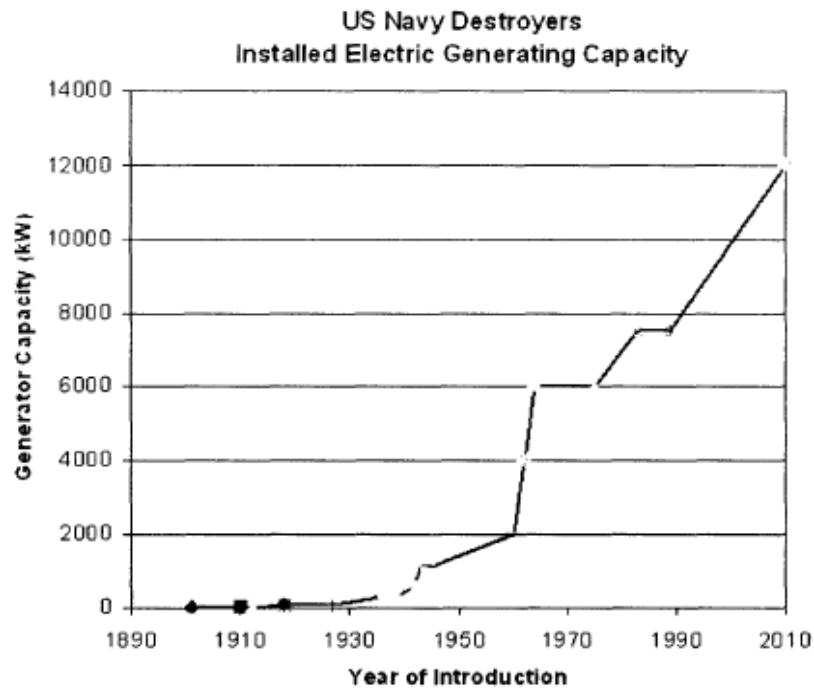


Figure 1-1: Electric Generating Capacity of US Navy Destroyers (1910-2010 projected)

Figure 1.4 [9]

The second and third diagnostic demonstrations occurred on an auxiliary sea water pump. The motor is connected to the pump by a flexible coupling. As the coupling failed, researchers could see a spike in the the magnitude of the ripple in the startup transient at 43Hz. This result was consistent with a 5th-order induction motor simulation. [9, 10]

NILM has also been used as a diagnostic for HVAC systems. Fault detection for rooftop air-conditioning units was demonstrated. The author was able to detect compressor leakage from run cycle data, as well as state of charge of the system from the startup transient of the compressor motor. Figure [1.5] clearly shows the difference in startup transients with different physical states. [11]

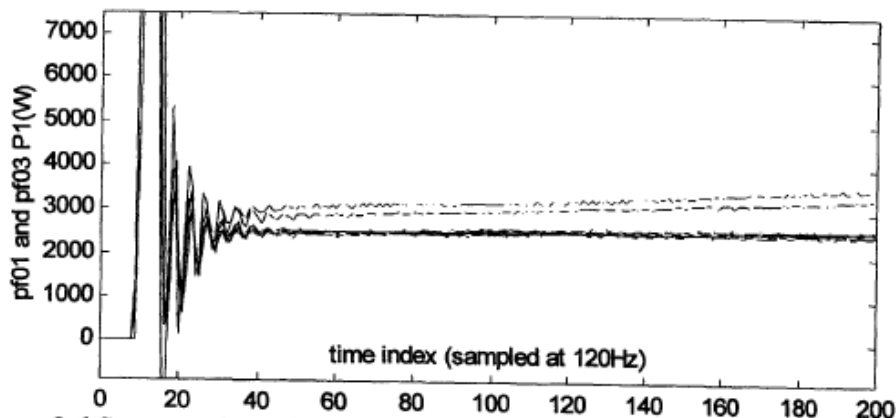
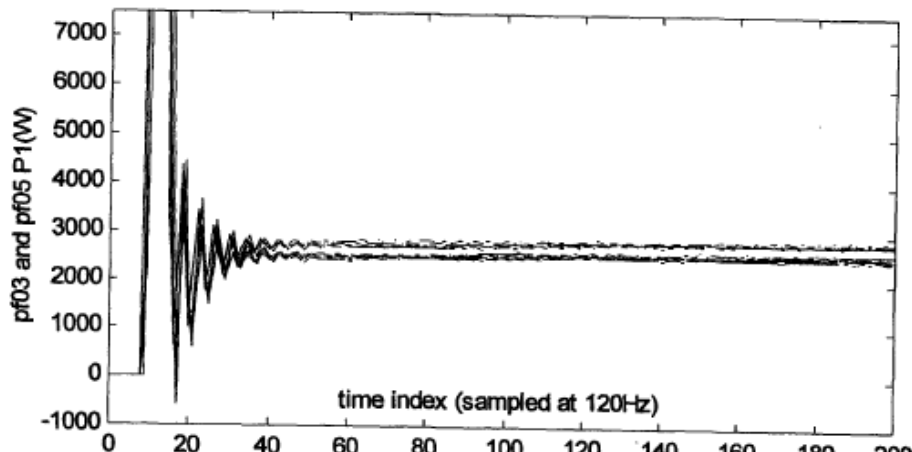


Figure 2.6 Start transients: lower seven traces normal, upper two traces 20% undercharge. For clarity, only two of the four undercharge traces are shown.

Figure 1.5 [11]

References:

- [1] Laughman, C., D. Lee, R. Cox, S. Shaw, S. Leeb, L. Norford, P. Armstrong, "High Performance Commercial Building Systems: Advanced Nonintrusive Monitoring of Electric Loads," *IEEE Power and Energy Magazine*, March/April, 2003, pp. 56- 63.
- [2] Steve Shaw. *System Identification Techniques and Modeling for Nonintrusive Load Diagnostics*. PhD thesis, MIT, February 2000.
- [3] Robert Cox. *Minimally Intrusive Strategies for Fault Detection and Energy Monitoring*. PhD thesis, MIT, September 2006.
- [4] Kwangduk Lee. *Electric Load Information System based on Non-Intrusive Power Monitoring*. PhD thesis, MIT, June 2003.
- [5] James Paris. *A Framework for Non-Intrusive Load Monitoring and Diagnostics*. MEng thesis, MIT, February 2006.
- [6] Patrick Bennett. *Using the Non-Intrusive Load Monitor for Shipboard Supervisory Control*. MS thesis, MIT, June 2007.
- [7] S. Shaw and Leeb, S., "Identification of Induction Motor Parameters from Transient Stator Current Measurements," IEE Transactions on Industrial Electronics, vol. 46, no. 1, February 1999, pp. 139-149.
- [8] Norbert Doerry, *Next Generation Integrated Power System: NGIPS Technology Development Roadmap*, Washington Navy Yard DC: Naval Sea Systems Command.
- [9] Thomas DeNucci. *Diagnostic Indicators for Shipboard Systems using Non-Intrusive Load Monitoring*. MS thesis, MIT, June 2005.
- [10] William Greene. *Evaluation of Non-Intrusive Monitoring for Condition Based Maintenance Applications on US Navy Propulsion Plants*. MS thesis, MIT, June 2005.
- [11] Peter Armstrong. *Model Identification with Application to Building Control and Fault Detection*. PhD thesis, MIT, September 2004.

Chapter 2: Machine Design

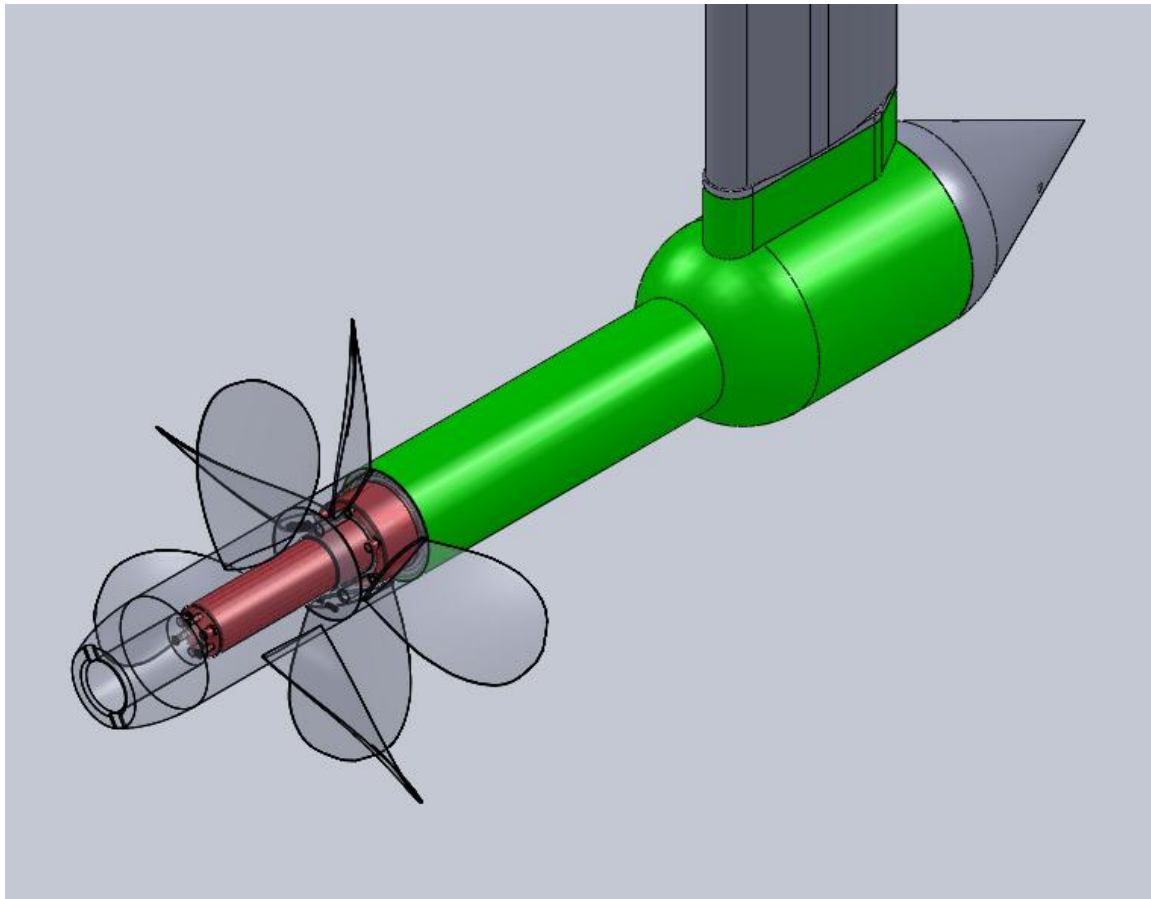


Figure 2.1: Isometric view of complete machine.

The device consists of an inner and outer shaft connected to the rotor and stator, respectively, of the motor. These concentric shafts are held in an outer housing that contains the motor and electrical hardware. It is closed by a top cap that allows access to the brushes and hall sensor on the outer shaft. The motor is fed by brushes through slip rings attached to the outer shaft. There is a conical tail cone that screws in and allows access to the motor and provides a method for locking the inner shaft and allowing testing of a single propeller with something else mounted to the inner shaft.

The machine is designed to run with each shaft turning at 1000 RPM in opposite directions at about 9 N-m.

The motor is a Kollmorgen KBM-25H03, a brushless permanent magnet machine with ten poles. The motor was selected for its power density, as minimum diameter is important for propeller performance, and minimum length is required to allow the cantilevered design to function properly. Table 2.1 contains motor parameters [1].

KBM(S)-25 Performance Data and Motor Parameters	KBM(S)-25X02-X	
	Units	Value
Continuous Stall Torque at 25°C ambient		
	N-m	8.75
	lb-ft	6.45
Continuous Current I _c	Arms	5.18
Peak Stall Torque (25°C winding temp)		
	N-m	29.7
	lb-ft	21.9
Peak Current I _p	Arms	22
Rated Continuous Output Power at 25°C ambient		
P Rated	Watts	2545
HP Rated	HP	3.41
Speed at Rated Power	RPM	4000
Torque Sensitivity K _t		
N-m/Arms	Arms	1.73

Ib-ft/Arms	Arms	1.27
Back EMF Constant Kb	Vpk/kRPM	148
Motor Constant Km		
	N-m/vwatt	0.733
	Ib-ft/vwatt	0.541
Resistance (line to line) Rm	Ohms	3.7
Inductance Lm	mH	19
Inertia Jm		
	Kg-m ²	6.78E-04
	Ib-ft-s ²	5.00E-04
Weight Wt		
	Kg	3.5
	lb	7.72
Max Static Friction Tf		
	N-m	1.63E-01
	Ib-ft	0.12
Cogging Friction (Peak to Peak) Tcog		
	N-m	0.132
	Ib-ft	9.70E-02
Viscous Damping Fi		
	N-m/kRMP	3.95E-02
	Ib-ft/kRPM	2.91E-02
Thermal Resistance	TPR/°C/watt	0.56

Number of Poles P		10
-------------------	--	----

Table 2.1: Motor specifications.

Runout Spec .1mm

The biggest design challenge is meeting the motor runout specification. The motor is cantilevered off the shafts, and the allowable runout is only .1 mm, per the manufacturer data sheet [1]. The tolerances on the motor are loose enough that they would take half of the allowable runout and impose micron-level tolerances on concentricity and roundness on the shafts where they mate with the motor parts. The interface is now designed to be bonded. The fluid properties of Loctite will center the motor in the bore.

Shaft bending must be included in the tolerance stack-up. Without tweaking the shafts, it came to about 25% of the allowable runout.

First, motor force was calculated. It was assumed that this force would act at the very end of the shaft. For centrifugal force, it was assumed that the entire mass of the motor would be displaced by the maximum runout at the maximum design speed of the machine. This turned out to be small next to the magnetic attractive forces. For the motor, the magnets were assumed to be as strong as anything available at 1.3 Tesla, and magnet heights and air gap were pulled from the manufacturer-supplied solid model. The value was again calculated at maximum runout.

To calculate side forces, the motor gap (space between rotor and stator) must first be defined to be sinusoidally varying.

$$g = g_0 - x \cos \theta$$

The remnant magnetic flux density is a function of the gap.

$$B_r = B_0 \frac{h_m}{h_m + g} \cos(p\theta + \delta)$$

Then we must calculate radial force.

$$F_r = \frac{B_r^2}{2\mu_0}$$

Radial force is integrated to calculate side force.

$$F_x = l \int_0^{2\pi} F_r \cos \theta R d\theta$$

Expand radial force equation.

$$F_r = \frac{B_0^2}{2\mu_0} \left\{ \frac{h_m}{h_m + g_0 - x \cos \theta} \right\}^2 \cos^2(p\theta + \delta)$$

Assume $x \ll h_m + g$.

$$\frac{1}{1+x} \sim 1-x$$

$$\frac{h_m}{h_m + g_0 - x \cos \theta} = \frac{h_m}{h_m + g_0} \left(1 + \frac{x}{h_m + g_0} \cos \theta \right)$$

Combine everything.

$$F_r = \frac{B_r^2}{2\mu_0} \left(\frac{h_m}{h_m + g_0} \right)^2 \left(1 + \frac{x}{h_m + g_0} \cos \theta \right)^2 \cos^2(p\theta + \delta)$$

Assume \cos^2 term washes out as it is symmetric and will not affect side force calculations.

$$F_r = \frac{B_r^2}{2\mu_0} \left(\frac{h_m}{h_m + g_0} \right)^2 \left(1 + \frac{x}{h_m + g_0} \cos \theta \right)^2$$

$$F_x = \frac{\left(B_0 \frac{h_m}{h_m + g} \right)^2}{4\mu_0} \frac{Rl2x}{h_m + g_0} \int_0^{2\pi} \cos^2 \theta d\theta$$

$$F_x = \frac{\left(B_0 \frac{h_m}{h_m + g} \right)^2}{4\mu_0} \frac{Rl2\pi x}{h_m + g_0}$$

Results of this calculation are shown in table 2.2.

Motor Mass (Complete) [kg]	3.72		
Motor Mass (Complete) [lbs]	7.22		
Air Gap [mm]	0.695		
Air Gap [in]			
Max Speed [RPM]	1100		
Max Speed [rad/s]	115.1917306		
Rotational Radial Force [N]	4.936118148	using complete mass at max displacement	
mu0	1.25664E-06		
Rotor Length [m]	0.083		
Rotor Diameter [m]	0.06373		
B [Tesla]	1.3		
magnet height [mm]	3.15		
Max Force [N] (magnetic pressure, one side... not			

used)			
Magnetic Max Force at max displacement [N]	97.52608889		
Max Force [N]	102.462207	23.02522	lbs
Sum of shaft Displacements from bending [mm]	0.024404381		

Table 2.2: Shaft bending analysis.

Max Displacement [mm]	0.1
Max Displacement [in]	0.003937008
Loctite 609 max gap [in]	0.005
Loctite 609 max gap [mm]	0.127
Shear Strength [N/mm ²]	15.8
Shear Strength @ 100degC [N/mm ²]	11.85
Total Shear [N-m]	3855.87694
Rotor Diameter Tolerance (+)	0.025
Rotor Radius Tolerance (+) [mm]	0.0125
Stator Diameter Tolerance (-)	0.087
Stator Diameter Tolerance (-) [mm]	0.0435
Rotor/Stator tolerance stack-up	0.056

Table 2.3: Tolerance stack-up.

Front Bearing				
housing bore radius [mm]	0.00254			

shaft bore diameter radius [mm]	0.00254			
force displacement [mm]	0.00762	0.0003		
concentricity [mm]	0.01			
sum [mm]	0.0227			
Rear Bearing				
housing bore radius [mm]	0.00254			
shaft bore diameter radius [mm]	0.00254			
force displacement [mm]	0.00762			
sum [mm]	0.0127			
				Assuming Interference Fit...
displacement at back of rotor from bearings [mm]	0.019153081			0.019153081
Bending in dish				
dish thickness [mm]	5			
dish effective width [mm]	23.8125			
dish height [mm]	23.4405			
Dish moment [N-m]	9.733909669			
E	7.00E+10			
I	248.046875			
angular deflection	1.31408E-11			
Radial deflection at aft end [mm]	1.24838E-09			1.24838E-09
outer shaft concentricity [mm]	0.005	0.000197		0.03
inner shaft concentricity[mm]	0.005			0.03
Total displacement	0.109557463			0.103557463

Table 2.4: total displacement.

For bending calculations, bearings are modeled as distributed supports with no tilt stiffness. On the inner shaft, the smallest shaft diameter is assumed for the whole shaft. On the outer shaft, the portion of the shaft with the smallest area moment is again used. The portion around the motor stator is stiffer than the shaft portion. The transition section from the shaft portion of the outer shaft to the motor attachment was modeled as a vertical bar the thickness of the dish and the width of the shaft portion. The deflection angle was calculated with a torque equal to the length of the motor section multiplied by the total of motor attractive force and centrifugal force. This angle was the multiplied by the motor section length and added to the displacement calculated earlier.

The calculations start with the external forces and moments. M_b is a bending moment applied to the end of the shaft and F_p is a force at the end of the shaft. W is the bearings, which are modeled as a distributed supports.

$$q = F_p(x)_{-1} + M_p(x)_{-2} + w_1(x - x_1)^0 - w_1(x - x_2)^0 + w_2(x - x_3)^0 - w_2(x - x_4)^0$$

$$\frac{d^2 M_b}{dx^2} = q$$

$$M_b = EI \frac{d^2 V}{dx^2}$$

The equation is then integrated to solve for V .

$$\frac{d^3 V}{dx^3} = \frac{1}{EI} [F_p(x)^0 + M_p(x)_{-1} + w_1(x - x_1)^1 - w_1(x - x_2)^1 + w_2(x - x_3)^1 - w_2(x - x_4)^1 + C_1]$$

$$M_b = \frac{d^2 V}{dx^2} = \frac{1}{EI} \left[F_p(x)^1 + M_p(x)^0 + \frac{w_1}{2}(x - x_1)^2 - \frac{w_1}{2}(x - x_2)^2 + \frac{w_2}{2}(x - x_3)^2 - \frac{w_2}{2}(x - x_4)^2 + C_1 x + C_2 \right]$$

$$\frac{dV}{dx} = \frac{1}{EI} \left[\frac{F_p}{2}(x)^2 + M_p(x)^1 + \frac{w_1}{6}(x - x_1)^3 - \frac{w_1}{6}(x - x_2)^3 + \frac{w_2}{6}(x - x_3)^3 - \frac{w_2}{6}(x - x_4)^3 + \frac{C_1}{2}x^2 + C_2 x + C_3 \right]$$

$$V = \frac{1}{EI} \left[\frac{F_p}{6} \langle x \rangle^3 + \frac{M_p}{2} \langle x \rangle^2 + \frac{w_1}{24} \langle x - x_1 \rangle^4 - \frac{w_1}{24} \langle x - x_2 \rangle^4 + \frac{w_2}{24} \langle x - x_3 \rangle^4 - \frac{w_2}{24} \langle x - x_4 \rangle^4 + \frac{C_1}{6} x^3 + \frac{C_2}{2} x^2 + C_3 x + C_4 \right]$$

The boundary conditions are applied and used to solve for the constants.

The results of these calculations are shown in table 2.2.

Completing the tolerance stackup are the simple tolerances, bearing deflection on both ends, bearing bore tolerance, and concentricity error between bearing surface and motor.

Bearing bore numbers are taken from the bearing selection guide. The rear bearing is a tight press fit and front bearing is oversized by the same amount. The rear bearing reverses the tolerances specified in the selection guide. This gives a .0006" undersize on the rear inner bearing bore, and the same oversize on the front bore [2].

Loctite 609, an adhesive happy with small gaps, is used for assembly. If necessary, the motor will be shimmed in place to keep it concentric on the shaft.

O-ring seals

There are two o-rings in the design, located at the tail cone and the top cap. Per the Parker design guide, the o-ring is squished to 80% of its free height, and the groove is 30% larger on the outer diameter [3].

Surface roughness is spec'd to 32uin RMS, but 64uin to 128uin is adequate [3]. On the top cap itself and the back end of the outer housing, these surfaces may be fly-cut to spec. On the top cap portion of the outer housing and the tail cone, the sealing surface is at the bottom of the groove. These surfaces will be smoothed with 600-grit sand paper by hand. To account for this process, the grooves are machined .002" shallower than the depth suggested by the 20% squish.

Corners must be round to .005" radius larger to avoid cutting the o-ring, and walls must be within 5 degrees of vertical (concave) [3].

Top Cap

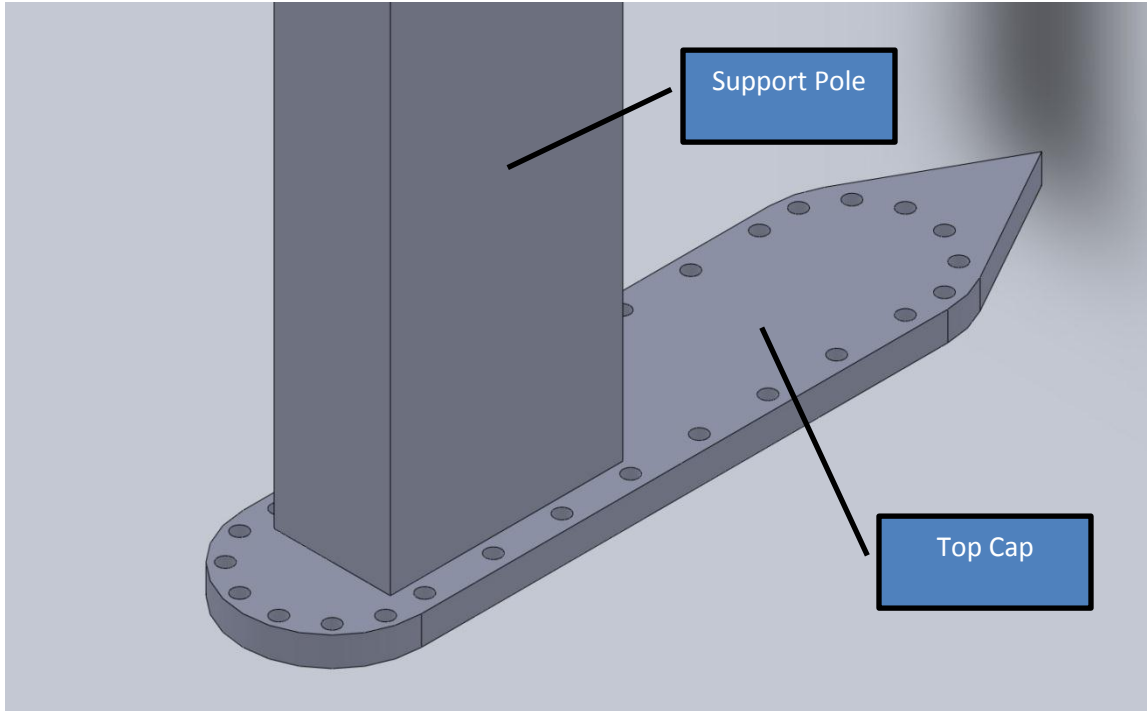


Figure 2.2: Top cap and support pole.

The top cap is designed to hold the machine and allow access to the brushes for servicing or replacement. It is not anticipated that it will be removed often.

Following best design practices, bolts are spaced 5 diameters on the straight lines and every 30 degrees at the ends and are M3 buttonheads. The holes are all sized to clear the M3 bolt. There is a 1.5mm space between the bolt and the edge. To provide this spacing on the outside and allow clearance between bolt heads and the square tube, the sail must be 39 mm wide.

The support that holds the machine is a 1"x2" aluminum tube with 1/8" walls, welded on to the top cap. The wires carrying motor power and signal and the sump line are run through the tube.

The tube is surrounded by a Hall Spar 171 Spreader section to remove drag forces from the tube. The fairing is anchored to the carriage so the force transducer will not see force from stagnation pressure on the support. The top cap, square tube, and Spreader section fairing are shown below.

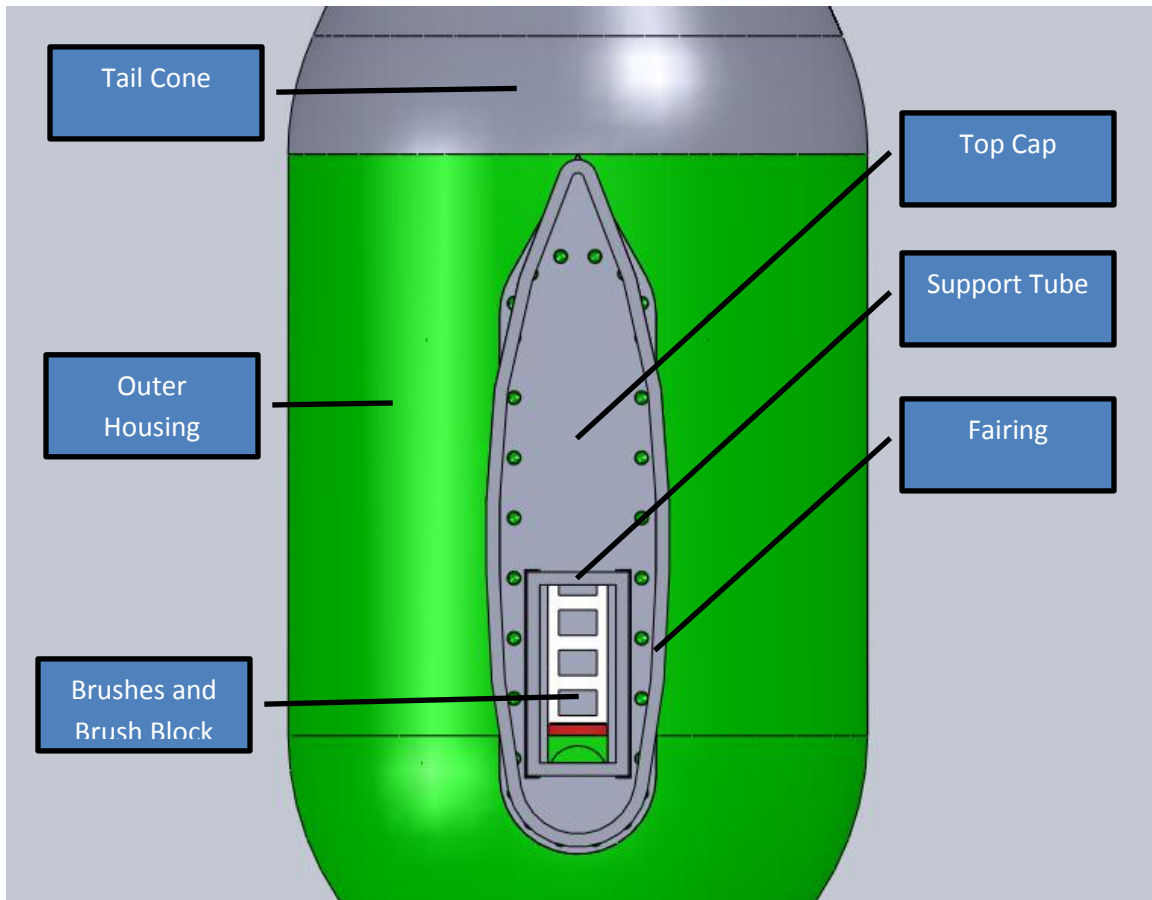


Figure 2.3: Top view of machine.

Bearing Preload

	bore	shaft	load	work height	free height	spring rate
	in	in	lbs	in	in	lbs/in
SSB-0185	1.850394	1.524409	29.00035	0.096689	0.15	776.58
SSB-0295	2.952756	2.526378	46.08583	0.122311	0.2	1073.508

Table 2.5: Bearing preload spring specifications.

Preload	Inner Bearing Axial Rating	Inner bearing preload	Outer Bearing Axial Rating	Outer bearing Preload
%	lbs	lbs	lbs	lbs
3	1380	41.4	2780	83.4

Table 2.6: Bearing preload calculations.

The bearings are of the angular-contact variety, so they must be pre-loaded to maintain radial alignment. The mechanical contact is made at an angle, so axial force pushes on a cone, causing it to self-center. They are loaded to 3% of bearing thrust capacity, which comes to ~40lbs on the inner bearing and ~80lbs on outer bearing. To achieve these numbers with a standard Smalley Wave Spring two springs must be stacked, and they must be compressed by .06" and .08", respectively. Wave springs add in series when stacked with the waves in phase and in parallel when stacked out of phase. In this case, they are stacked in phase to increase stiffness. Tolerances are spec'd small on the length and washers are spec'd large (two at .001" tolerance) to ensure that error in spring preload is on the high side [2]. Table 2.6 shows calculations.

Motor Attachment

The motor is attached with Loctite 609 with 7471 accelerator. This was recommended for steel-on-aluminum by the manufacturer due to differences in coefficient of thermal expansion of the materials.

Rotary Seals

The rotary seals are Parker PolyPaks, which are o-ring loaded lip seals made of urethane. They are designed for pistons in hydraulic seals, so they're more than adequate to deal with a few psi of water. The design includes two sets, one set in front of each bearing. All are captured with washers on both sides that are then held in place with snap rings. On the fore seals, the snap rings are located on the shaft (not the housing) for convenience. This has the consequence of preferring motion on the exterior of the seal, where surface speeds are higher. The aft seals are captured by the housing [4].

The front seals are operated outside of the manufacturer's recommendations. The bores are oversized and the shafts undersized by a few ten-thousandths to accommodate the bearings. Given their intended purpose, they should be capable of sealing water at a few psi. The tolerances for the aft bearings are within suggested tolerances for the seals [4].

The only other relevant requirement is that the seals not exceed 200degF [4].

Figure 2.4 shows the front outer bearing, preload spring, spring washer, seal, seal washers, and snap rings. The assembly between the inner and outer shafts is the same.

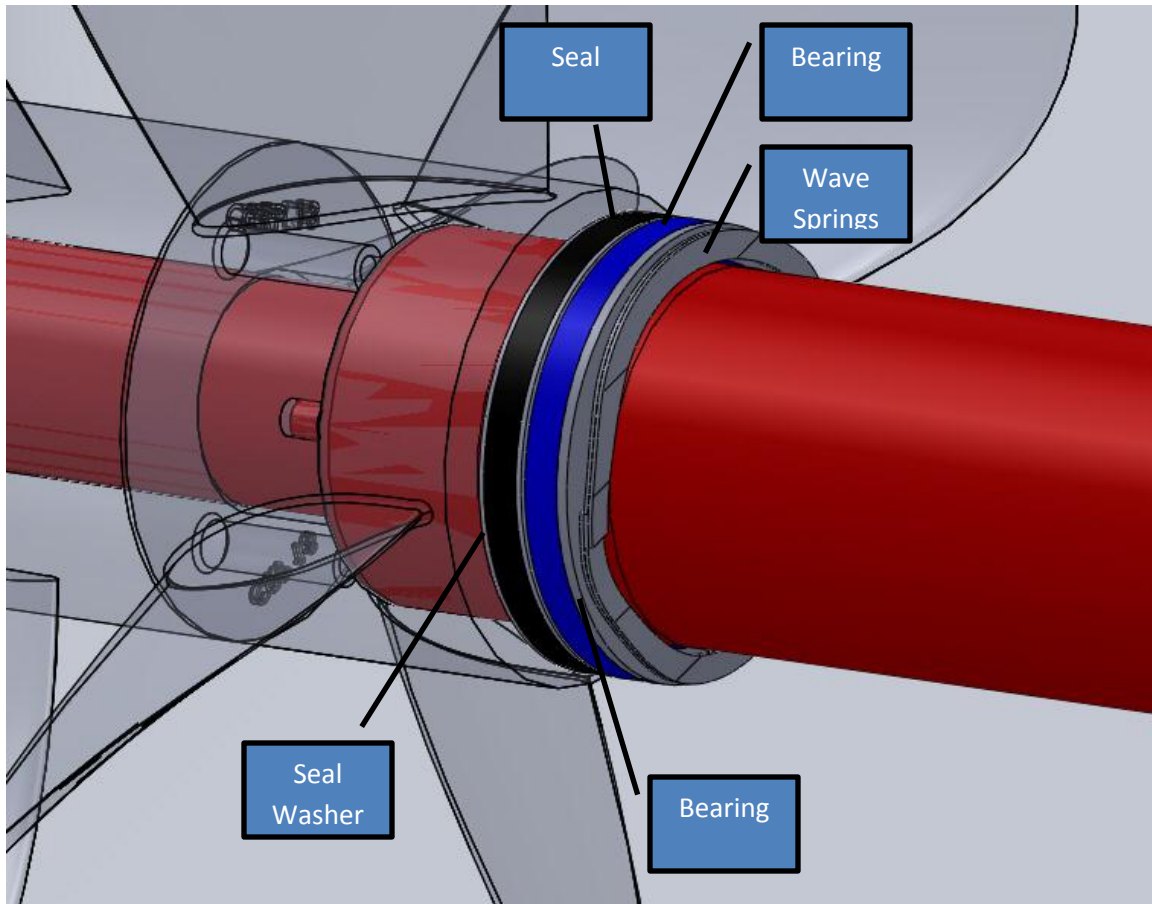


Figure 2.4: front bearing, seal, preload detail.

Motor Brushes/Slip Rings/Insulators

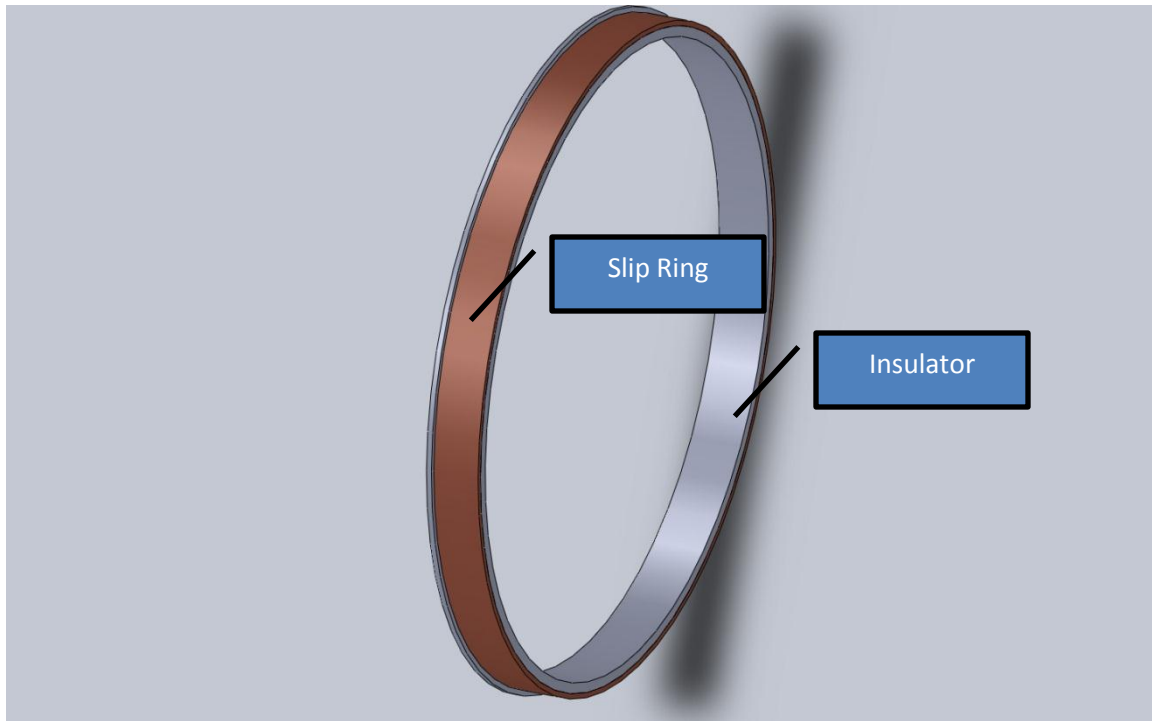


Figure 2.5: Slip ring and insulator.

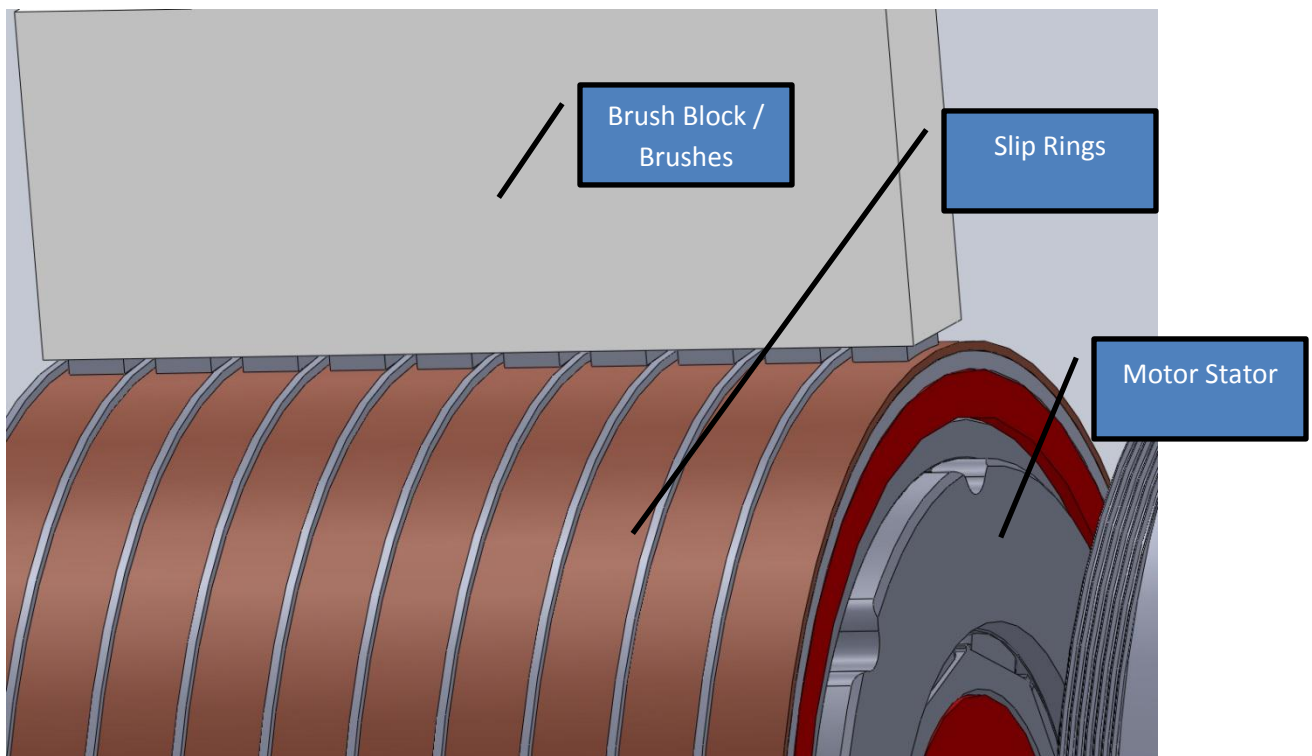


Figure 2.6: Slip ring assembly, brush block assembly, and motor.

Slip rings reside on the outside of the outer shaft where it contains the motor. Three rings transmit power to the three phases of the motor. Five rings transmit commutation signals from the hall sensors in the motor. Two connect a thermistor used for overload detection.

Power brushes are sized to handle the maximum continuous motor current of 5.18 Arms. A brush $\frac{1}{4}$ " x $\frac{3}{8}$ " is sufficient, allowing more than 7 Arms if a current limit of 80 A/cm^2 is observed. Signal brushes are a silver compound optimized for low voltage drop [5].

Slip rings are sized 9 mm x 1 mm as this is a convenient size for packaging purposes, given that the brushes are only 6.35 mm wide and the cross-sectional area of the ring far exceeds that of the wiring. There are 10 rings and the section of the outer shaft that contains the motor is ~100 mm long. Insulators are made of G-10 and are effectively a ring with a lip.

The brush block must be fitted in to the outer housing such that it lines up with the slip rings.

Each brush is 6.35mm wide, and rings are 9mm wide. This leaves 1.325 mm allowable on each brush/ring combo. The holder is toleranced .05 mm long, each holder .05 mm short. This leaves .5mm to play with on positioning the brush block in the assembly or for the shafts to move axially during operation. The brush block will be installed as far aft as possible to make up for displacement in the preload springs should the machine ever be run in reverse.

Inner Shaft

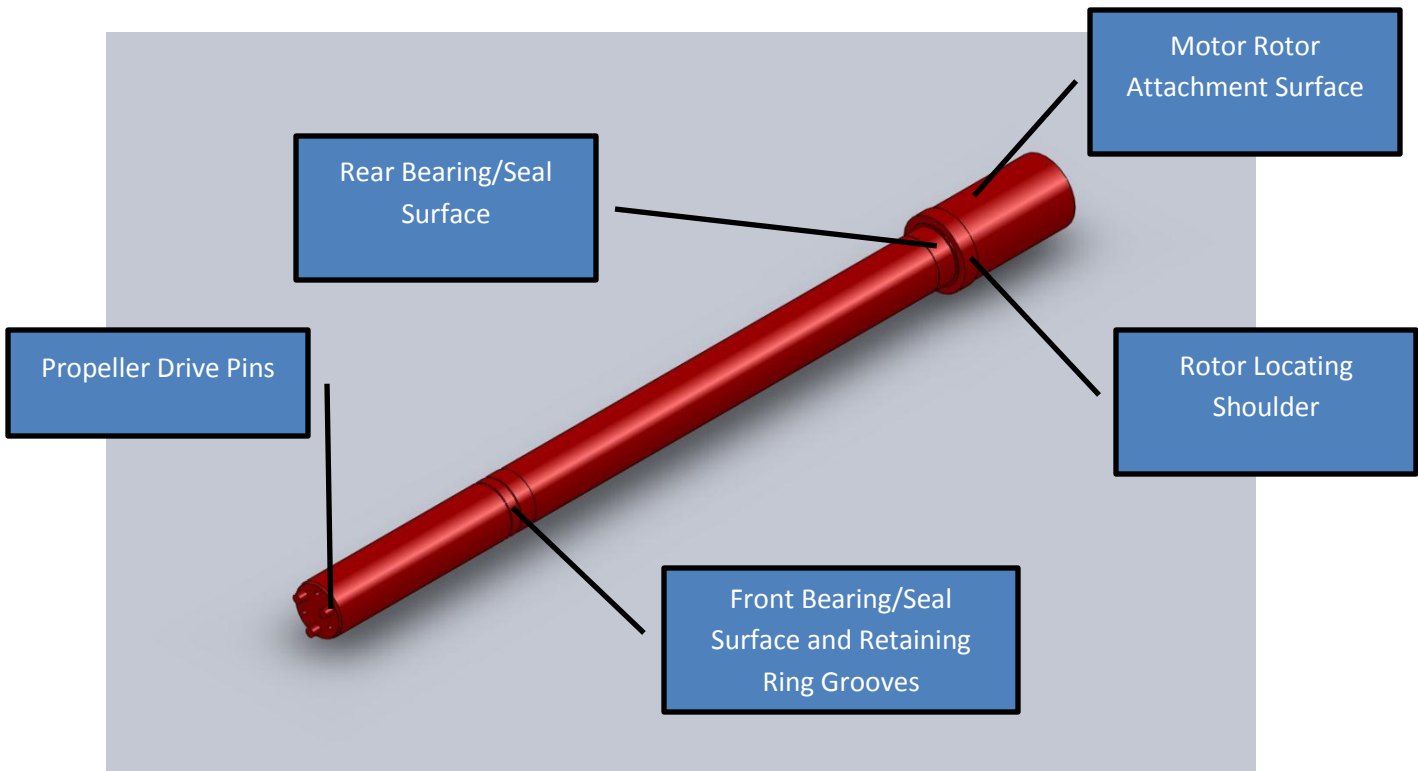


Figure 2.7: Inner shaft.

The inner shaft is mated to the rotor of the motor. The critical parts are the motor interface, the bearing surfaces, and the length between the snap ring and bearing surface.

The inner shaft consists of a motor mounting surface, a ridge to axially align the motor, a bearing standoff block, an aft bearing and seal surface, a fore bearing and seal surface, a snap ring groove to capture the bearing preload spring and washers, a snap ring groove to capture the fore seal, and studs on the front to transmit torque to the propeller.

The bearing surface diameters are taken from bearing selection guide. The rear bearing is a tight press fit (bore undersized and shaft oversized by a few ten-thousandths) and front bearing is over/undersized by the same amount.

A hexagonal hole cut to allow a 1" hex rod to lock inner shaft to tail cone.

Studs on shaft	
Aluminum shear strength [Mpa]	82.7
Stud diameter [mm]	6.35
Stud Area [m^2]	3.16692E-05
Stud Shear Force [N]	2619.044283
Torque [N-m]	33.26186239
Number of Studs	3
Total Torque [N-m]	99.78558717

Table 2.7: Torque transmission calculations.

Three bolt holes are used to affix the prop, and three studs transmit torque. $\frac{1}{4}$ " diameter studs have a shear force of $3.16692 \times 10^{-5} \text{ m}^2 \times 82.7 \text{ MPa} = 2619.044283 \text{ N}$ (shear strength) for a torque capacity of 33 N-m for each stud at a 12.7 mm radius. Propeller Drive Pins are repeated for the outer shaft, as the studs are twice as far from the center. Shear force is doubled for the outer shaft, resulting in a value of the inner studs. Table 2.7 shows these calculations.

Outer Shaft

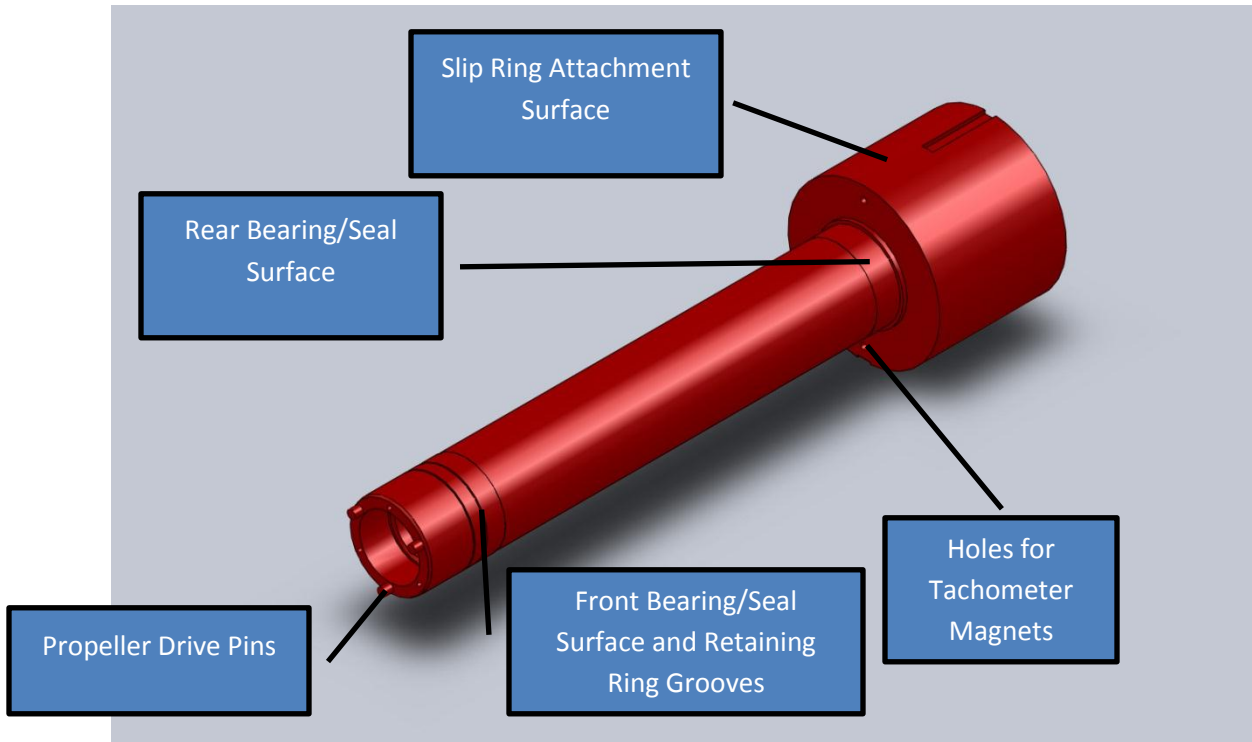


Figure 2.8: Outer shaft.

The outer shaft has the same features as the inner shaft on the exterior and propeller end. The prop is secured with three M4 bolts and torque is transmitted by three $\frac{1}{4}$ " studs machined on the end.

The bearing surface diameters are taken from bearing selection guide. The rear bearing is a tight press fit (bore undersized and shaft oversized by a few ten-thousandths) and front bearing is over/undersized by the same amount [2].

The end is chamfered to allow installation of seals.

There are wire cutouts on the exterior of the motor portion to allow wires from the slip rings to pass underneath the other slip rings. The wire sizes are 26AWG for signal wires and 14AWG for the power wires, as these are the wires coming out of the motor from the manufacturer. The signal wires have a diameter of .051" with insulator, and there are 7 conductors. The slot is then 10mm x 1.5mm. The power wires have a diameter of .11" with insulator and there are 3 conductors. The slot is then 8.5 mm x 2.85 mm.

To record the speed of the outer shaft, there is a hall sensor mounted in the outer housing. There are holes in the front of the motor section of the outer shaft for mounting magnets. The magnets are nominally 5mm x 4mm. They will be epoxied in place.

Outer Housing

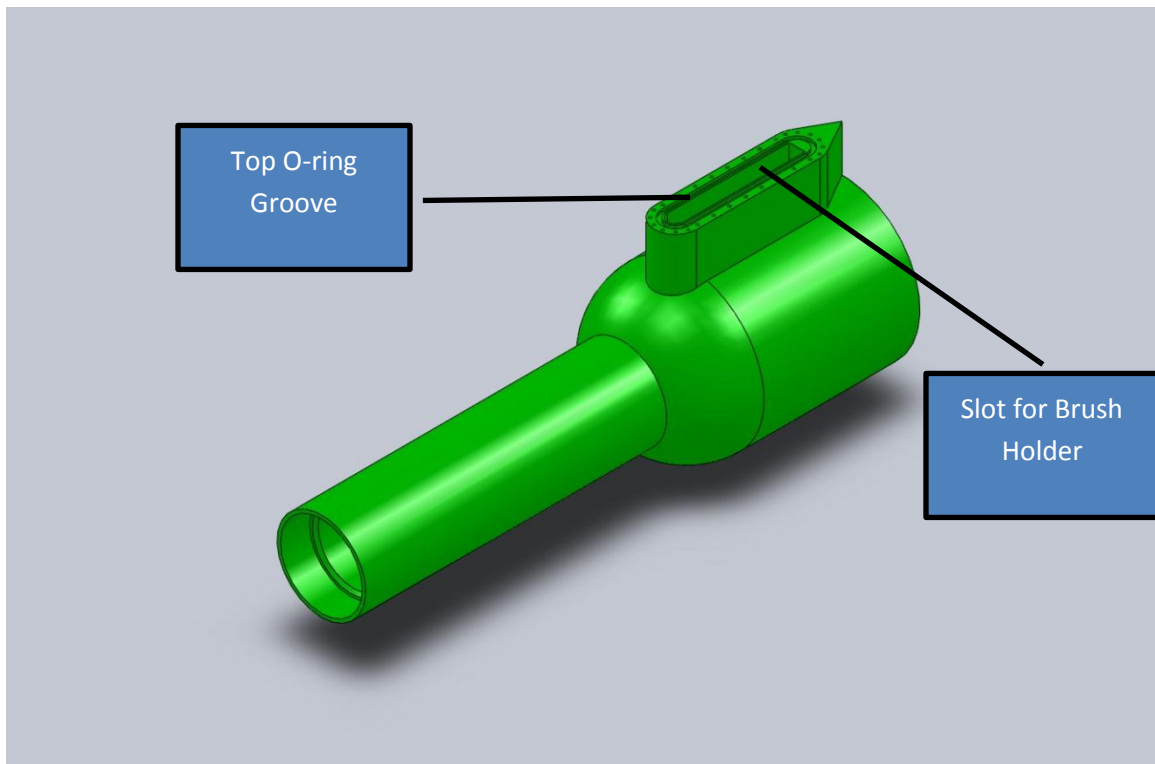


Figure 2.9: Outer housing.

The outer housing contains the inner/outer shaft and motor assembly, the electrical hardware to feed the motor and measure the speed of the outer shaft, and a sump line to empty water from the bottom of the machine should a seal leak. This line will be attached to a vacuum pump.

For the outer housing, the bearing diameters and spacing between bearings are only critical dimensions. These are taken, again, from the bearing selection guide. The bore is oversized on both ends to avoid a tight press fit, as accuracy on the outer shaft isn't needed.

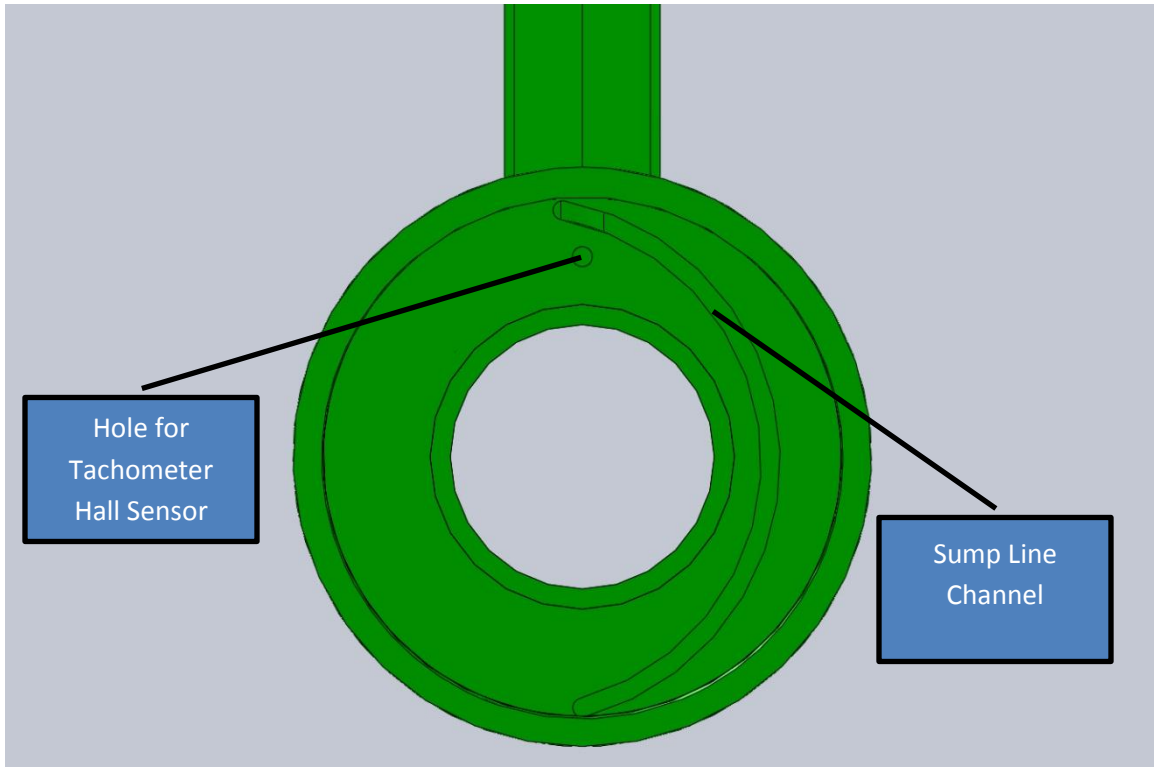


Figure 2.10: Rear view of outer housing.

At the rear of the housing is a threaded section to attach the tail cone. The threads are 1mm pitch and they extend 14 turns. The rear surface must be finished to 32-128 μ in to seal with the tail cone o-ring [3].

Inside of the housing at the front of the motor chamber is a hole for a hall sensor and a groove for the bilge tube. The hall sensor hole is nominally 5mm to match the magnet holes in the outer shaft. The groove is 3/16" to accommodate the tube. The path of the groove is inconsequential so long as it intersects the hole drilled from the top and reaches the bottom of the housing.

The electronics are contained in the sail on top. The brush block is glued in to a 15mm slot joining the motor housing section with the top of the sail. The top of the sail contains an o-ring groove for sealing purposes. It is sized to use a standard 94 mm o-ring with a 3 mm cross section. It is 80% of the height of

the uncompressed o-ring and 130% the width. The bottom of the groove will be finished with 600-grit sandpaper and a pencil. Radii on corners must be .005" to avoid damaging the o-ring.

The bolt holes on top are clearance drilled to $\frac{1}{4}$ diameter below the bottom of the o-ring groove to avoid problems with mushrooming when the bolts are tightened. The hole is then threaded like normal.

Bolts are spaced 15mm (five diameters) apart. On the rounded ends, they are spaced 30 degrees apart. Since a clearance hole is 3.2 mm for a 3 mm bolt, the holes must be accurate to true position within .1 mm.

Tail Cone

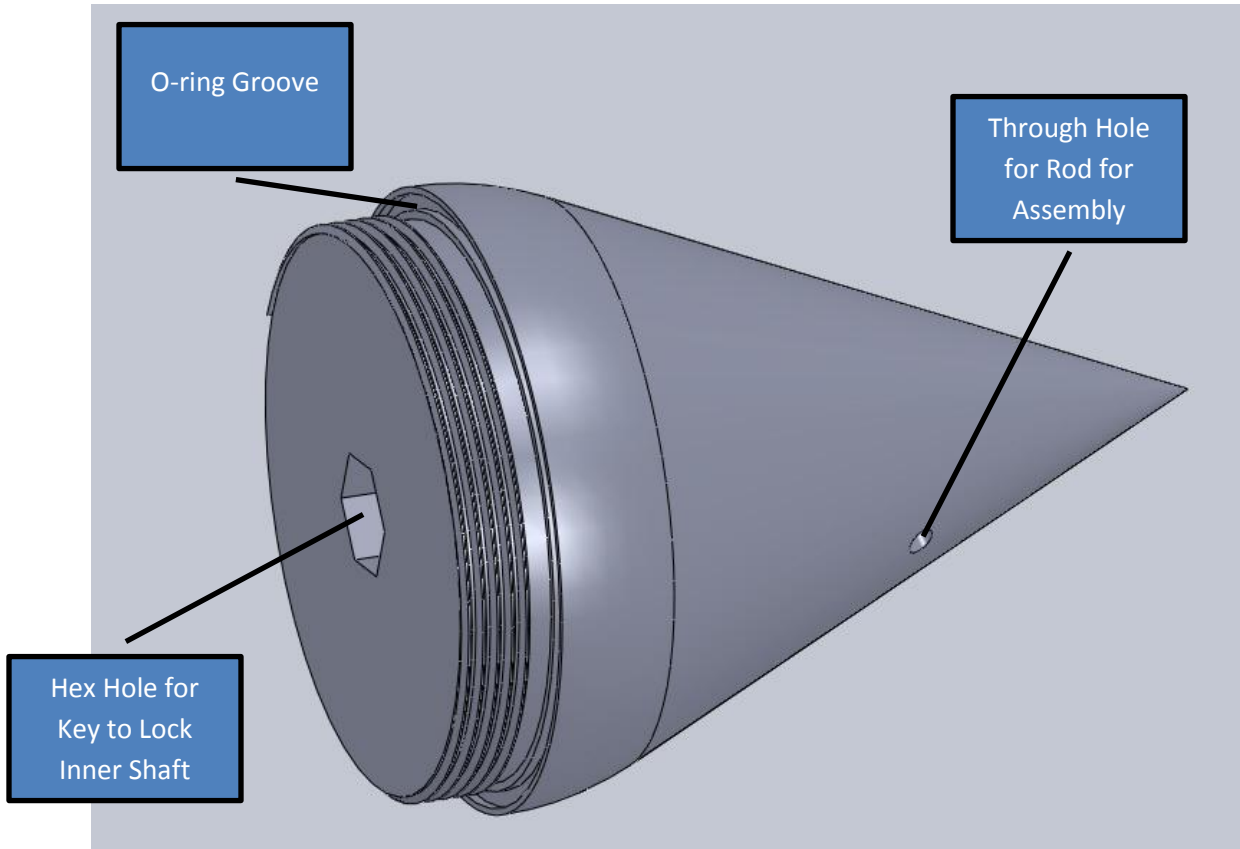


Figure 2.11: Tail cone.

The relevant features in the tail cone are the hexagonal hole, the o-ring groove, and the threads.

Outside of the o-ring groove, a 1.5mm lip is required to avoid damage. This requirement drives the outside diameter of the whole device. The ID of the o-ring groove is toleranced $+.1/-0.000$ mm. The o-ring groove is 30% wider than the uncompressed ring. Corners are radiused .005" [3].

The thread is 3.5 mm pitch to match the outer housing, with ten threads set off 2 mm from the surface where the o-ring groove is cut.

A 1" hex hole is cut in the center to allow locking of the inner shaft to run only the outer shaft. The device may be used to test a single propeller with something stationary mounted to the inner shaft. Tolerances are not tight. McMaster lists aluminum hex rod with a $+\text{-} .0025$ " tolerance. The hole is sized at $1.0025^+ .0025^- .000$.

To mount the tail cone, a $\frac{1}{4}$ " hole is drilled perpendicular to allow a rod to be inserted. Torque may then be exerted to seat the o-ring.

Assembly

The aft seals and associated washers and snap rings will be inserted in to the housing and outer tube. The motor parts will be installed on the shafts with loctite 609 and accelerator. The bearings will be heated and installed on the inner and outer shafts.

The inner shaft will then be pressed in to the heated outer shaft. The front bearing, washers, preload spring, and snap ring will be installed at the front. The seal and associated washers and snap ring will be installed at the front.

The slip rings, insulators, and magnets, along with associated wiring will be installed on the outer shaft.

The sump tube will be installed in the outer housing.

The inner and outer shaft assembly will be pressed in to the outer housing, which will be heated. The front bearing and associated washers and snap rings will be installed. The front seal and associated washers and snap rings will be installed.

The brush block will be glued in to the outer housing with epoxy. Care must be taken to ensure that the brushes line up with the slip rings. This may require shimming of the brush block. After the epoxy has cured, brushes will be fit in to the bores and connected electrically. At this point, the motor may be run.

The tail cone will be screwed in with the o-ring in place.

A hall sensor is affixed to a dowel and slid in to place

The top cap will be bolted down with the o-ring in place.

Heat assembly

Heat eliminates the requirement for press-fitting the aft, inner bearings. The outer bore is heated to expand it and allow easy insertion of the bearing. The limiting factor here is the captured seals at the rear of the device. They can only withstand 200degF. Assuming room temp is 70F, maximum allowable temperature rise is 130F (55C).

Aluminum coeff of expansion [K^-1]	2.22E-05
Max temperature [C]	55
Bore [in]	3
undersize [in]	-0.0003

bearing OD [in]	3
bearing oversize [in]	0.0003
Bore expansion [in]	3.0037E+00
Bore [in]	1.875
undersize [in]	-0.0002
bearing OD [in]	3
bearing oversize	0.0002
Bore expansion	1.8773E+00

Table 2.8: Heat assembly calculations.

Both inner and outer bearings may be installed by heating the shafts instead of pressing the bearings. To install the outer bearing, .0006" expansion is needed. 55 deg C gives .0037" on the bore inside the outer housing. For the inner bearing, .0004" is needed. 55 deg C gives .0023" on the bore inside the outer shaft.

References:

[1] *Kollmorgen Frameless Motor Selection Guide* at

http://www.kollmorgen.com/website/common/download/document/Kollmorgen_KBM_Selection_Guide.pdf

[2] *Kaydon Reali-Slim Ball and Roller Bearings: Catalog 300* at

http://www.kaydonbearings.com/downloads/catalog300/Kaydon_Catalog_300.pdf

[3] *Parker O-ring Handbook: ORD 5700* at

http://www.parker.com/literature/ORD%205700%20Parker_O-Ring_Handbook.pdf

[4] *Parker Fluid Power Seal Design Guide* at

<http://www.parker.com/literature/Engineered%20Polymer%20Systems/5370.pdf>

[5] Appendix A

Chapter 3: Machine Construction

The picture below shows the bare aluminum parts laid out in an exploded view.



Figure 3.1: Machine components.

Parts were received and then taken to be black anodized. Bearing and sealing surfaces were masked by the anodizer as to not upset the tolerances on the precision surfaces. The other surfaces were etched (a chemical process that cleans and removes a small amount of material) prior to anodizing to counteract the material growth during anodizing.

During the anodizing process, the coating penetrates the aluminum, then deposits material on the outside. A part will grow a few ten-thousandths of an inch on each surface. A round part may gain .001" in diameter.

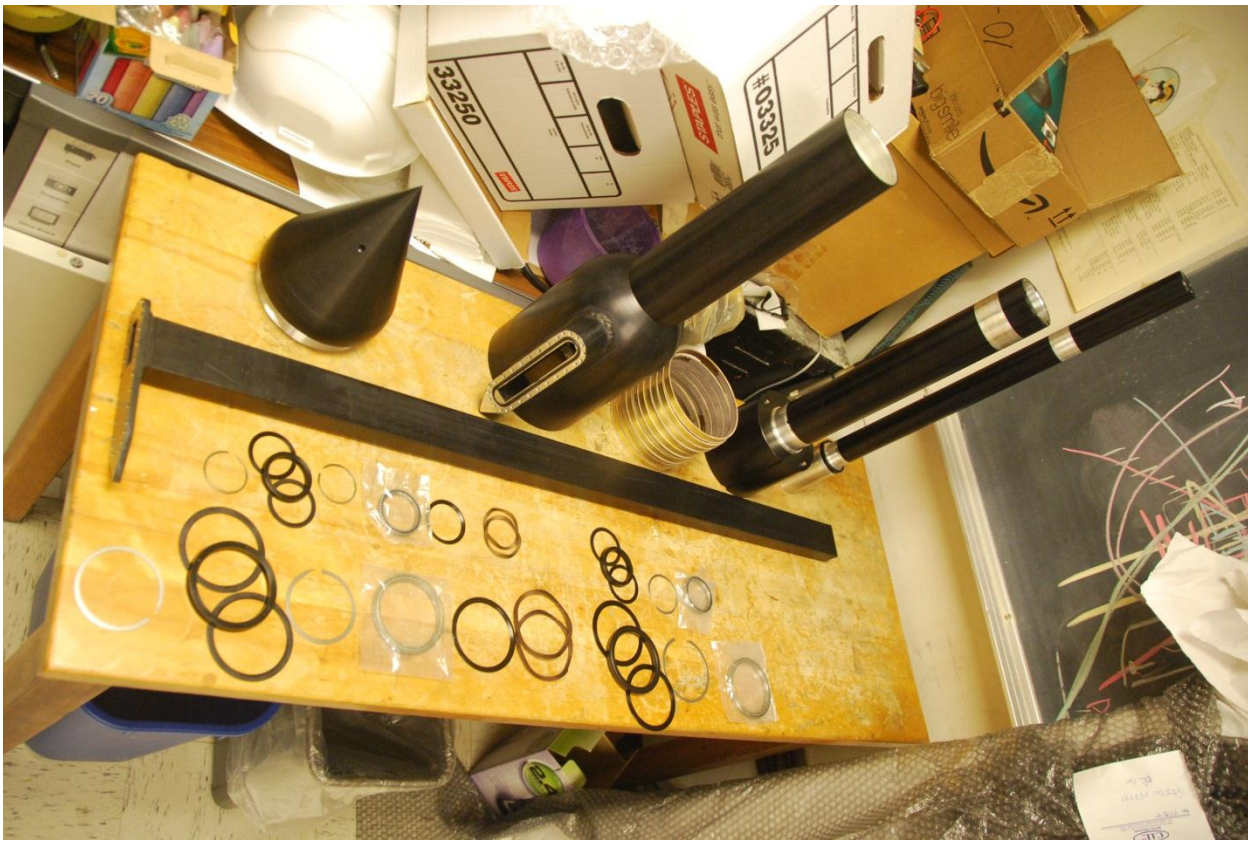


Figure 3.2: Anodized machine parts.

The first order of business was affixing the rotor to the inner shaft and the stator to the outer shaft. The plan was to glue both pieces in place with Loctite 609 as recommended by Loctite for steel parts on aluminum shafts. As delivered, the parts presented a .001" to .002" interference fit. The outer shaft was heated with a heat gun until the motor was able to slide in to place, while the inner shaft was dipped in liquid nitrogen and the rotor slid on. We could not heat the rotor enough to make it fit on the shaft, as the magnets would cease to be magnets if they were heated beyond the curie temperature.

While putting the rotor on the outer shaft, we decided we could put the rear inner bearing on in the same manner instead of pressing it on. The bearing caught on a burr on the front bearing surface, preventing it from going further. By the time we went to pull it back off, the inner race had cooled and contracted. Since it is an angular contact bearing, this was enough to allow the bearing to be pulled apart with very little force.

Once the bearing came apart, the 40 balls inside spread out on the lab floor. After finding and cleaning them, grease was applied to the separator to hold the balls in place inside the outer race, and they were reinserted one-by-one with a pair of tweezers. The inner race was then carefully inserted and pressed in to place.

After reassembly, the bearing was again cleaned with petroleum solvents and then repacked with bearing grease.



Figure 3.3: Motor parts and shafts.

The burr on the front bearing surface was removed with a piece of emory cloth before tapping the rear bearing in to place. Instead of pressing the bearing on, a slide hammer of sorts was machined out of a piece of aluminum pipe. It was sized to fit freely around the inner shaft. The front end was chamfered such that it only contacted the inner race of the bearing. This device was used to hammer the bearing past the front bearing surface and on to the rear bearing surface, which was sized to be a tight press fit. This time, the bearing went on with no issues.



Figure 3.4: Installation tool for bearings.

The rear seal, seal washers, and retaining ring were then inserted in to the inner bore of the outer shaft. The inner shaft was then inserted part way in to the seal, which served to center it in the outer shaft. The rotor was then wrapped with paper to prevent damage when inserting it in to the rotor. Once roughly inside, a mallet was used to gently coax the rear inner bearing in to its bore in the outer shaft. The bearing preload springs were dropped in between the inner and outer shafts, followed by the inner spring washer. The bearing was inserted using the same tool used to tap the rear inner bearing in to place. The retaining ring was expanded to fit around the inner shaft, then the tool was used again to compress the bearing preload springs and seat the retaining ring with a tapping motion.

$\frac{1}{4}$ " diameter by $\frac{1}{2}$ " long steel pins were then tapped in to the three holes in the inner and outer shafts. At this point, the rotating assembly and motor were assembled.

Upon rotating the shaft by hand, we decided that the seal was much too tight for our application. We removed the inner shaft, again wrapping paper around the rotor to avoid damaging it. The rear seal was removed. We decided that we would use only a front seal, and that we would remove the o-ring designed activate the lip seal, leaving a much more compliant seal. We felt justified in doing this, as the seals are designed for use in hydraulic systems at several thousand psi, while our application will see a maximum of a few psi in water. This decision was later validated as the machine does not leak when assembled correctly.



Figure 3.5: Assembled inner/outer shafts and outer housing.

Before proceeding further with construction, we decided to wire the motor and run it. The Kollmorgen AKD drive was wired in only to find that it could not be set up to run a motor with hall sensor feedback for commutation. Luckily, a Copley Xenus drive used for a previous student, Jarod Ketcham's motor project, was available. This drive was wired in, using an Ethernet cable for the five sensor leads and a 4-14 cable with a braided shield around it for the motor leads. The wiring diagram and wiring scheme colors are shown below. Power and signal grounds are placed next to one another and in between signal and power lines in the hope of reducing interference.

The stator was initially fit in to the outer shaft with heat. When the inner shaft was installed, the use of the slide hammer tool to seat the front retaining ring caused the stator to move slightly. We decided that we would pull the stator out a ways, add Loctite, and then press it back in. The heat gun was used to expand the outer shaft, Loctite was applied, and the stator was pressed back in, never to be removed.

vga connector pin (at controller)	function	standard ethernet wire color	brush slot	sensor board wire color
2	+5V	brown/white	1	blue
3	hall U	orange	2	brown
5	gnd	orange/white	5	green
6	hall V	green/white	3	orange
9	hall W	blue/white	4	yellow
	function	wire color	brush slot	motor wire color
-	motor gnd	green	6	brown, but lone wire soldered to outer shaft
-	motor U	white	7	blue
-	motor V	black	8	brown
-	motor W	red	9	purple

Table 3.1: Wiring table.

Once the motor ran, the slip rings needed to be installed around the stator section of the outer shaft. The slip rings consisted of a G-10 fiberglass insulator surrounded by a brass slip ring. There are channels cut in the section of the outer shaft around the stator to allow wires to be run to the slip rings. To wire them in, it was necessary to cut a groove in the fiberglass insulator from the inside. One at a time, a groove was cut, the appropriate wire was cut to length and soldered to the slip ring, epoxy was used to cover the connection, then the ring was pressed on to the shaft, taking care to keep the wire in place. The following pictures illustrate this process.

The larger wires for the motor leads were much more of a problem to solder to the brass rings.



Figure 3.6: Slip ring installation.

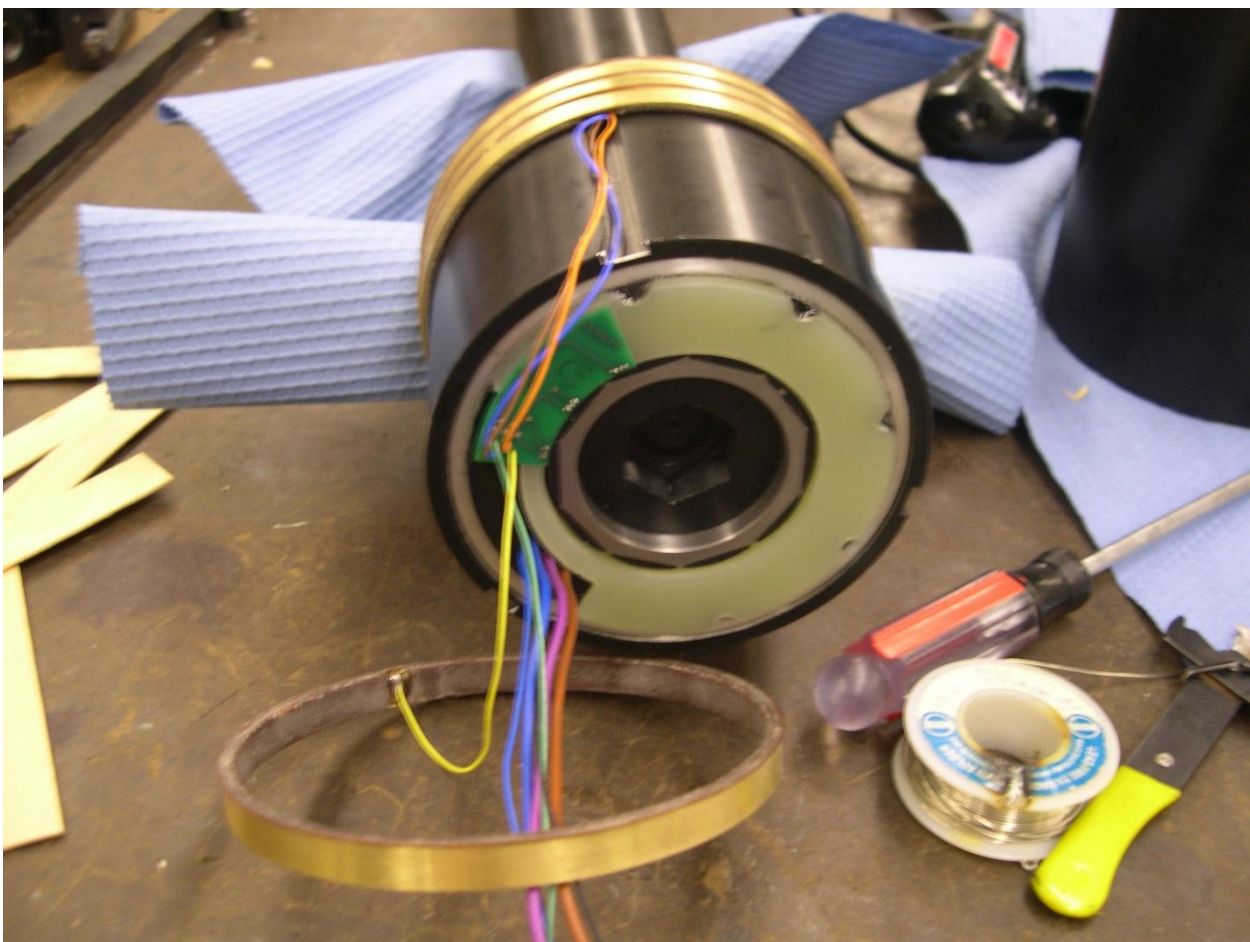


Figure 3.7: Slip ring connection detail.



Figure 3.8: Slip ring close-up.

When the outer shaft was anodized, it was apparently not etched first, meaning the diameter grew by a few ten-thousandths. This caused the outer bearings to not fit easily over the front of the outer shaft. This situation was rectified by a lot of time spent sanding down the anodizing on the outer shaft with a piece of emory cloth.

Once the bearings fit over the outer shaft, the rear bearing was test-fit in to the outer housing. Like the inner rear seal, the outer rear seal was left out. This left just the retaining ring to keep the bearing in place. Luckily, the bearing bore in the outer housing was right on spec, and the bearing dropped in. The front bearing bore in the outer housing was specified a little large to allow the bearing to slide for preload purposes. It was delivered a slightly small, so emory cloth was again used to open up the bore so that the bearing would slide properly. When finished, the bore was approximately .001" larger than the outer race of the bearing.

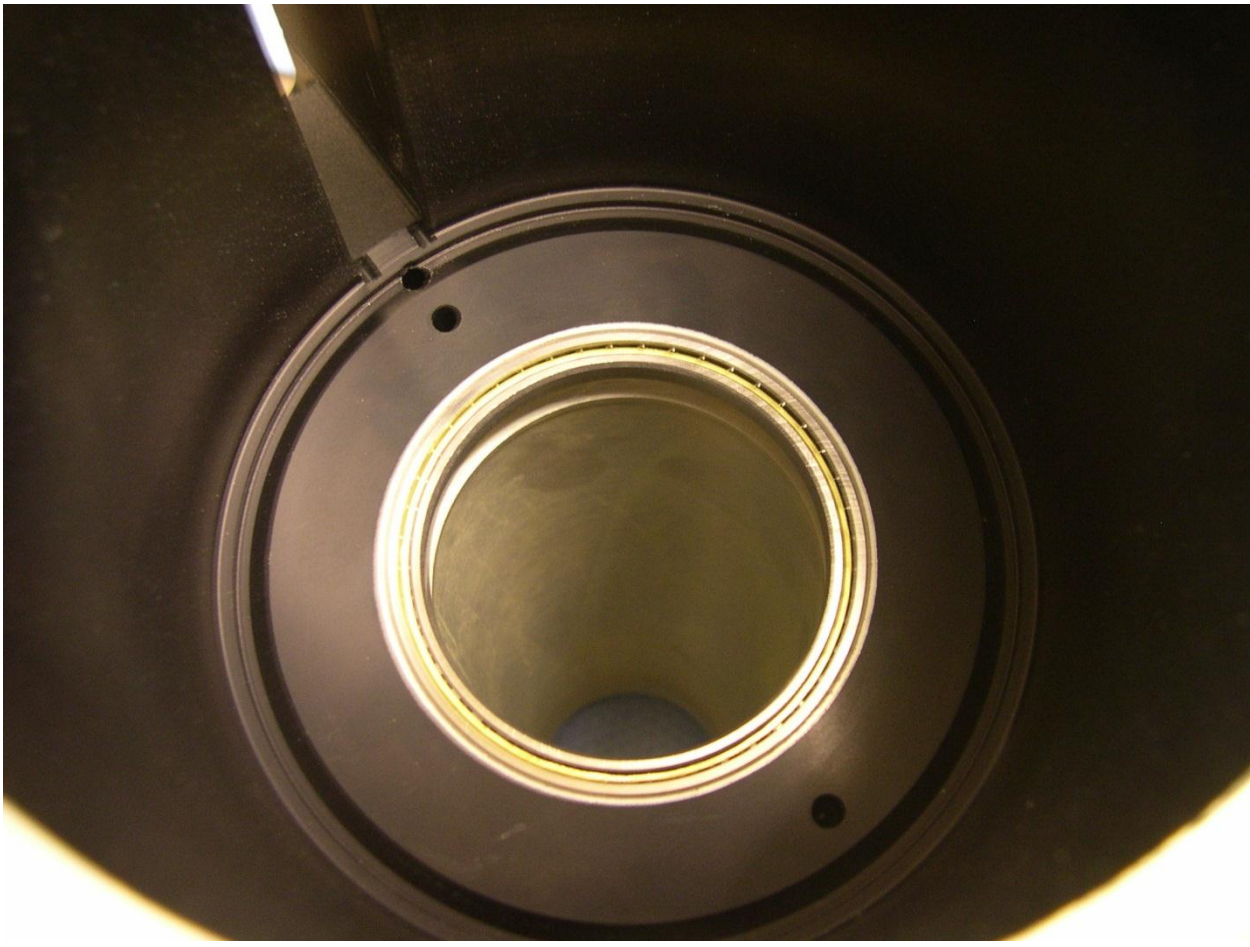


Figure 3.9: Bearing test-fit.

There is a hall sensor installed to measure speed of the outer shaft. The sensor is installed in a channel milled in a 15mm wooden dowel. This dowel is then inserted in a hole from the top of the device, placing the sensor in a hole drilled in the outer housing. The test-fit of the device can be seen below.

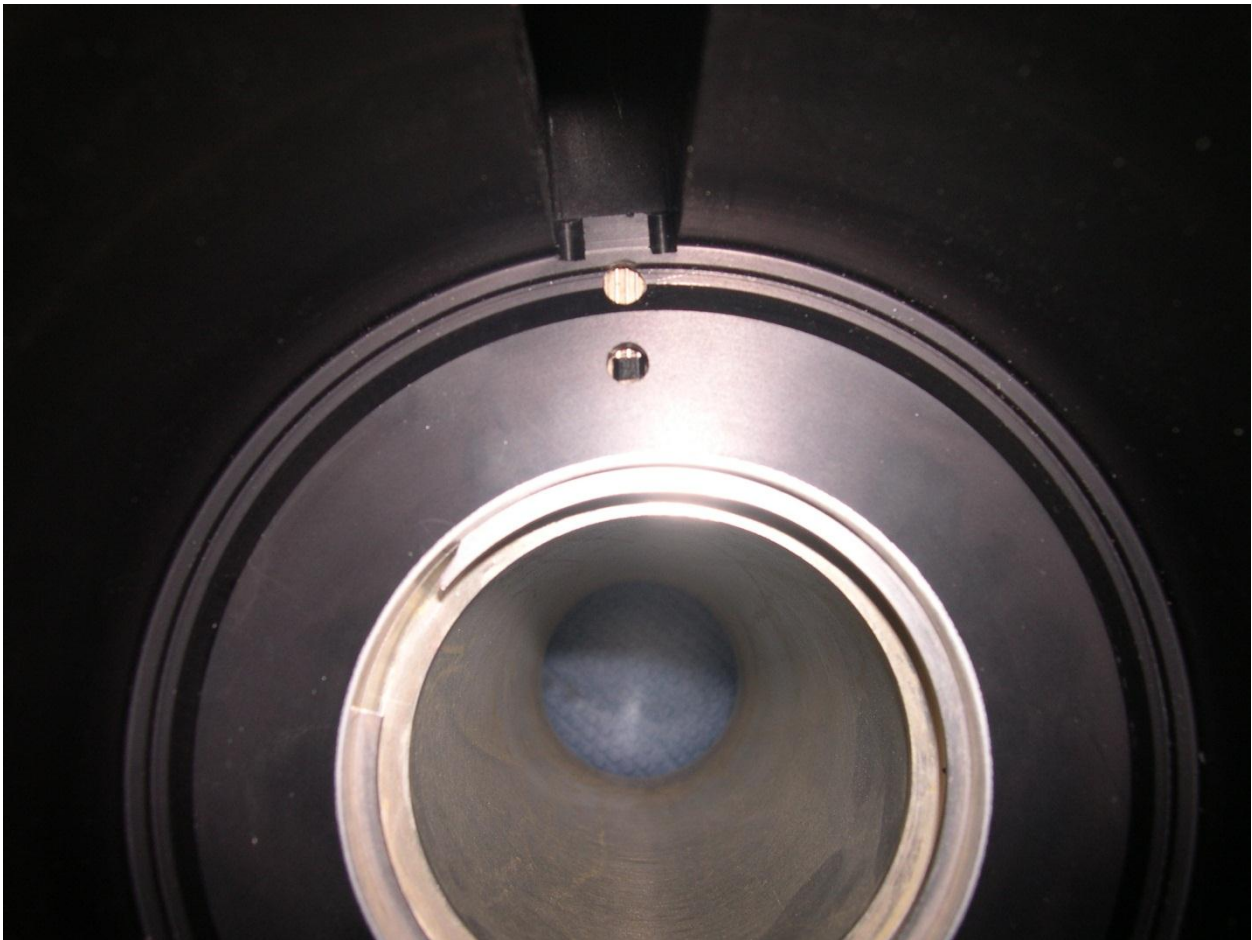


Figure 3.10: Tachometer hall sensor test-fit.

The brush block was 3D printed in the lab. Brushes were sanded slightly to make them slide easier in their bores. The picture below shows the brush block and brushes being test-fit in to the outer housing prior to installation of the rotating assembly.

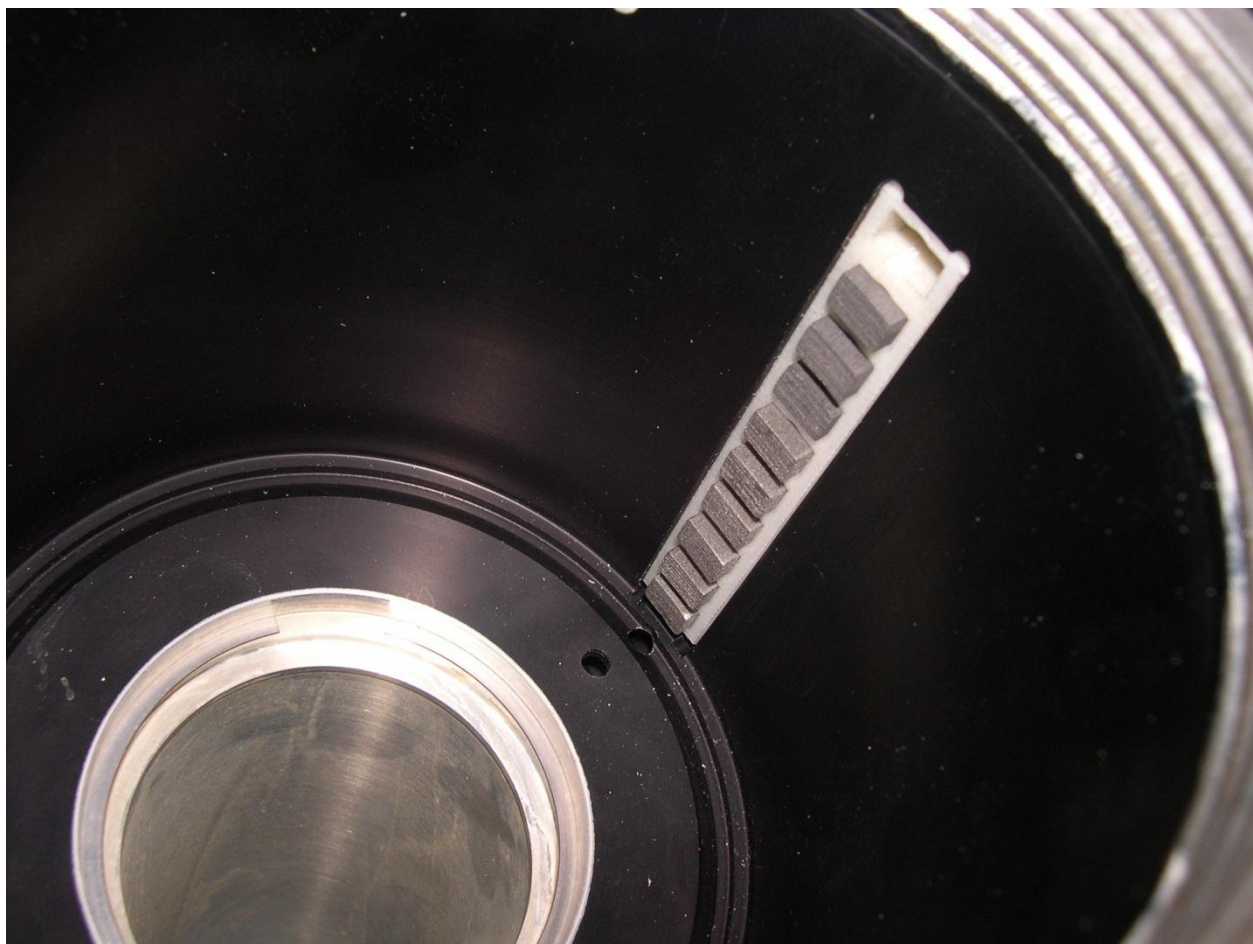


Figure 3.11: Brush block test-fit.

A sump line was added to enable pumping water out of the housing should there be a leak. This line was glued with 10-minute epoxy in a groove machined in to the housing for precisely this purpose.

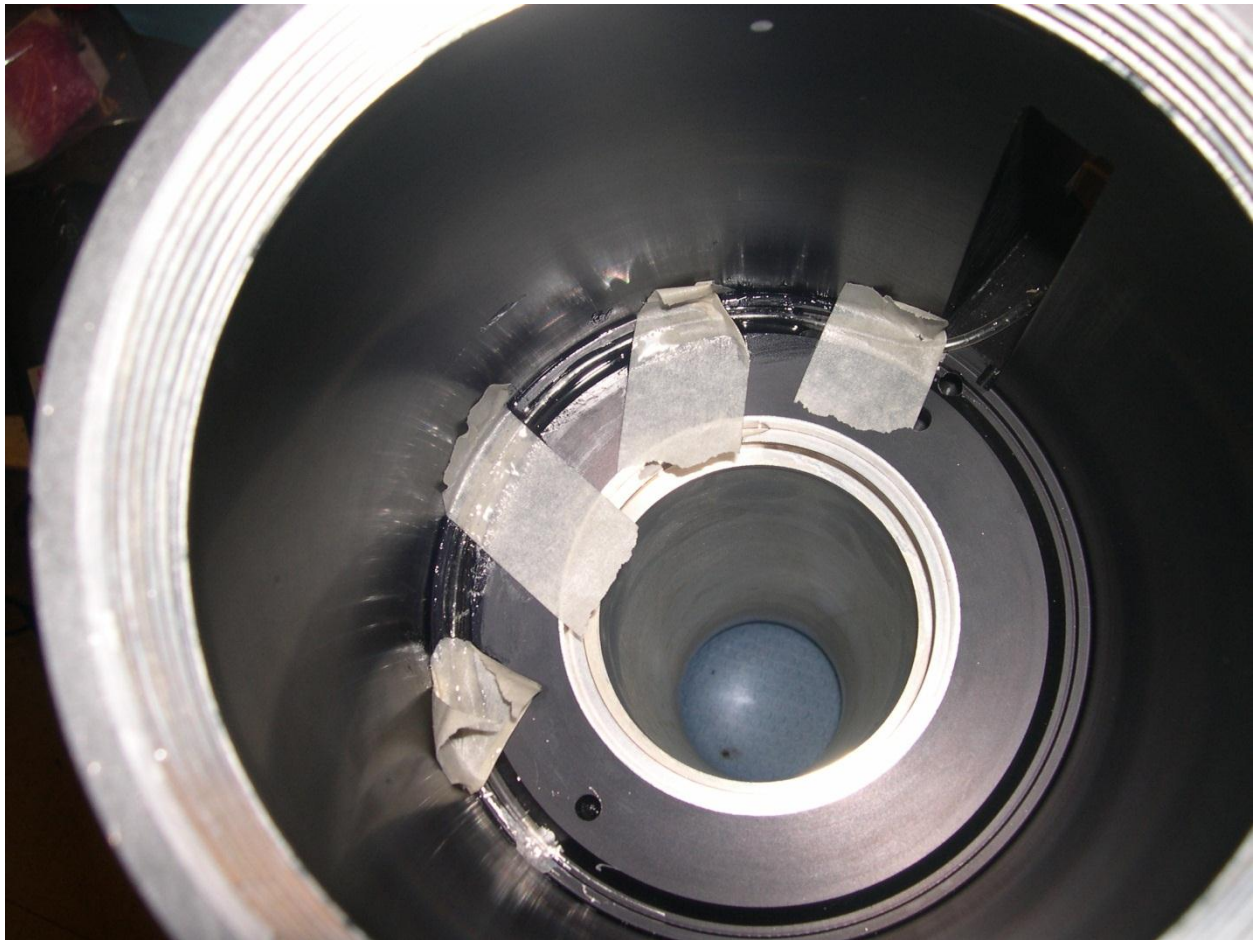


Figure 3.12: Sump line installation.

Before the rotating assembly could be inserted in to the outer housing, the outer rear bearing was tapped in to place using a tool similar to the one that had been fabricated for the same job on the inner shaft. Small magnets were glued in to their bores with Loctite 609 to trigger the hall sensor installed in the outer housing.

The rotating assembly was then carefully inserted in to the outer housing. Then , much the same as the inner shaft/outer shaft assembly, the preload springs, bearing washer, and retaining ring were installed to capture the rotating assembly in the outer housing. The pictures below show the rotating assembly

installed in the outer housing with the sump line visible.



Figure 3.13: Assembled machine.

The next picture shows the slip ring through the slot machined to allow insertion of the brush block and brushes.

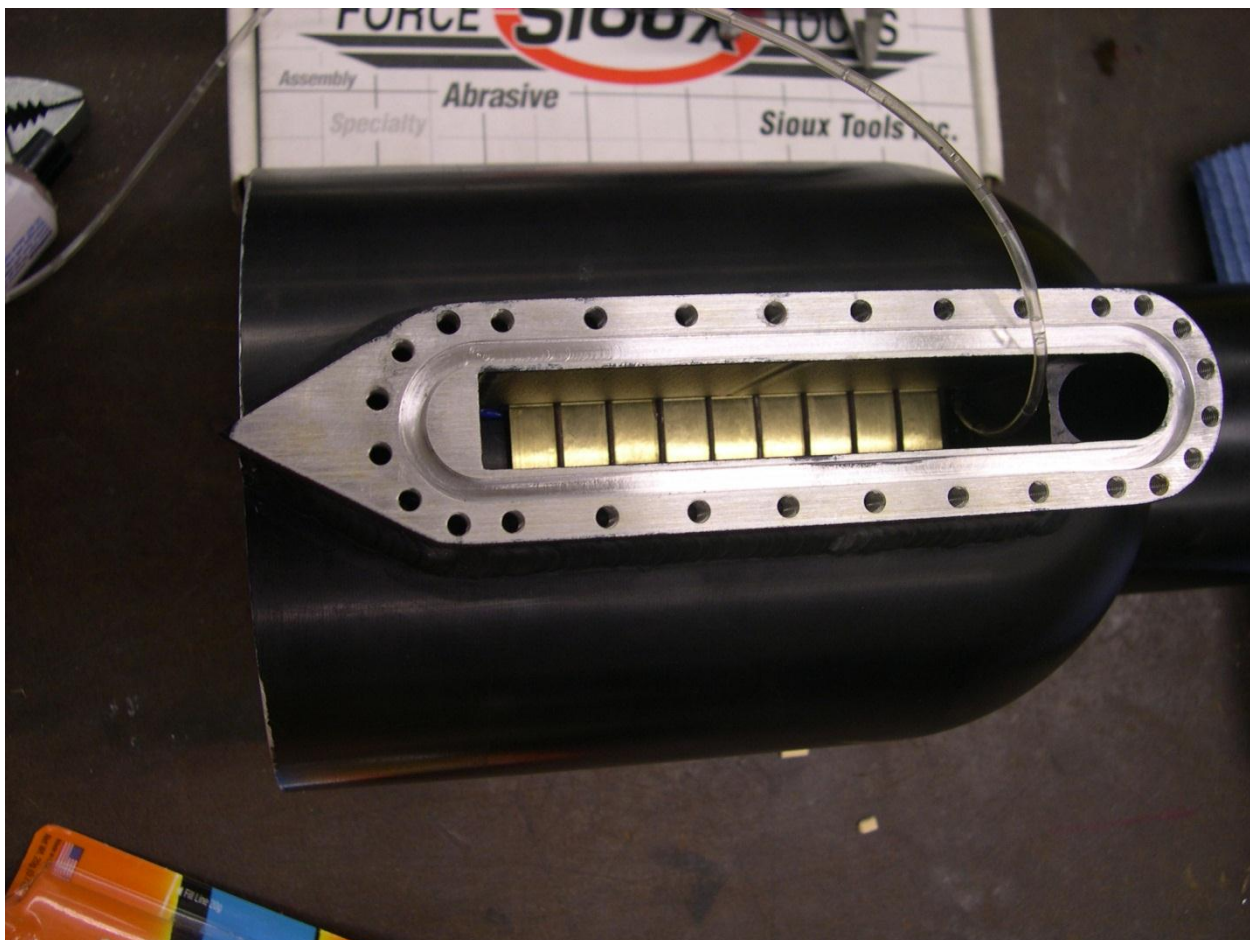


Figure 3.14: Slip rings viewed from top.

Holding brushes in their bores was left as an afterthought. The brush holder was designed to protrude in to each brush slot and center the spring. It is held in place when the top cap is bolted on. The part was 3D printed in the lab. The picture below shows the brush holder.

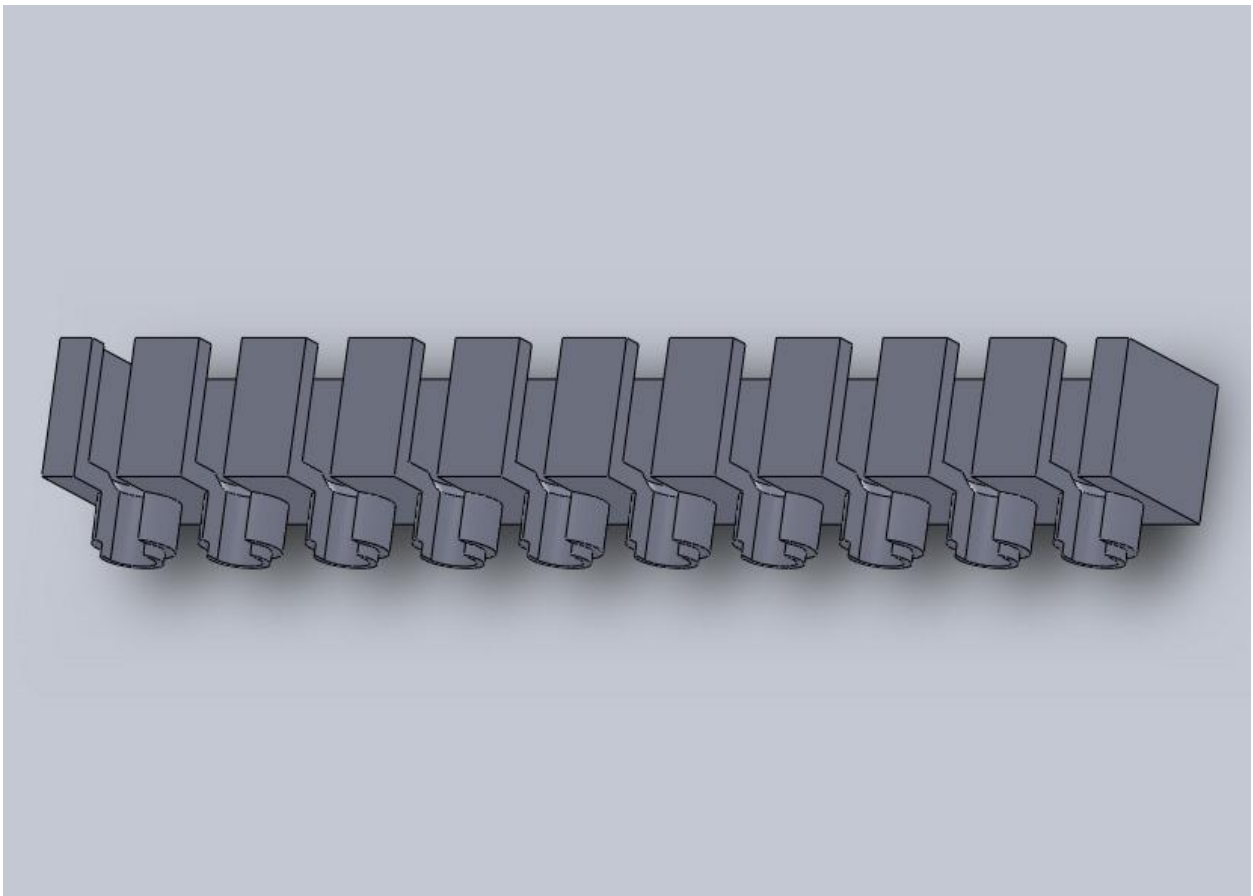


Figure 3.15: Brush holder.

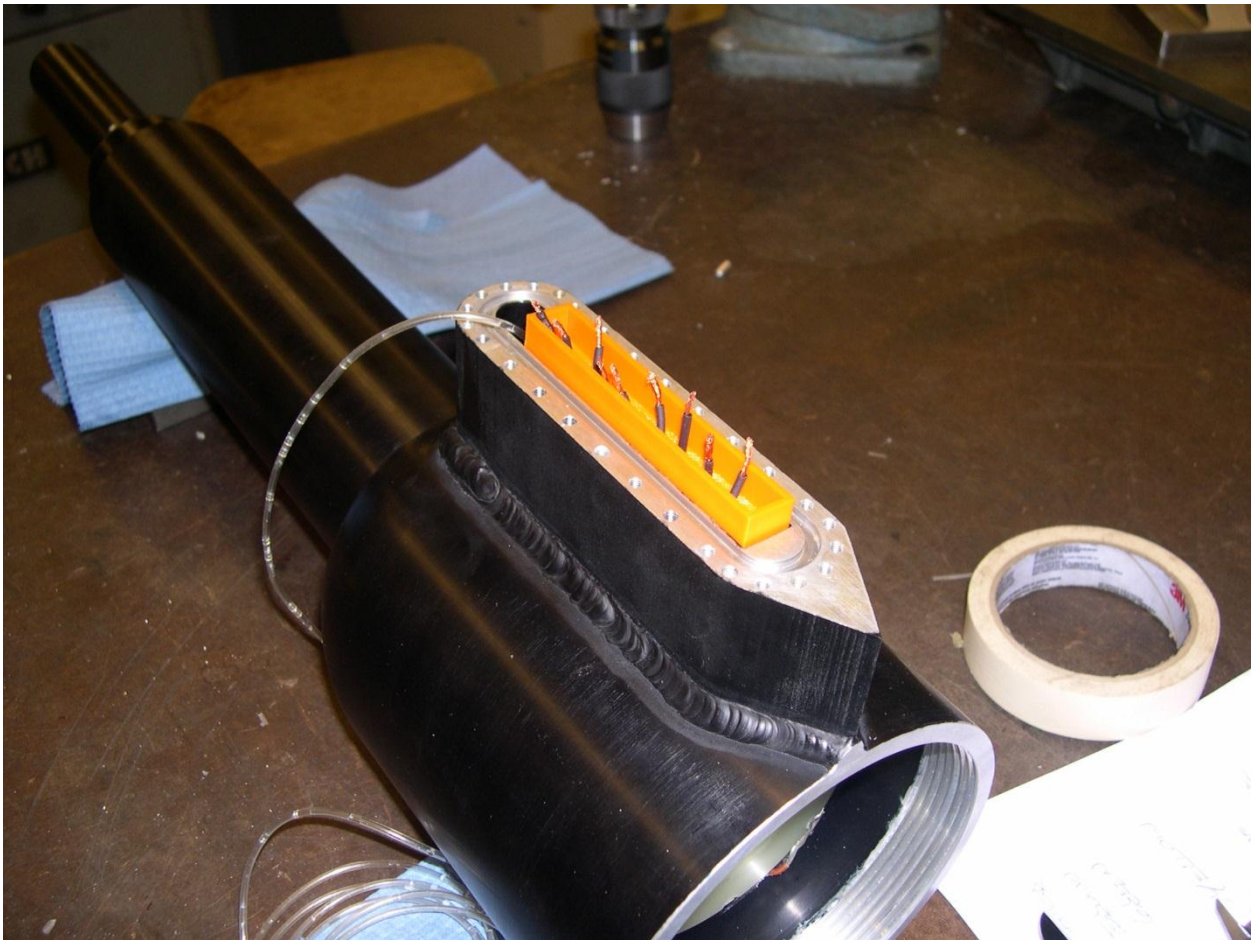


Figure 3.16: Brush holder and brush leads.

Since the propellers were 3D printed, tolerances were not good enough to mate with the shafts without help. The front propellers needed to be reamed to 1.5", and the rear propellers needed to have a 2.5" bore. We located a 1.5" reamer, which we used to cut off excess material in the inner shaft propeller. The outer shaft propellers were affixed to a rotary table on a mill, and then an endmill was used to cut off material while the propeller hub was rotated. The holes that mate with the drive pins in the end of the shaft also needed to be reamed to 17/64". This allowed propellers to be easily seated on the shaft.



Figure 3.17: Assembled machine.

If the machine were designed again, there are a few changes that I would make. First, the brushes should be held in place prior to the top cap being installed. Testing the machine with the top cap

removed involved securing wood scraps across the top with zip ties. Bolting the top cap requires care to align wires properly. Second, I would make the sail taller to allow more room for wiring. The wires are currently a tight fit, though this may be in part caused by the brush holder. Care must be taken during assembly to ensure that nothing binds and the brushes are free enough to make good contact with the slip rings. Third, I would make the pole that holds the machine longer. The 1" width is fine, but having more room to run wires would make assembly easier. A 4" length would free up wiring space in the sail and provide additional stiffness to the machine on the test stand.

Chapter 4: Motor Math

Motor torque may be calculated from current going in to the motor. It is thus necessary to determine torque as a function of current.

Torque for a permanent magnet DC motor, or any machine with saliency is given by the following formula.

$$T = p \frac{q}{2} (\lambda_d I_q - \lambda_q I_d) \quad (1)$$

Where p is number of pole pairs, q is number of phases in the machine, λ is flux, and I is current. The d and q subscripts refer to the two axes of the machine. The d-axis is aligned with the magnetic flux in the rotor, and the q-axis is offset by 90 degrees.

Flux on each of the two axes is given by formula (2).

$$\lambda_{dq} = L_{dq} I_{dq} + \lambda_R = T L_{ph} T^{-1} I_{dq} + \lambda_R \quad (2)$$

The inductance and current in each winding must be transformed across to the rotor to calculate current. This is done with a Park's transform, which is dependent on rotor position. The transform matrix and its inverse are shown in formulas (3) and (4), respectively.

$$T = \frac{2}{3} \begin{bmatrix} \cos\theta & \cos(\theta - \frac{2\pi}{3}) & \cos(\theta + \frac{2\pi}{3}) \\ -\sin\theta & -\sin(\theta - \frac{2\pi}{3}) & -\sin(\theta + \frac{2\pi}{3}) \\ \frac{1}{2} & \frac{1}{2} & \frac{1}{2} \end{bmatrix} \quad (3)$$

$$T^{-1} = \begin{bmatrix} \cos\theta & -\sin\theta & 1 \\ \cos(\theta - \frac{2\pi}{3}) & -\sin(\theta - \frac{2\pi}{3}) & 1 \\ \cos(\theta + \frac{2\pi}{3}) & -\sin(\theta + \frac{2\pi}{3}) & 1 \end{bmatrix} \quad (4)$$

The remnant flux density of the magnets is aligned with the d-axis. Flux in the rotor frame is given by formula (5). Lambdaf is the remnant flux density of the magnets.

$$\lambda_R = \begin{bmatrix} \lambda_f \\ 0 \\ 0 \end{bmatrix} \quad (5)$$

Phase inductance is measured directly from the motor leads.

$$L_{ph} = \begin{bmatrix} L_A \\ L_B \\ L_C \end{bmatrix} \quad (6)$$

With these equations, torque may be backed out of the current waveforms.

Chapter 5: Experiment

The machine was taken to the tow tank at the US Naval Academy in Annapolis, MD for testing. The tow tank is a 380' long, 28' wide, and 16' deep tank of water with a carriage that travels the length of the tank at a defined speed. The machine was suspended in the water beneath the carriage, and attached via a force block to measure thrust produced.

The support tube is attached to a piece of 8020 that is then connected to force sensors and then to another piece of 8020. This piece is then clamped to the carriage with large c-clamps.

To avoid measuring force on the front of the tube, it is surrounded by a fairing that is anchored to the carriage directly. The fairing is a piece of extruded aluminum normally used as a spreader section in a sailboat. Two aluminum bars were machined to fit in the front and back of the fairing and used to attach the fairing to a frame built around the force sensors. Washers are used as spacers to properly center the fairing around the tube.

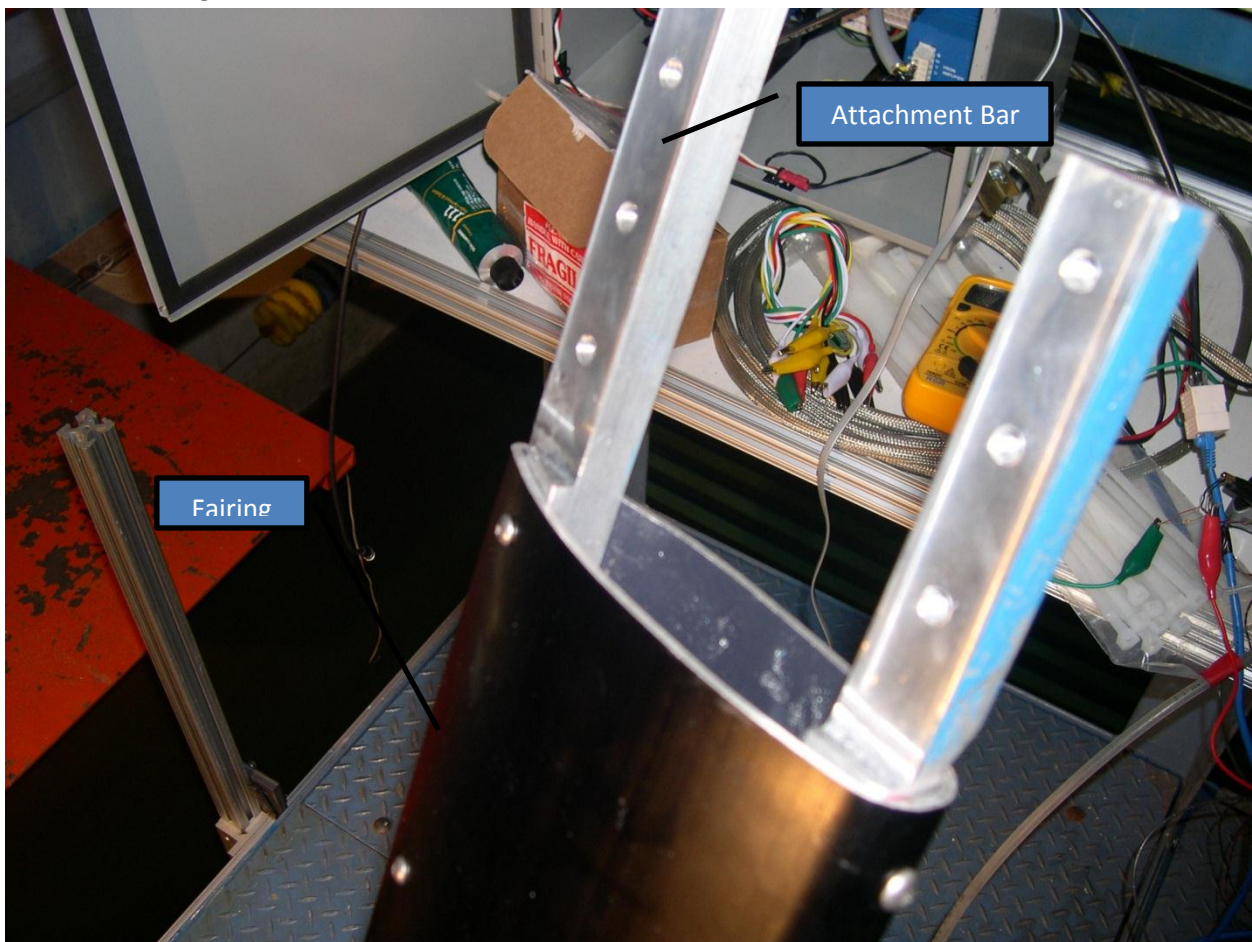


Figure 5.1: Fairing and attachments.

Figure 5.2 shows the fairing installed around the post and anchored to the strut on the right, which is anchored to the same piece of 8020 as the force sensors.

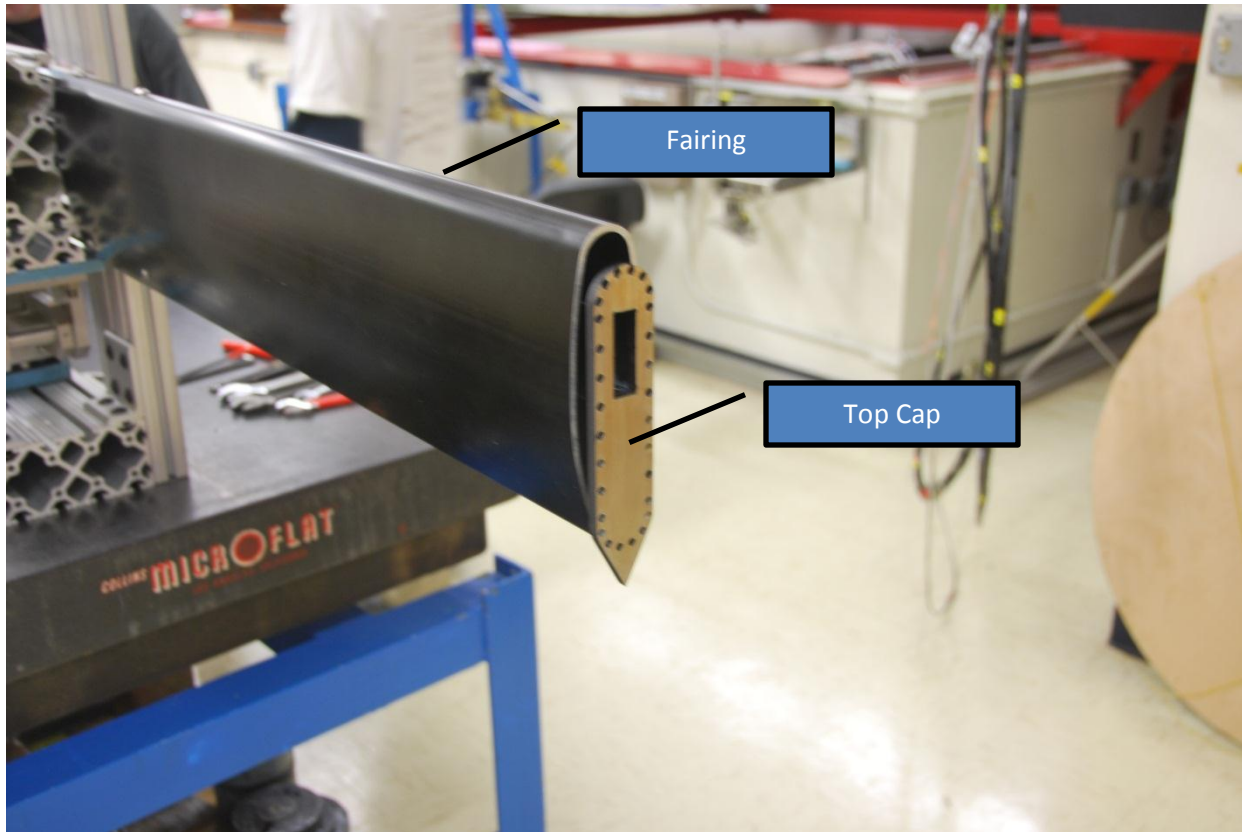


Figure 5.2: Fairing, support post, and top cap.

The picture below shows the device mounted to the carriage prior to being submerged. The force blocks are in red circles. The machine is mounted to the 8020 strut on the right, and the fairing and force blocks are mounted to the 8020 strut on the left, which is then secured to the carriage.

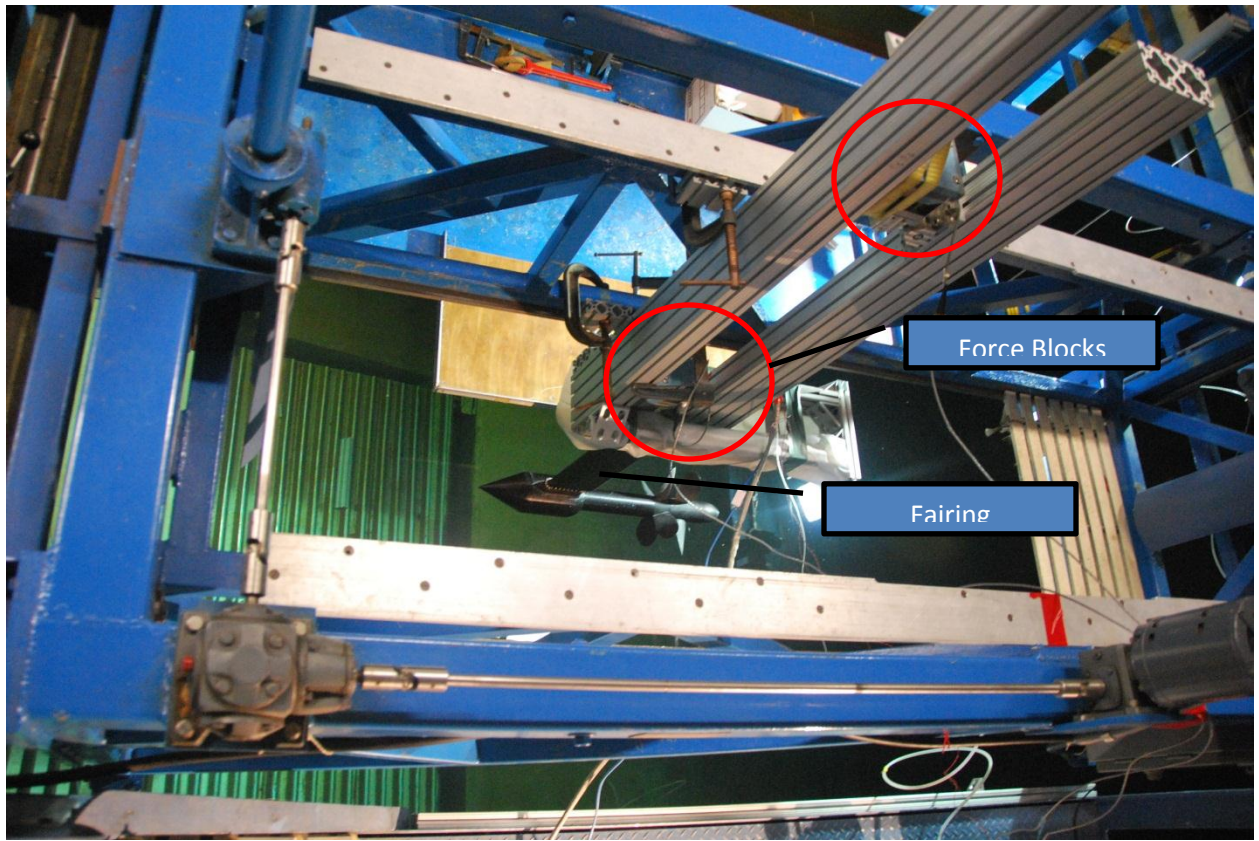


Figure 5.3: Machine mounted to test rig.



Figure 5.4: Tow tank carriage with machine.

These tests were attempted twice. On both trips, the motor failed at approximately 1 PM after being dropped in to the water at 9 AM by shorting one hall sensor lead to ground. This prevents the motor from running. On the first trip, a wire was pinched in the o-ring on top, allowing a small leak. It was initially assumed that this caused the short, but on the second trip, the same symptoms were observed. This time, the machine was assembled correctly, and the sump line confirmed that there was no leak.

After the first trip, the top cap, brushes, and tail cone were removed. The machine was allowed to sit in the lab for a week. The machine was then re-assembled and hall sensor function returned to normal. It is assumed that there is water inside the channel underneath the slip rings that contains the signal wires, as another cause that would fix itself after sitting for a week is not apparent.

Given that the problem re-occurred at about the same time both trips, condensation is a likely culprit. During testing at MIT, the machine was submerged in room-temperature water in a lab that has low humidity. At the Naval Academy, the water temperature is somewhere in the 40s, space temperature is in the 50s, and humidity is high. Water is likely condensing on the inside of the machine, as the sump line pulls air in, and the machine quickly cools to water temperature when it's not being run.

Chapter 6: Results

The motor has been demonstrated to work as designed. The device spins the two propellers in opposite directions as designed. In the one run where data was properly recorded, the relative speed was 480 RPM, and the individual speeds were approximately 210 RPM and 270 RPM on the outer and inner shafts, respectively.

The machine was also tested at MIT in both a trash can with propellers and in an aquarium without propellers to obtain seal torque measurements for a propeller experiment. In the trash can experiment, the device was positioned such that the nose and propellers were submerged while the rest of the machine was above the surface. The machine was then spun to between 140 and 160 RPM, where contra-rotation was demonstrated.

Figure 6.1 shows the current waveform (dark blue), the outer shaft tachometer waveform (light blue-green), and the fourier transform of the current. The current measurement is taken with a hall sensor current probe. The current waveform has a fundamental frequency of about 12.5 Hz, which correlates to a 150 RPM relative shaft speed, as the machine has ten poles. The outer shaft tachometer waveform measurement on the right has been corrupted by noise. The outer shaft is spinning at approximately .8 Hz, or 48 RPM. This differs from the later experimental results, as the machine is stationary.

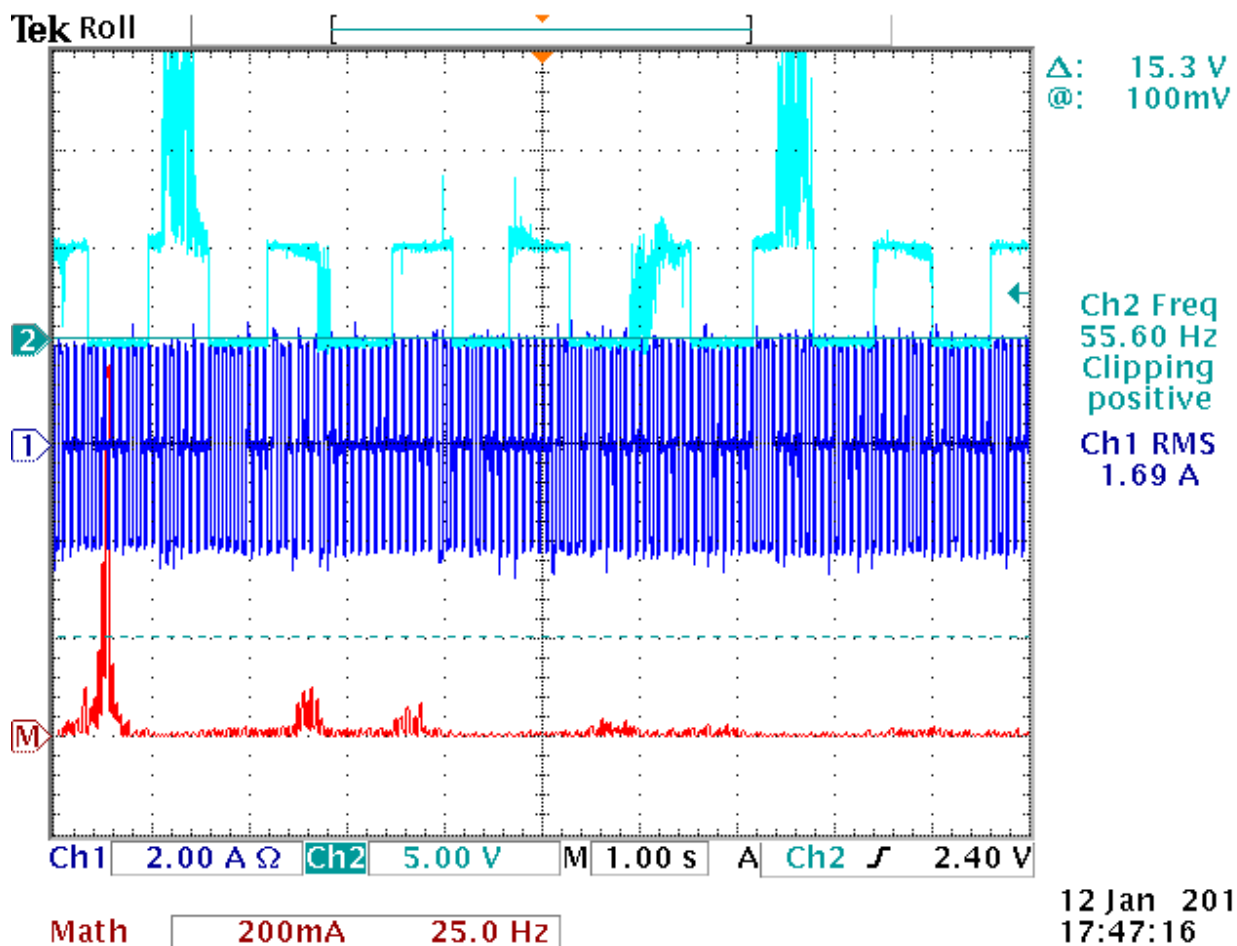


Figure 6.1: Current waveform, fft, and tachometer signal.

Figure 6.2 shows a similar test, demonstrating contra-rotation in the trash can with propellers. Note that there is 5th, 7th, 11th, and 13th harmonic present in the FFT of the current waveform.

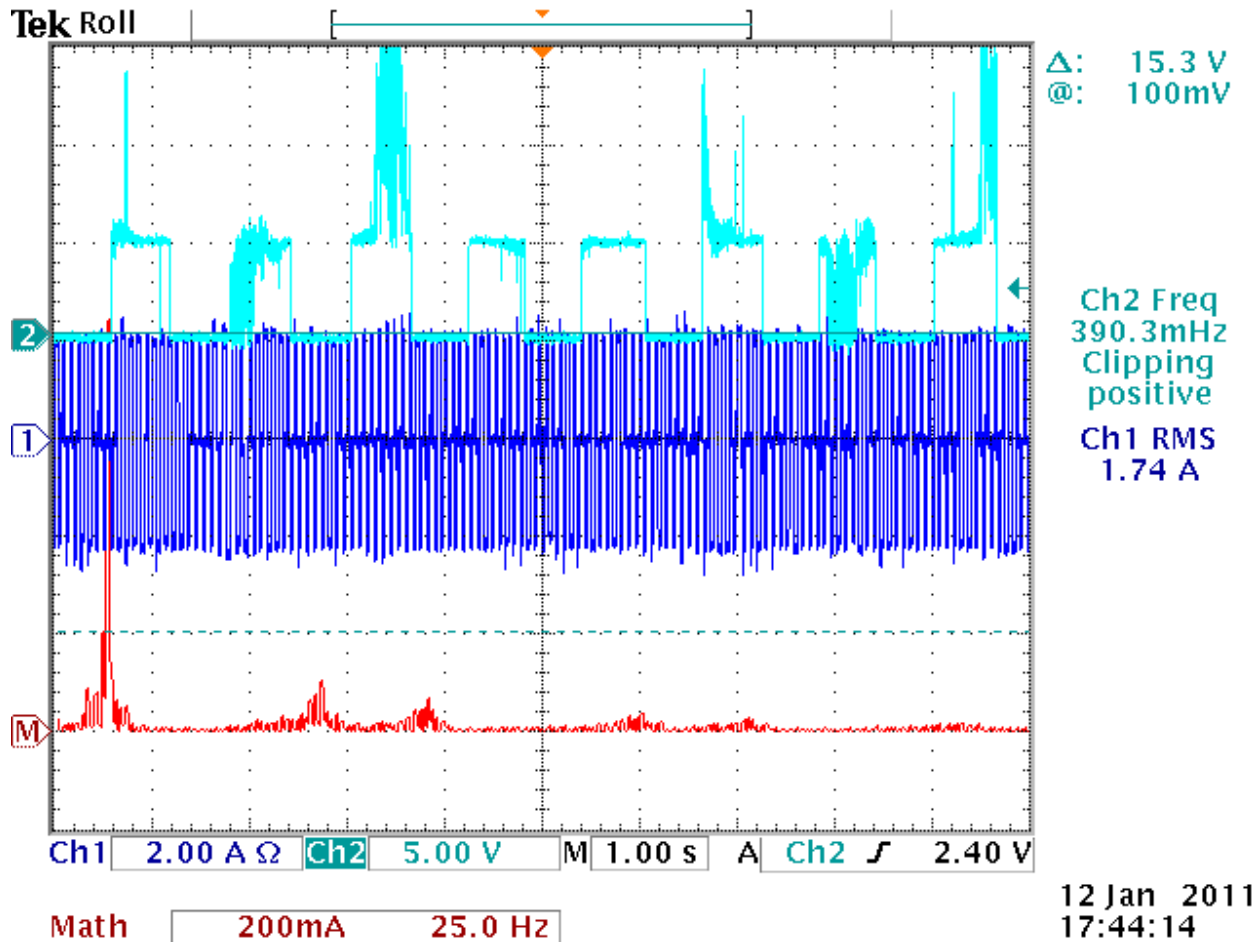


Figure 6.2: Current waveform, fft, and tachometer signal.

The machine was then taken back to the Naval Academy to test in the tow tank, where it was run with the contra-rotating propellers. We were hoping to see blade interactions once a torque waveform was pulled from the machine. Once back in the tow tank, we again had a problem with one of the hall sensors. This can be seen in the fourier transforms of the current waveforms. Figure 6.3 shows the measured current waveforms acquired with hall current sensors attached to the scope. Blue is U, red is V, and green is W.

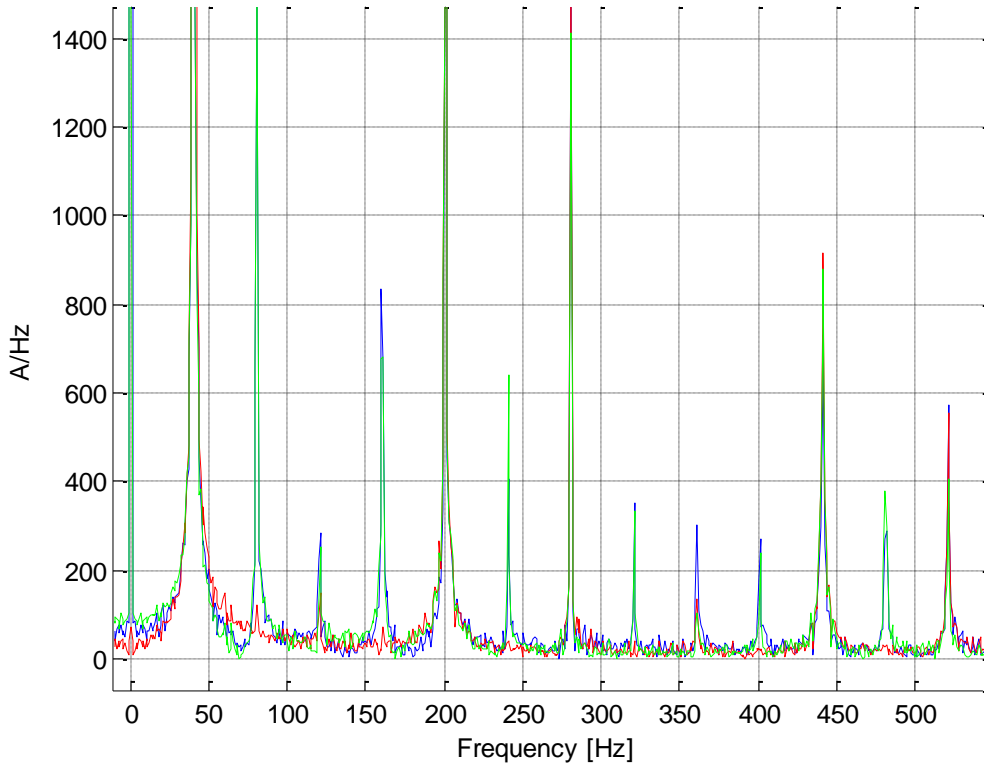


Figure 6.3: Fourier transforms of current waveforms.

Notice that V (red) is missing even harmonics that are present in U and W. This confirms that the W hall sensor was not operating properly during this particular test. This could be seen when setting up the machine phasing in the controller software. The V waveform also matches the scope traces from previous tests. 5th, 7th, 11th, and 13th harmonic are pronounced. In the previous tests, even harmonics are not present.

Sensor status may be checked in the software that runs the motor. When the shaft is rotated with the W sensor shorted, the controller becomes confused about rotor position. The following table shows the hall sensor states versus rotor position. It appears that the controller properly finds the middle state (360) when all sensors are shown as off. This causes it to think that the rotor is jumping immediately from 240 degrees to 360/0 and 360/0 to 120. This would cause 30th and a 60th harmonics (in relative shaft speed space) in both current and torque as there are 30 hall pulses (total, ten per sensor) per machine revolution and 60 state transitions (again, because it is a ten-pole machine).

	Rotor Position (degrees)					
Hall Phase	60	120	180	240	300	360
U	Red	Red	Red			
V			Red	Red	Red	
W	Red				Red	Red

Table 6.1: Hall sensor states and corresponding electrical angle.

To calculate torque, motor currents and inductances are transformed to the rotor frame. To perform this transformation, rotor position is necessary. Since it isn't recorded, a sine wave is fit to the current waveform in phase A.

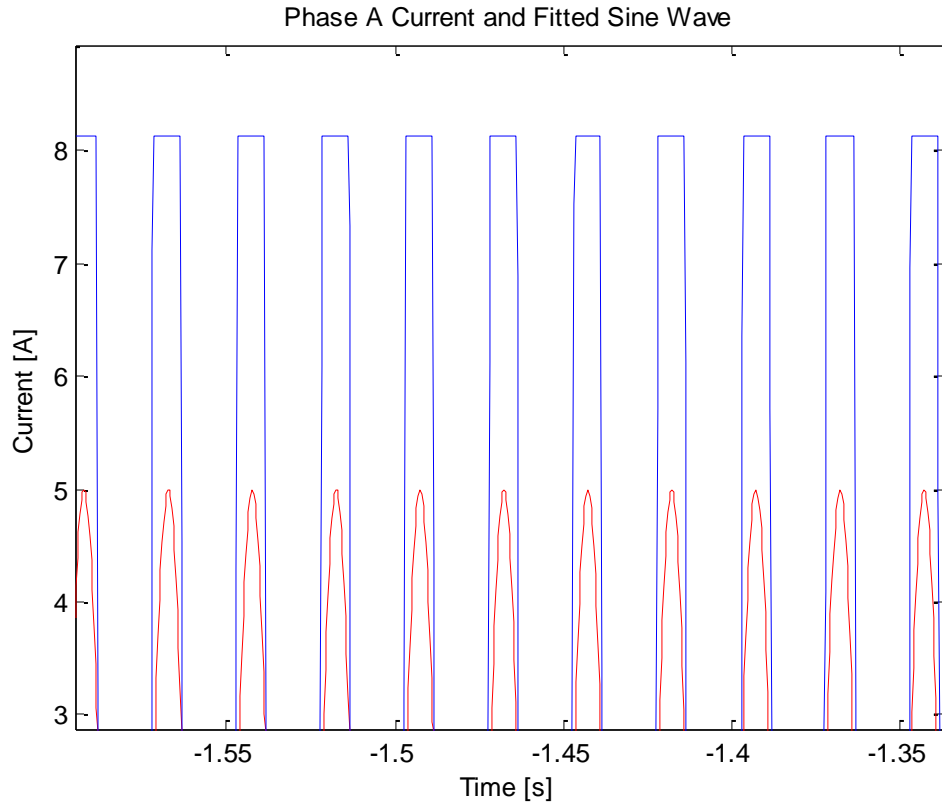


Figure 6.4: Phase U Current waveform (blue) and estimated rotor position (red).

Figure 6.4 shows the sine wave fit to the current data. The blue waveform is current, while the red one is the fitted sine wave. The fitted sine wave is used as a surrogate for shaft position for the Park's transform.

The currents and phase inductances are transformed to the rotor space as described in Chapter 3: Motor Math.

The motor torque waveform is shown in figure 6.5.

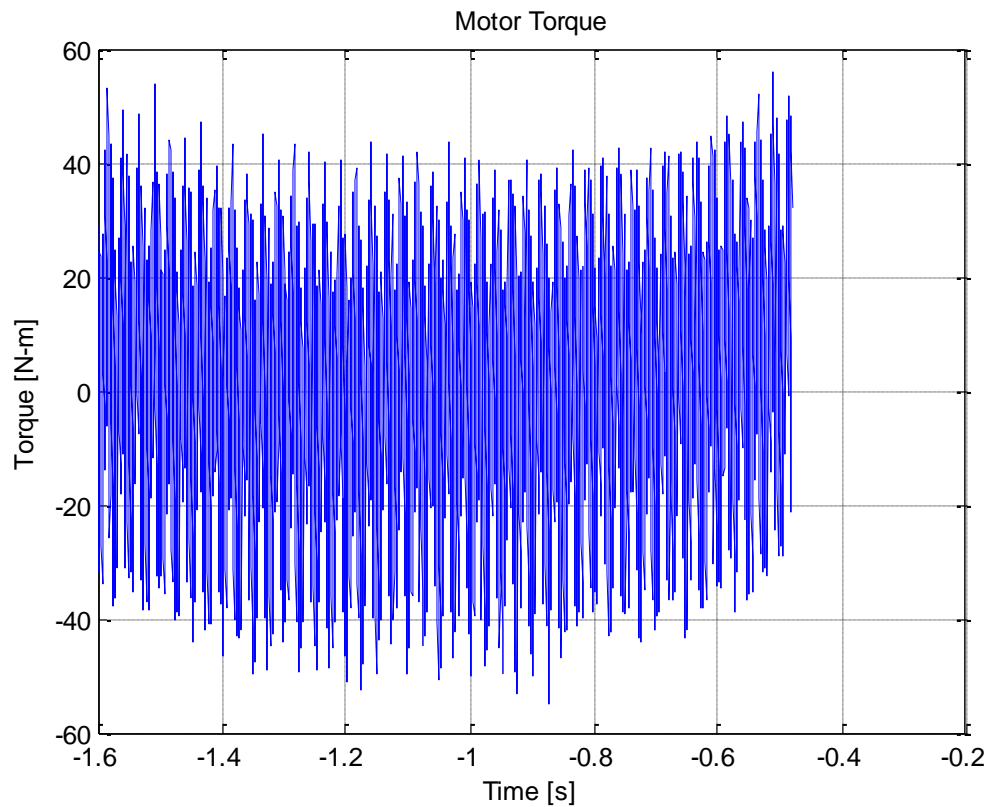


Figure 6.5: Calculated torque.

While the motor torque is very noisy, the frequency content should still show propeller performance. The average value of this waveform is 1.75 N·m, which is low, due to the failed sensor.

In a permanent magnet motor, torque is dependent on the angle of the current relative to shaft position. If current leads shaft position, positive torque is produced, and the machine runs as a motor. If shaft position leads, the machine runs as a generator. Figure 6.6 shows torque as a function of relative phasing.

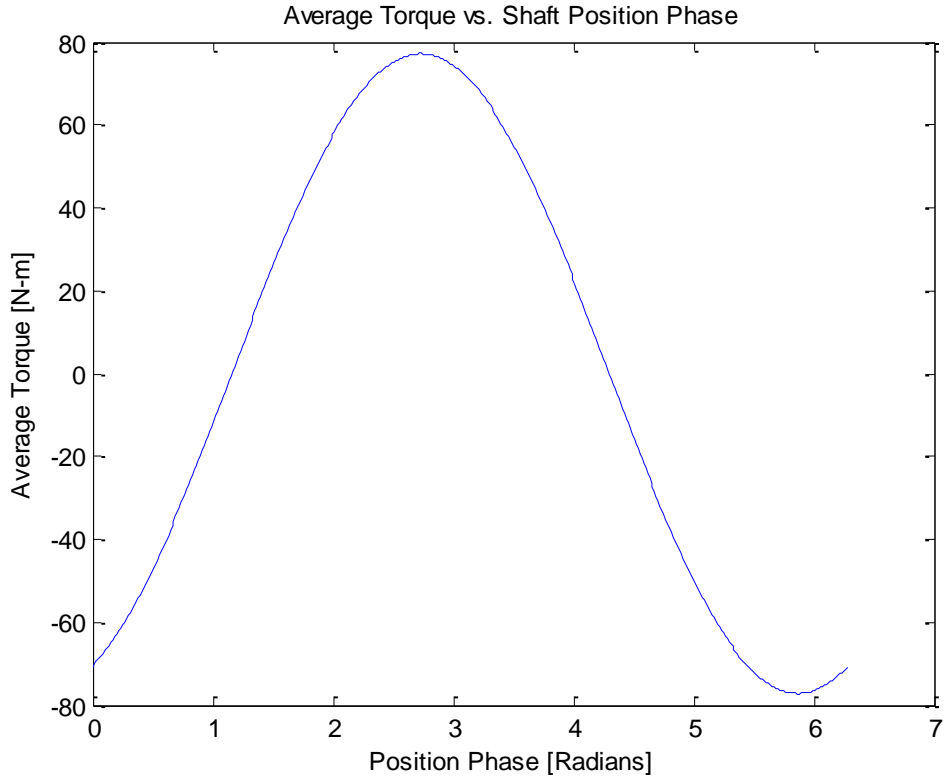


Figure 6.6: Machine Torque vs Shaft Position Phase.

Figure 6.7 shows outer shaft speed and relative speed, respectively. The first plot is a Fourier transform of the tachometer signal on the outer shaft. The peak is distorted, as it is zoomed in and there are not enough data points to create a smooth curve at this resolution. The second is a Fourier transform of the input current waveform. From this, the fundamental frequency shows relative shaft speed. Note that the second plot is electrical frequency, which is five times shaft frequency, as the motor is a ten pole machine.

When an FFT of the torque waveform is taken (figure 6.8), there are large spikes at 240 and 480 Hz. The rotation speed is right at 8 Hz, or 480 RPM, from the fft of the input current. The even harmonics predicted from the current waveforms are present. We expect to see propeller blade interactions at twelve times the relative speed, which would place a spike at 96 Hz. While there is noise in this frequency range, it does not stand out. It is likely hidden by the harmonics induced by the sensor failure.

Figure 6.9 shows this same information, but calculated at the phase angle corresponding to maximum torque. The harmonics described above are still present, suggesting that they are not artifacts of the math used to calculate torque.

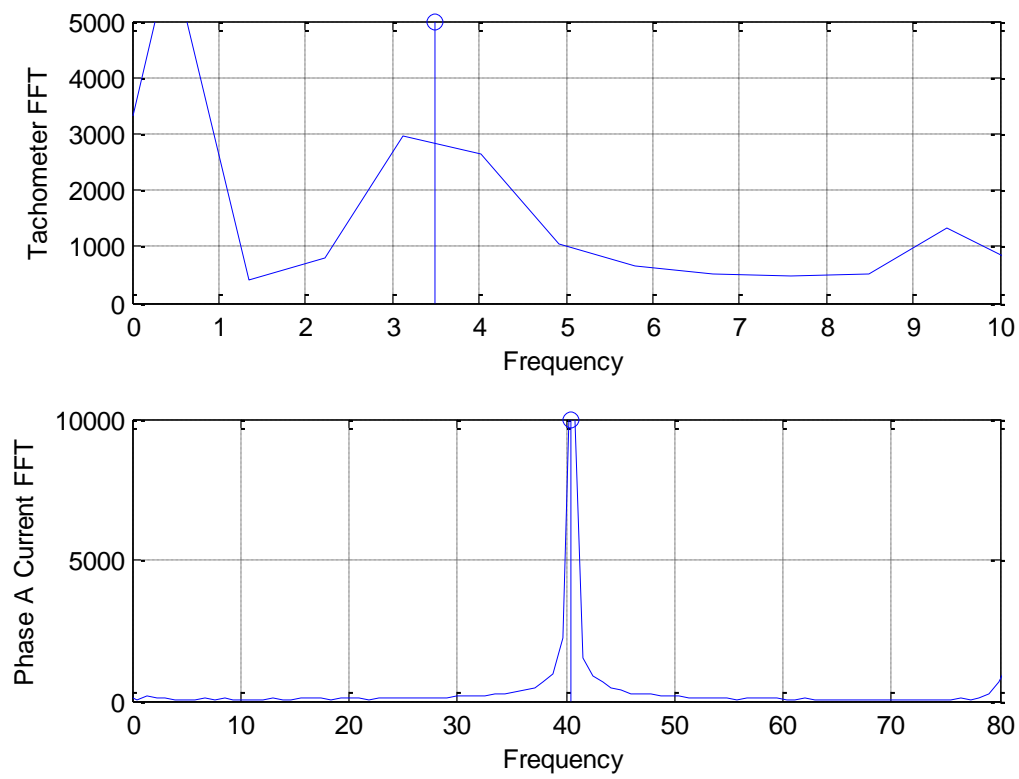


Figure 6.7: Frequency content of tachometer signal and current.

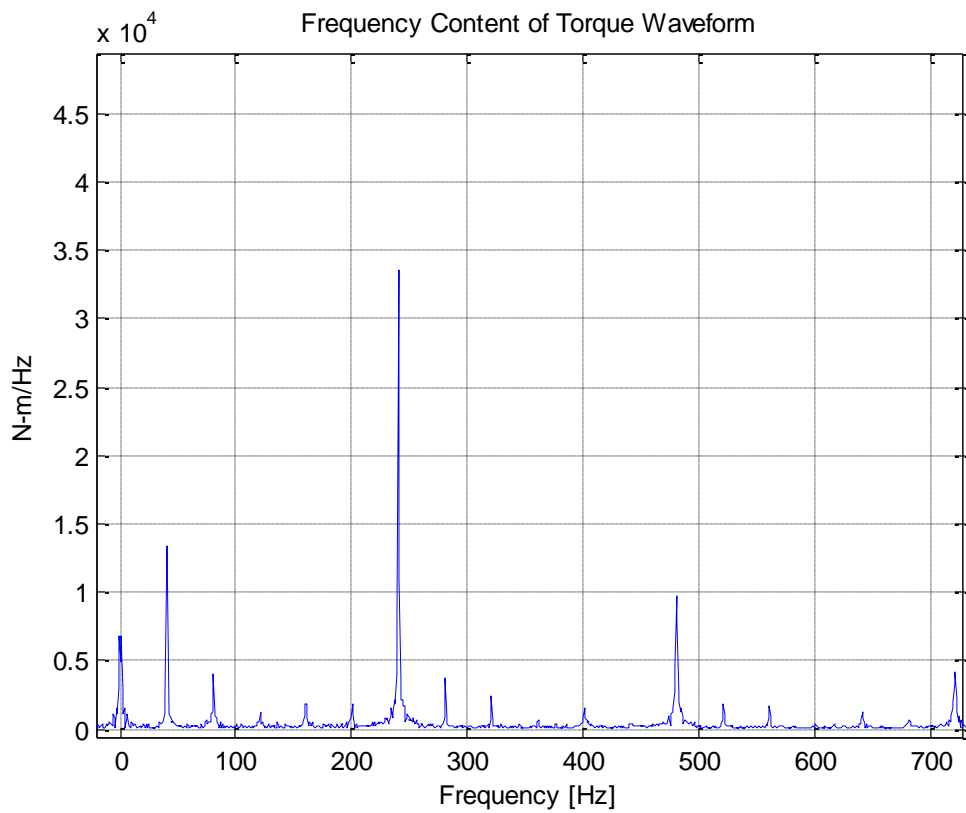


Figure 6.8: Frequency content of calculated torque.

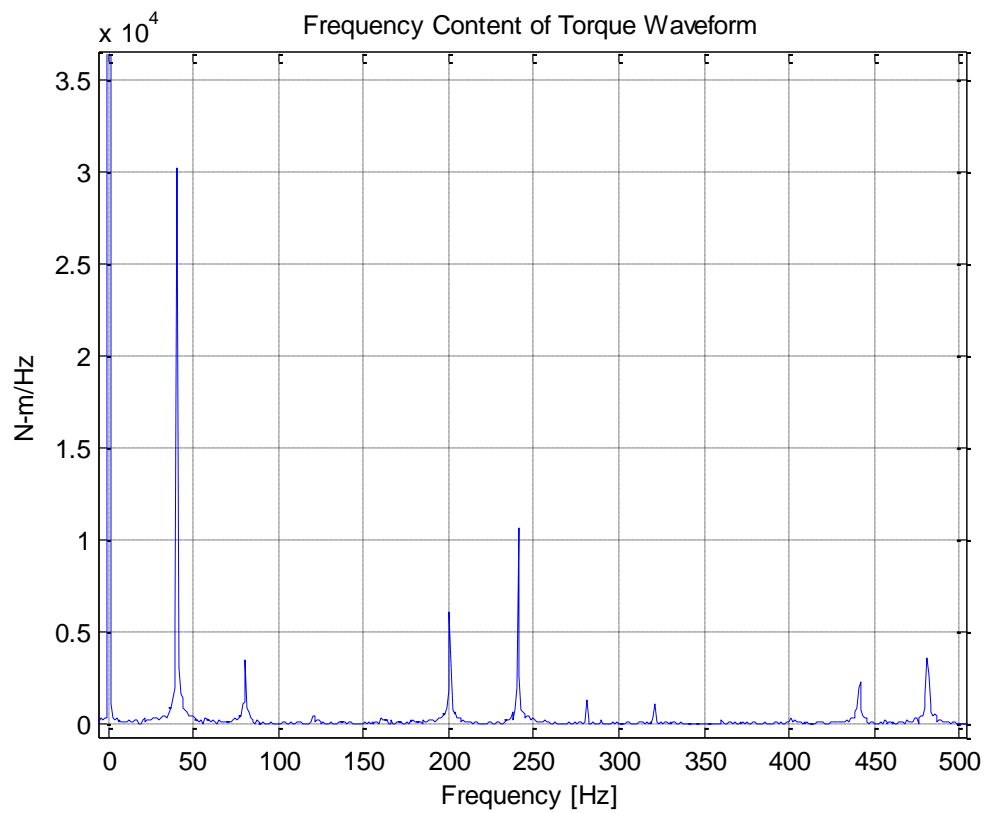


Figure 6.9: Torque Frequency Content at Phase Angle Corresponding to Maximum Torque.

Appendix A: Brush Data

MORGAN AM&T/NATIONAL ELECTRICAL CARBON PRODUCTS

251 Forrester Drive
Greenville, SC 29607-5328
(864) 458-7777

G R A D E D A T A S H E E T

Brush Grade . . . AY
Classification. ELECTROGRAPHITE
Resistivity . . . 0.000400 ohm inches
Strength . . . 3000 lbf/sq.inch
Bulk Density . . . 1.68 g/cubic cm.
Contact Drop . . M 1.3-1.8
Friction . . . M 0.2-0.29
Maximum Speed . . . 4000 ft/minute
Current Density . . 80.00 A/sq.inch
Metal 0 %

RECOMMENDED FOR STEEL OR BRONZE FIELD RINGS OF SYNCHRONOUS MOTORS AND WOUND ROTOR MOTOR RINGS UP TO 100 A/sqin & UP TO 4000 fpm. MINIMUM 4 psi SPRING PRESSURE RECOMMENDED. SUITABLE FOR SOME CONTACT APPLICATIONS.

Appendix B: MATLAB Code for Torque Calculations

```
close all
r1 = 1001;
r2 = 3800;
time = data(r1:r2,1);
Ia = data(r1:r2,2);
Ib = data(r1:r2,3);
Ic = data(r1:r2,4);
tach = data(r1:r2,5);
scopefft = data(:,6);

fs = 10000/4;

lambdaR = [1; 0; 0];
theta = 0;

Labc = [.0192; .019; .0193];

Iabc = [Ia'; Ib'; Ic'];

t = (1:size(Ia,1));
w = .1+2.30/3500;
phi = 3*pi/2-pi/6+pi/18-pi/36;
Idq = zeros(3,size(Ia,1));
Ldq = zeros(3,size(Ia,1));
lambdadq = zeros(3,size(Ia,1));

maxt = 0;
maxphi = 0;
phi = linspace(0,2*pi,400);
for k = 1:400
for i = 1:size(Ia,1)
    theta = w*t(i)+phi(k);
    T = 2/3.*[cos(theta) cos(theta-2*pi/3) cos(theta+2*pi/3);...
               -sin(theta) -sin(theta-2*pi/3) -sin(theta+2*pi/3);...
               1/2 1/2 1/2];
    Idq(:,i) = T*Iabc(:,i);
    Ldq(:,i) = T*Labc;
    lambdadq(:,i) = Ldq(:,i).*Idq(:,i)+lambdaR;
end
temp = mean(7.5*(lambdadq(1,:).*Idq(2,:)-lambdadq(2,:).*Idq(1,:)));
avgtorque(k) = temp;
if temp>maxt
    maxt = temp;
    maxphi = phi(k);
end
end
figure
plot(phi,avgtorque)
title('Average Torque vs. Shaft Position Phase')
xlabel('Position Phase [Radians]')
ylabel('Average Torque [N-m]')

phim = maxphi;
```

```

for i = 1:size(Ia,1)
    thetam = w*t(i)+phim;
    T = 2/3.*[cos(thetam) cos(thetam-2*pi/3) cos(thetam+2*pi/3);...
               -sin(thetam) -sin(thetam-2*pi/3) -sin(thetam+2*pi/3);...
               1/2 1/2 1/2];
    Idq(:,i) = T*Iabc(:,i);
    Ldq(:,i) = T*Labc;
    lambdadq(:,i) = Ldq(:,i).*Idq(:,i)+lambdaR;
end

figure
plot(time,5.*cos(w*t+phim),'r')
hold on
plot(time,Ia,'b')
plot(time, Ib,'g')
plot(time, Ic,'k')
hold off
title('Phase A Current and Fitted Sine Wave')
xlabel('Time [s]')
ylabel('Current [A]')

figure
hold on
plot(linspace(-fs/2,fs/2,size(Ia,1)),fftshift(abs(fft(Ia))), 'b')
plot(linspace(-fs/2,fs/2,size(Ia,1)),fftshift(abs(fft(Ib))), 'r')
plot(linspace(-fs/2,fs/2,size(Ia,1)),fftshift(abs(fft(Ic))), 'g')
xlabel('Frequency [Hz]')
ylabel('A/Hz')

figure
thoughta = Ia.*cos(w*t'+3*pi/2-pi/6+pi/18-pi/36);
thoughtb = Ib.*cos(w*t'+3*pi/2-pi/6+pi/18-pi/36+2*pi/3);
thoughtc = Ic.*cos(w*t'+3*pi/2-pi/6+pi/18-pi/36-2*pi/3);

plot(linspace(-fs/2,fs/2,size(Ia,1)),fftshift(abs(fft(thoughta))))
title('Frequency Content of Matched Sine Wave Mixed with Current Waveform')
xlabel('Frequency [Hz]')

for jk = 1:size(thoughta,1)
    intsuma(jk) = sum(thoughta(1:jk));
end
figure
plot(time,intsuma)
plot(linspace(-fs/2,fs/2,size(Ia,1)),fftshift(abs(fft(intsuma))))
Torque = 7.5*(lambdadq(1,:).*Idq(2,:)-lambdadq(2,:).*Idq(1,:));

figure
plot(time,Torque)
transform = abs(fft(Torque));
grid on
title('Motor Torque')
xlabel('Time [s]')
ylabel('Torque [N-m]')

```

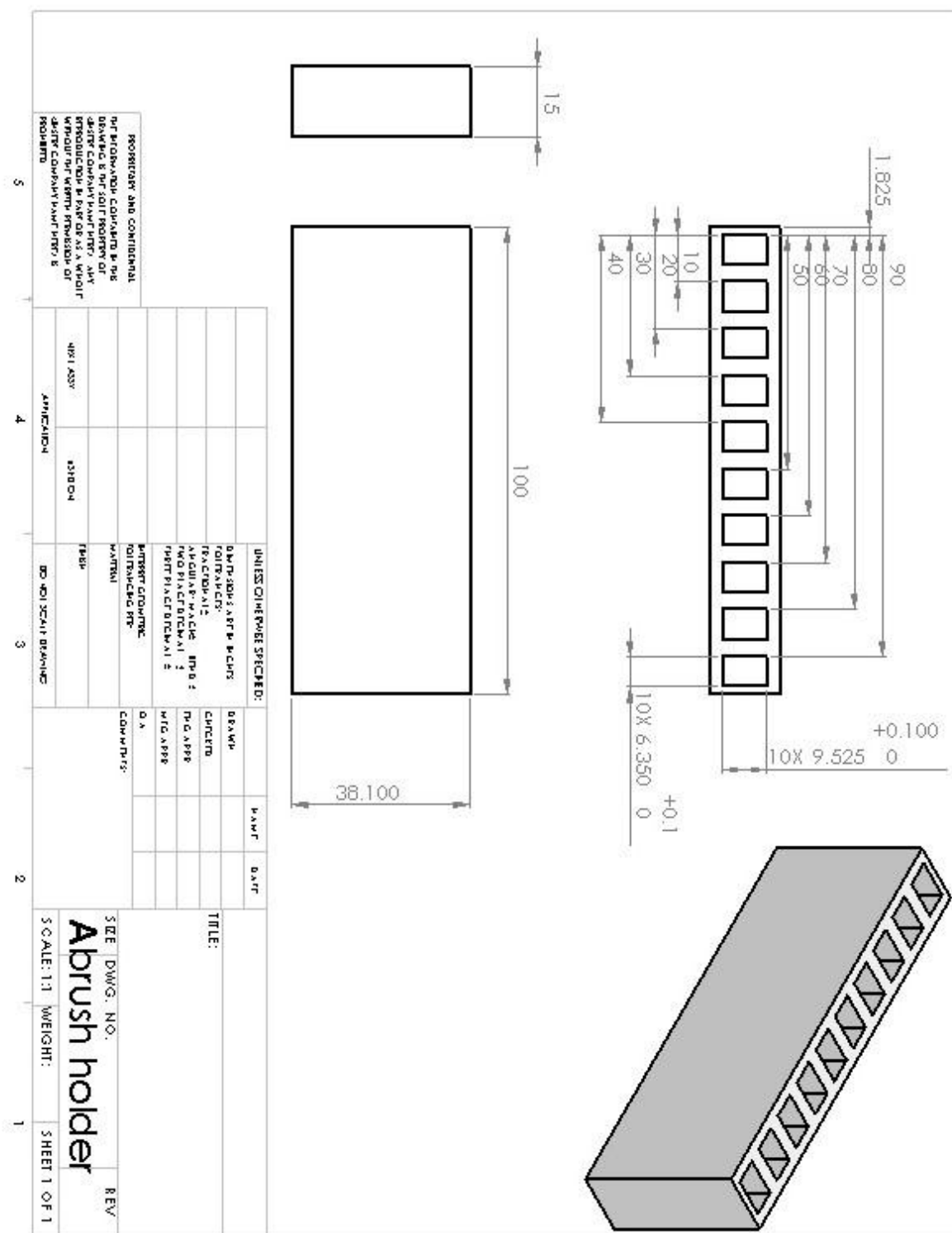
```

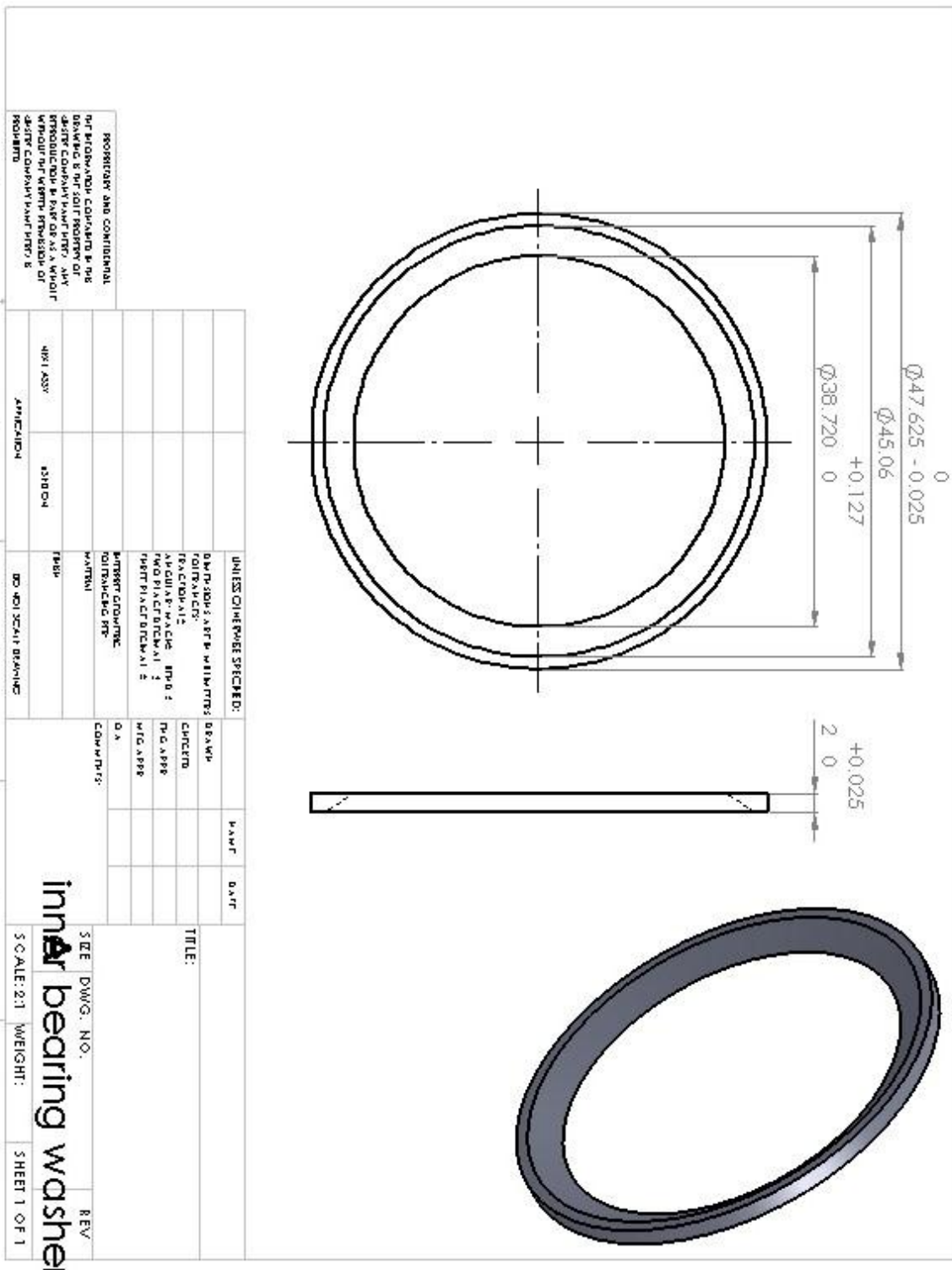
figure
subplot(2,1,1), plot(linspace(-
fs/2,fs/2,size(transform,2)),fftshift(abs(fft(tach))))
xlabel('Frequency')
ylabel('Tachometer FFT')
axis([0 10 0 5000])
grid on
hold on
stem(3.5,5000)
hold off
subplot(2,1,2), plot(linspace(-
fs/2,fs/2,size(transform,2)),fftshift(abs(fft(Ia))))
xlabel('Frequency')
ylabel('Phase A Current FFT')
axis([0 80 0 10000])
grid on
hold on
stem(40.43,10000)
hold off

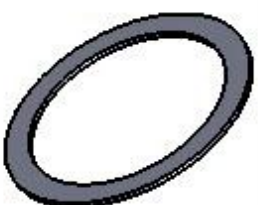
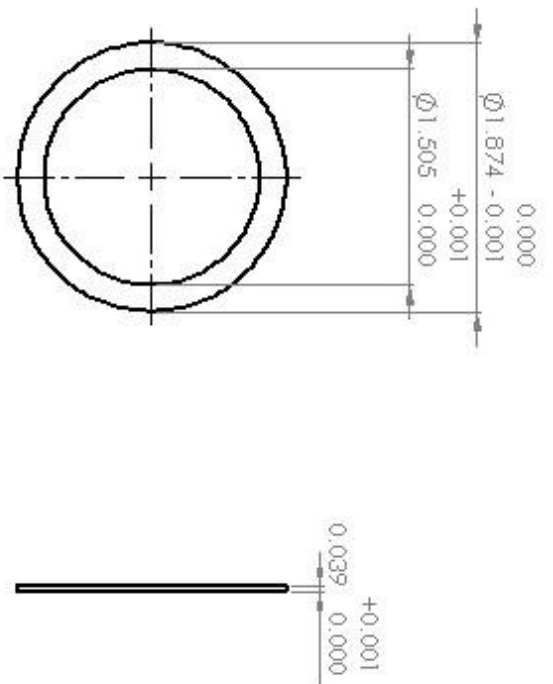
figure
plot(linspace(-fs/2,fs/2,size(transform,2)),fftshift(transform))
title('Frequency Content of Torque Waveform')
xlabel('Frequency [Hz]')
ylabel('N-m/Hz')
axis([0 750 0 5e4])
grid on

```

Appendix C: Machine Drawings

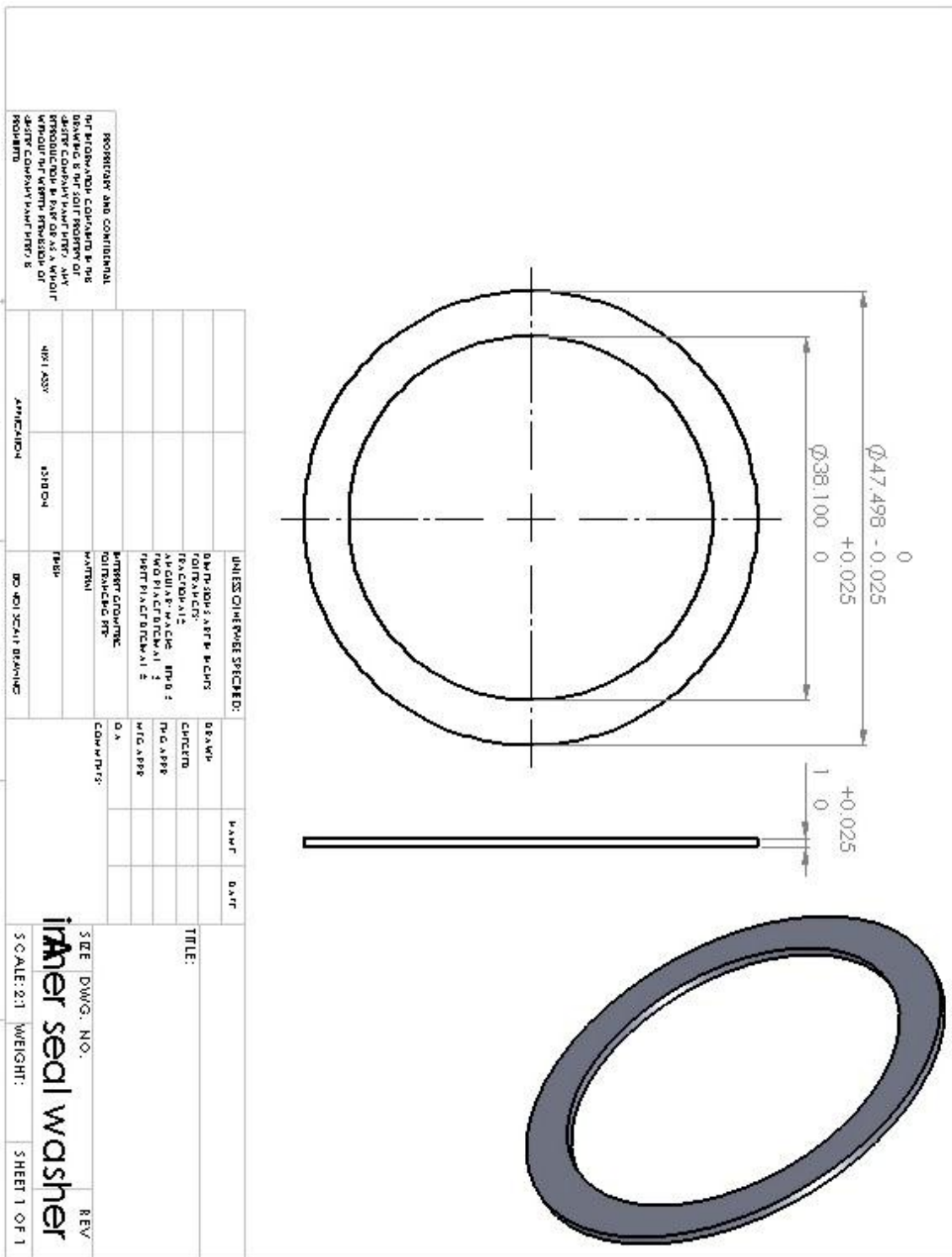


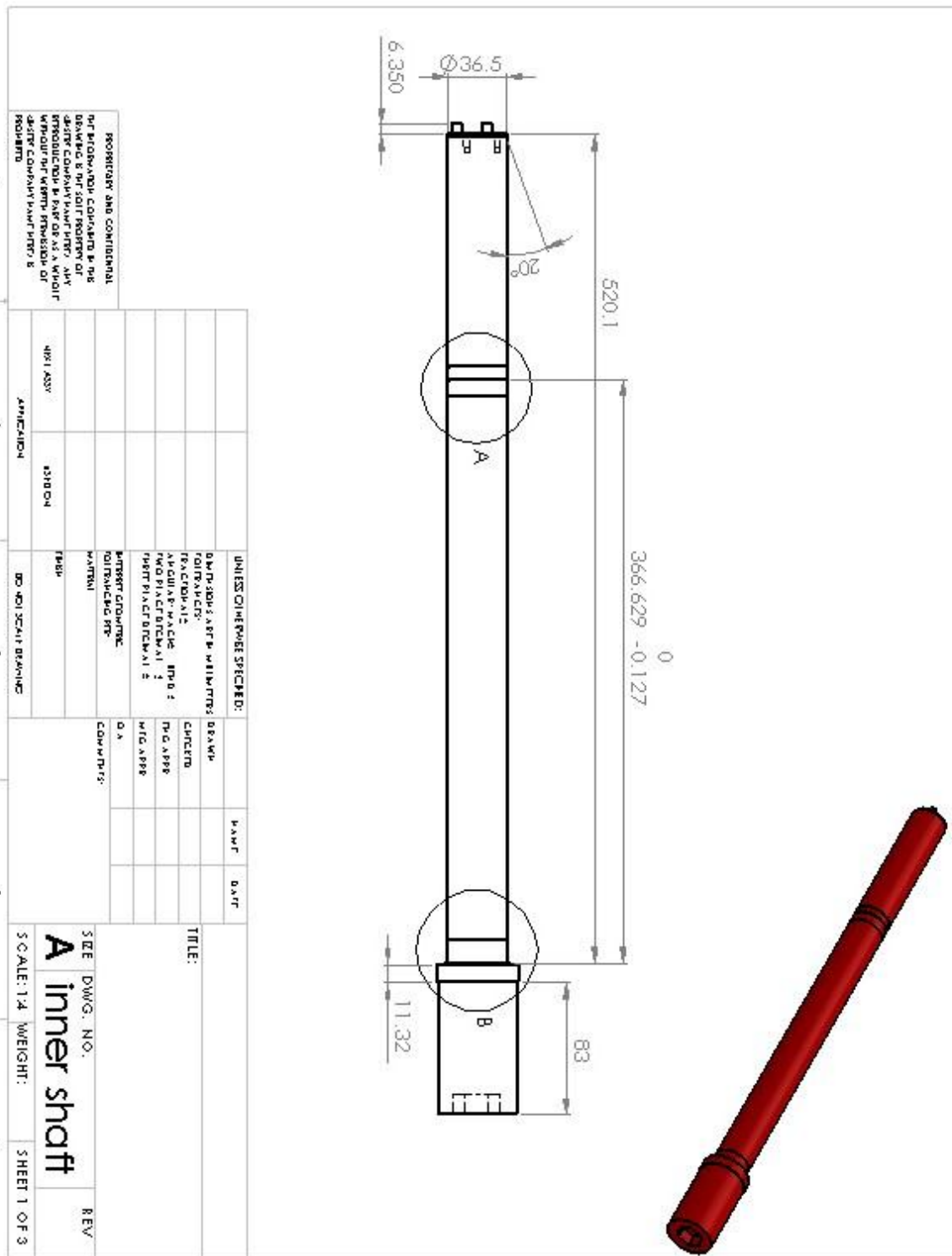


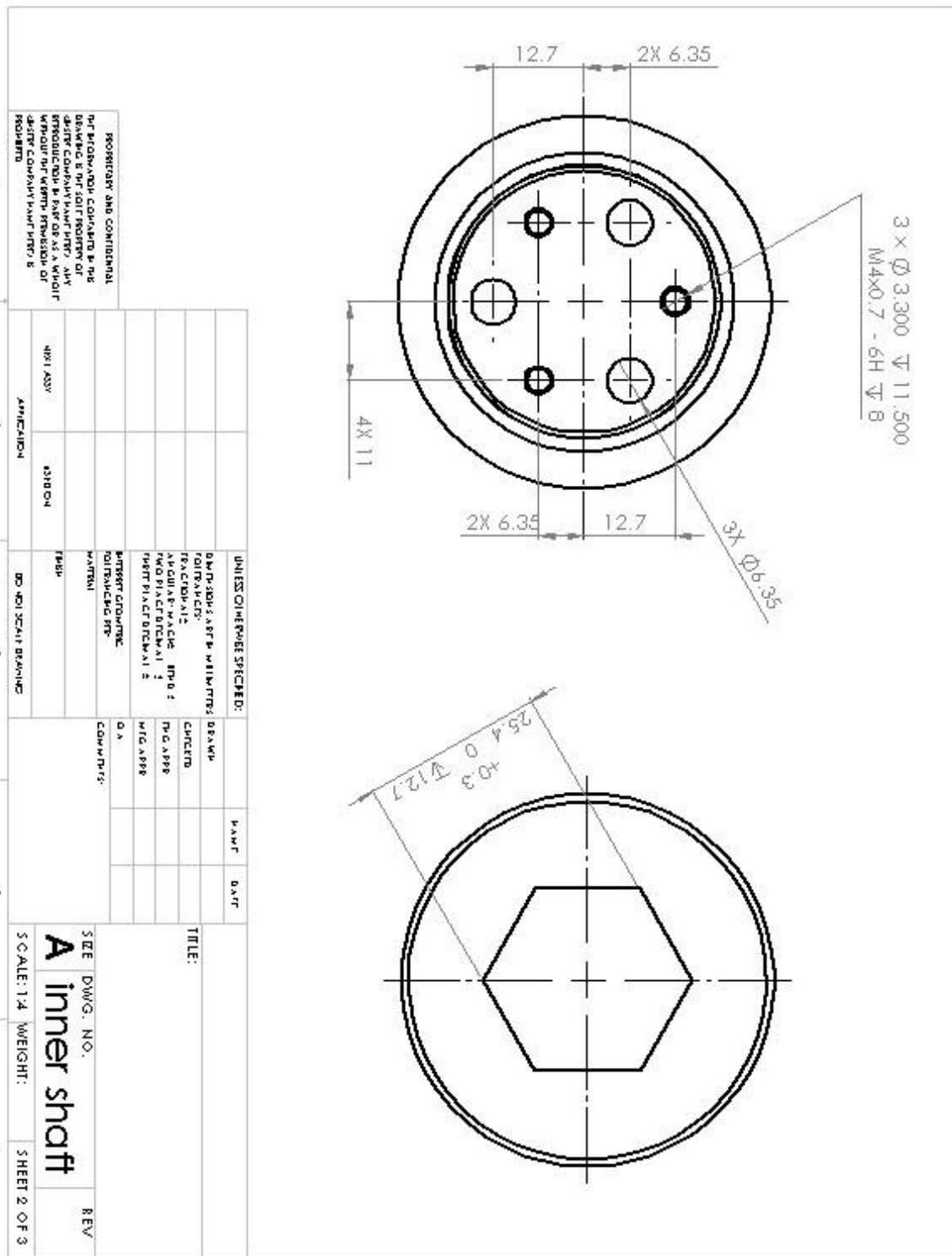


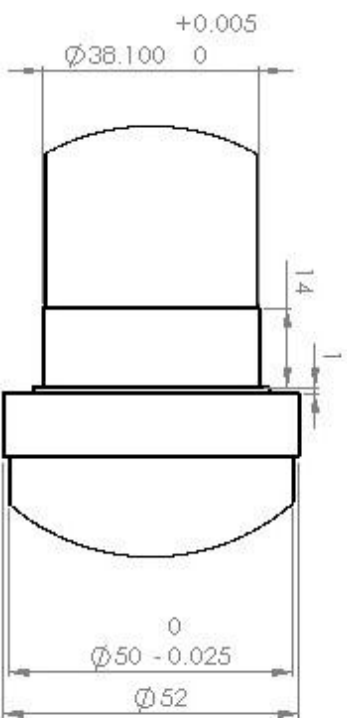
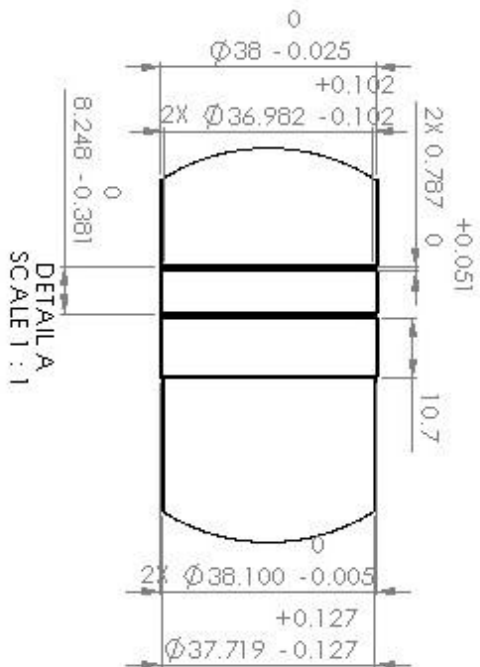
inner rear seal washer

PROPRIETARY AND CONFIDENTIAL			
NOT FOR GENERAL DISSEMINATION OR REPRODUCTION & NOT FOR PUBLIC PROPERTY NOT FOR COMMERCIAL PURPOSES, AND REPRODUCED FROM OR FOR USE AS A WHOLE WITHOUT WRITTEN PERMISSION OF THE COMPANY OWNERSHIP IS RESERVED.			
4821 ASSY	ISDN04	INSP	DO NOT SCALE DRAWING
ATTACHMENT			
UNLESS OTHERWISE SPECIFIED:		NAME	DATE
DIMENSIONS ARE IN INCHES	DESIGN		
EXPLANATORY	CHARTS		
TELEGRAMS	CHARTS		
ADDITIONAL MACHINES	PROJ. I		
NO. OF PLATES	PROJ. I		
PLATE PLATE MATERIAL	PROJ. I		
PICTURE DRAWINGS	PROJ. I		
PURCHASE DRAWINGS	PROJ. I		
ROTATING PARTS	PROJ. I		
MATERIAL	COMMENTS		
SIZE DWG. NO.		REV.	
SCALE: 1:1 WEIGHT:		SHEET 1 OF 1	
inner rear seal washer			





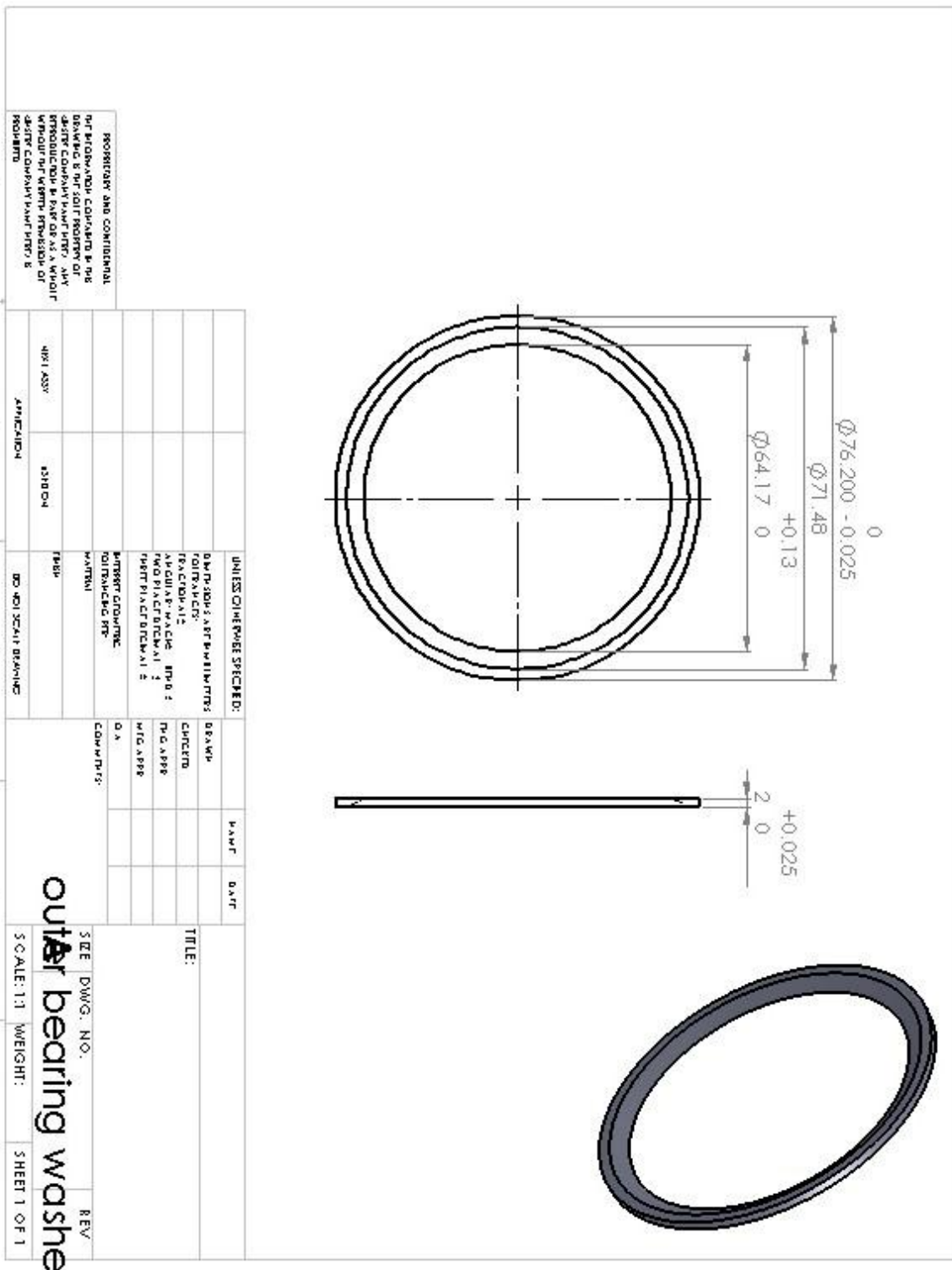


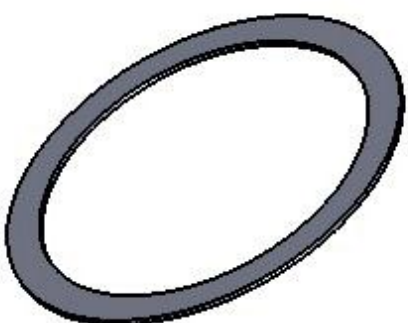
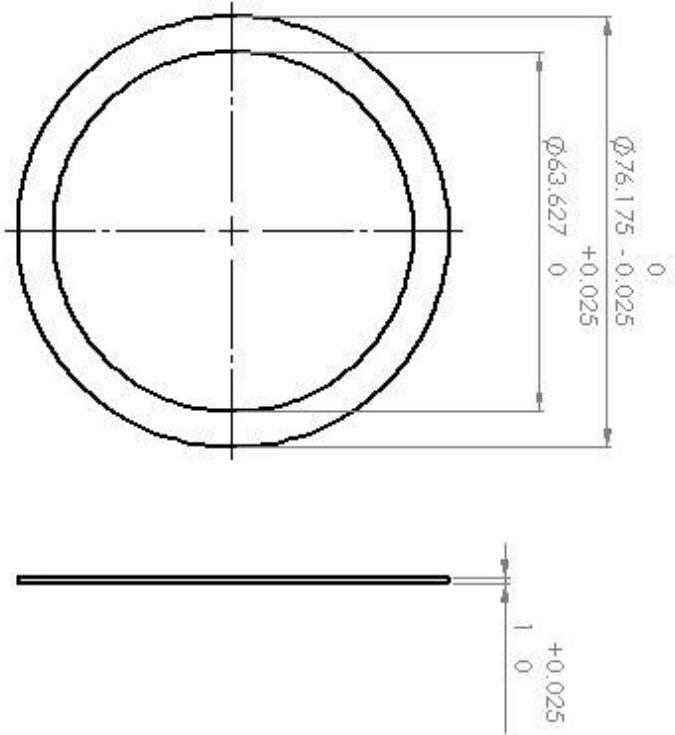


DETAIL B
SCALE 1 : 1

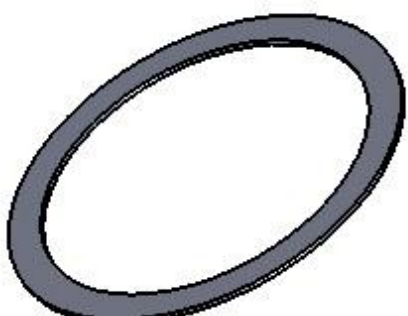
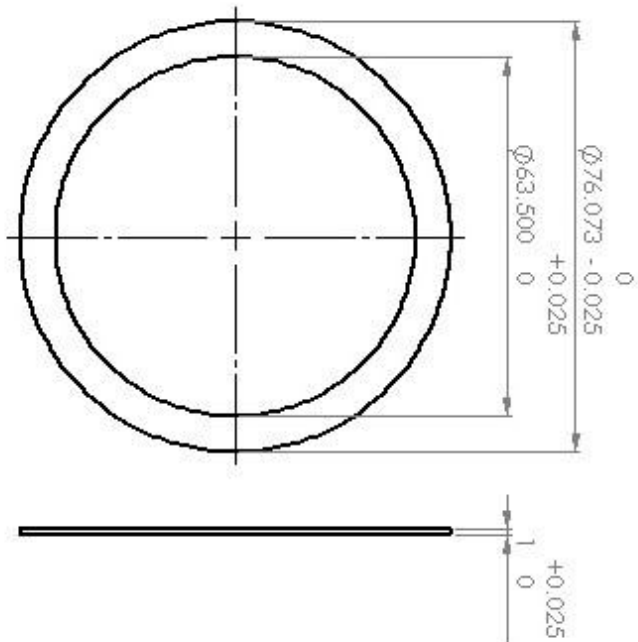
PROSPECTIVE AND CONCURRENT

6





outer rear seal washer

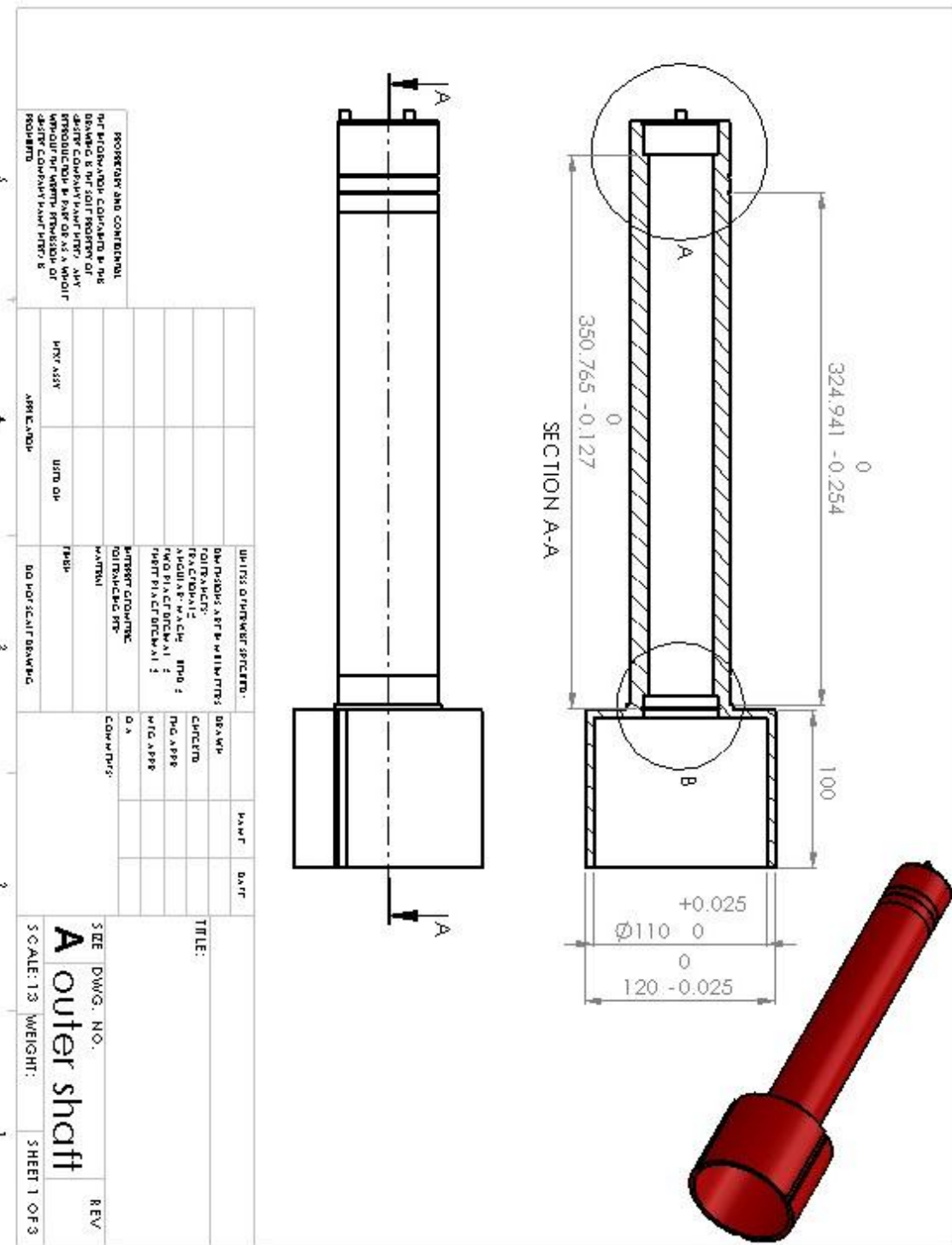


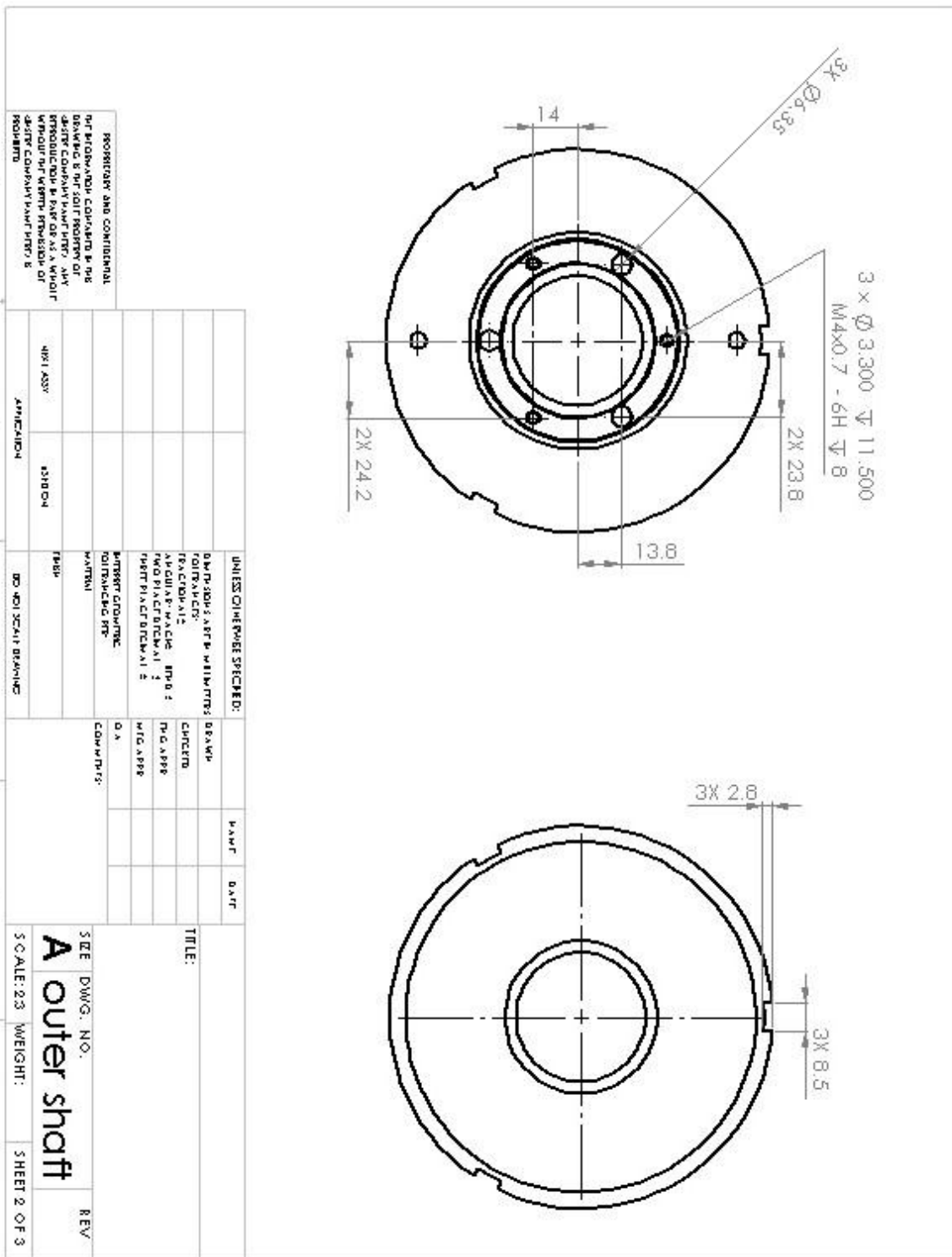
PROPRIETARY AND CONFIDENTIAL

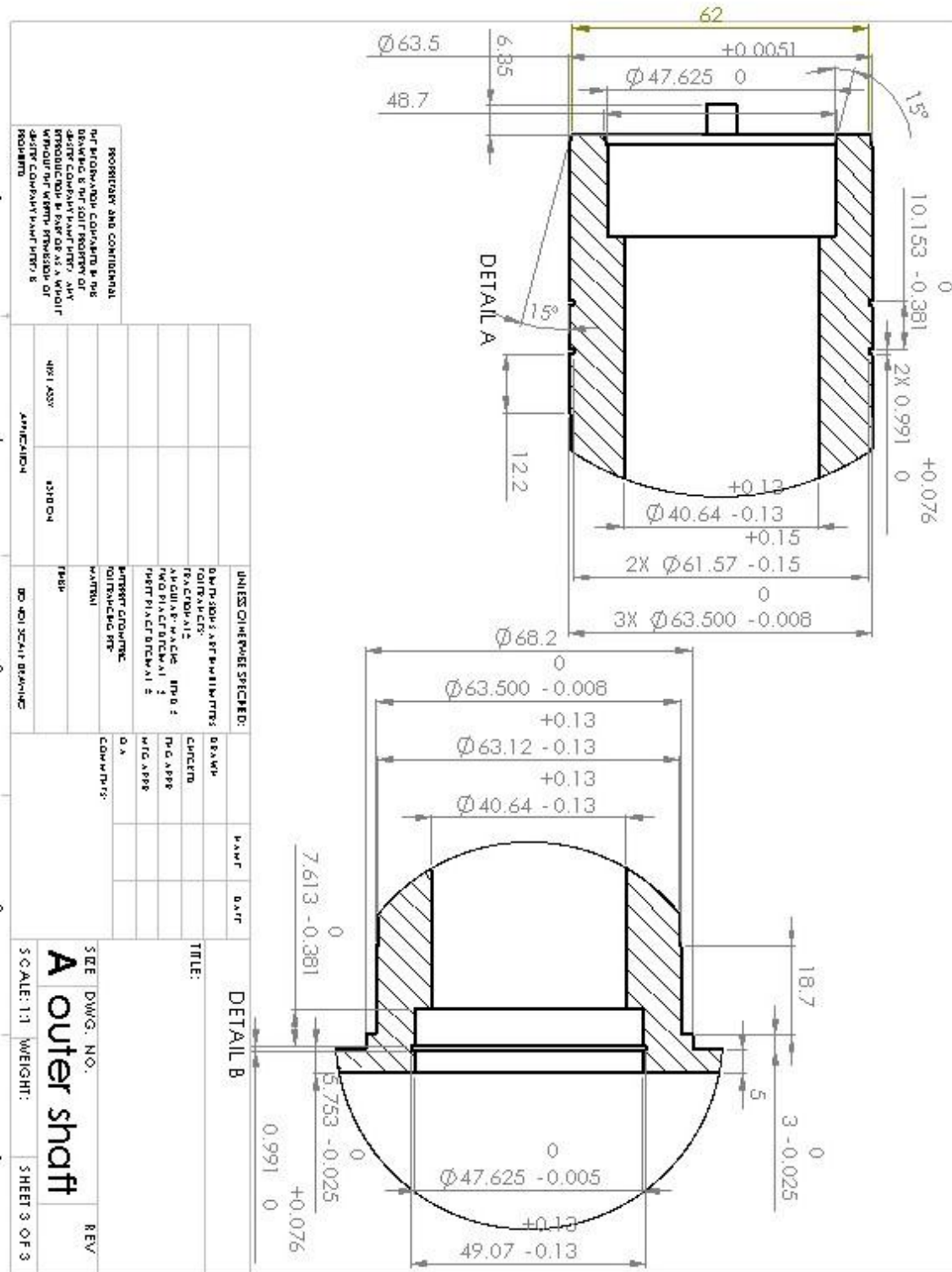
NOTIFICATION TO CONTRACTOR: DRAWING & MFG. PROPERTY OF
SANTA CLARA VALLEY WATER DISTRICT, CALIFORNIA.
PRODUCTION IS FOR USE AS A WHOLE
WITHOUT WRITTEN PERMISSION OF
SANTA CLARA VALLEY WATER DISTRICT.

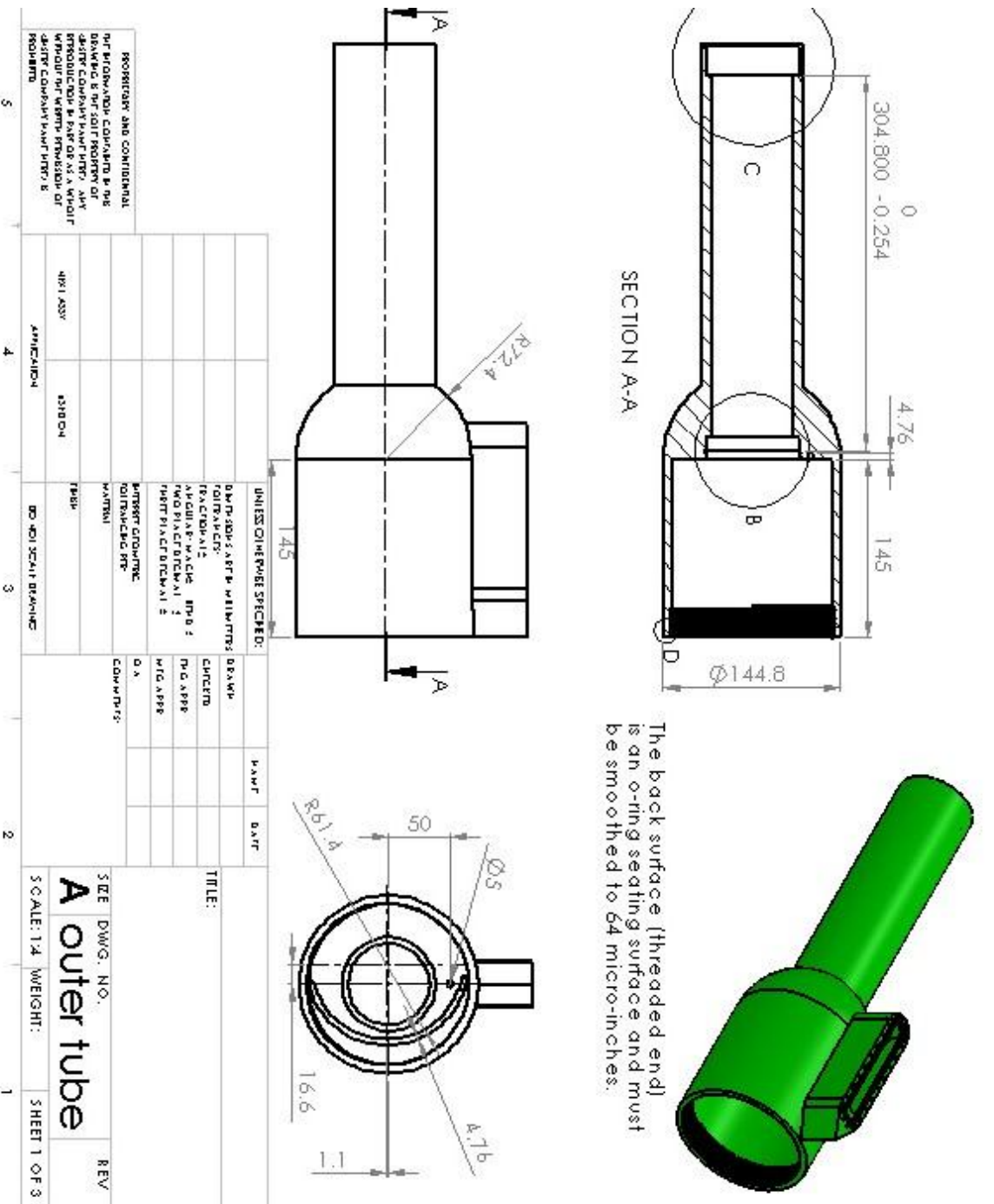
UNLESS OTHERWISE SPECIFIED:		INCHES	MM	INCHES	MM
DIMENSIONS ARE IN MILLIMETERS		DRAWN	PRINTED	DIA. IN	MATERIAL
ROTATED:					
EXCEPTIONS:					
AS DRAWN		INCHES	MM	INCHES	MM
NO PLATE THICKNESS		1/8	3.2	1/8	3.2
REPT PLATE THICKNESS		1/2	12.7	1/2	12.7
PART NUMBER:					
PART NUMBER:					
MATERIAL:					
COMMENTS:					
SIZE	DWG. NO.	REV.			
SC. 1:1	WEIGHT:				
SHEET 1 OF 1					

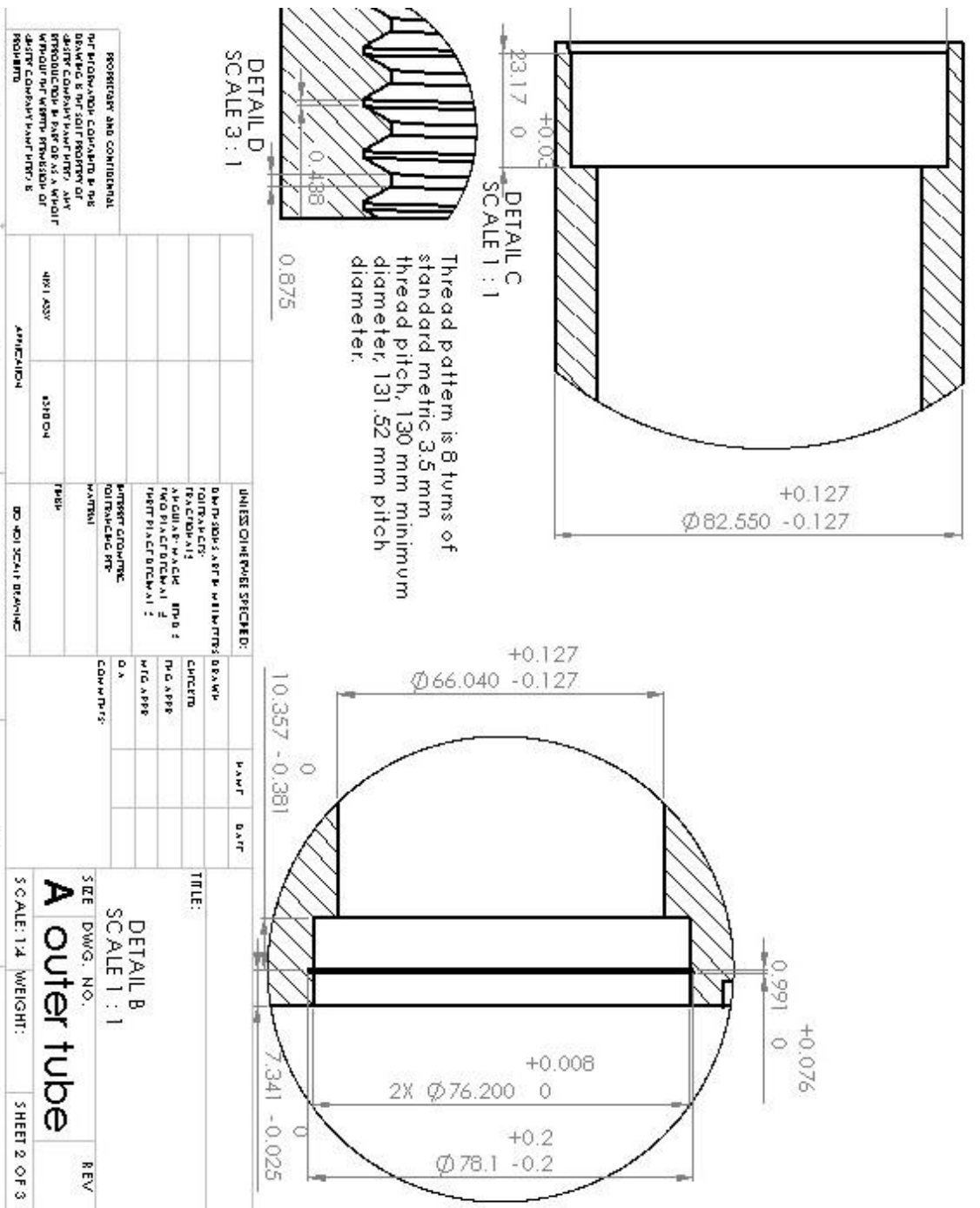
Oter seal washer

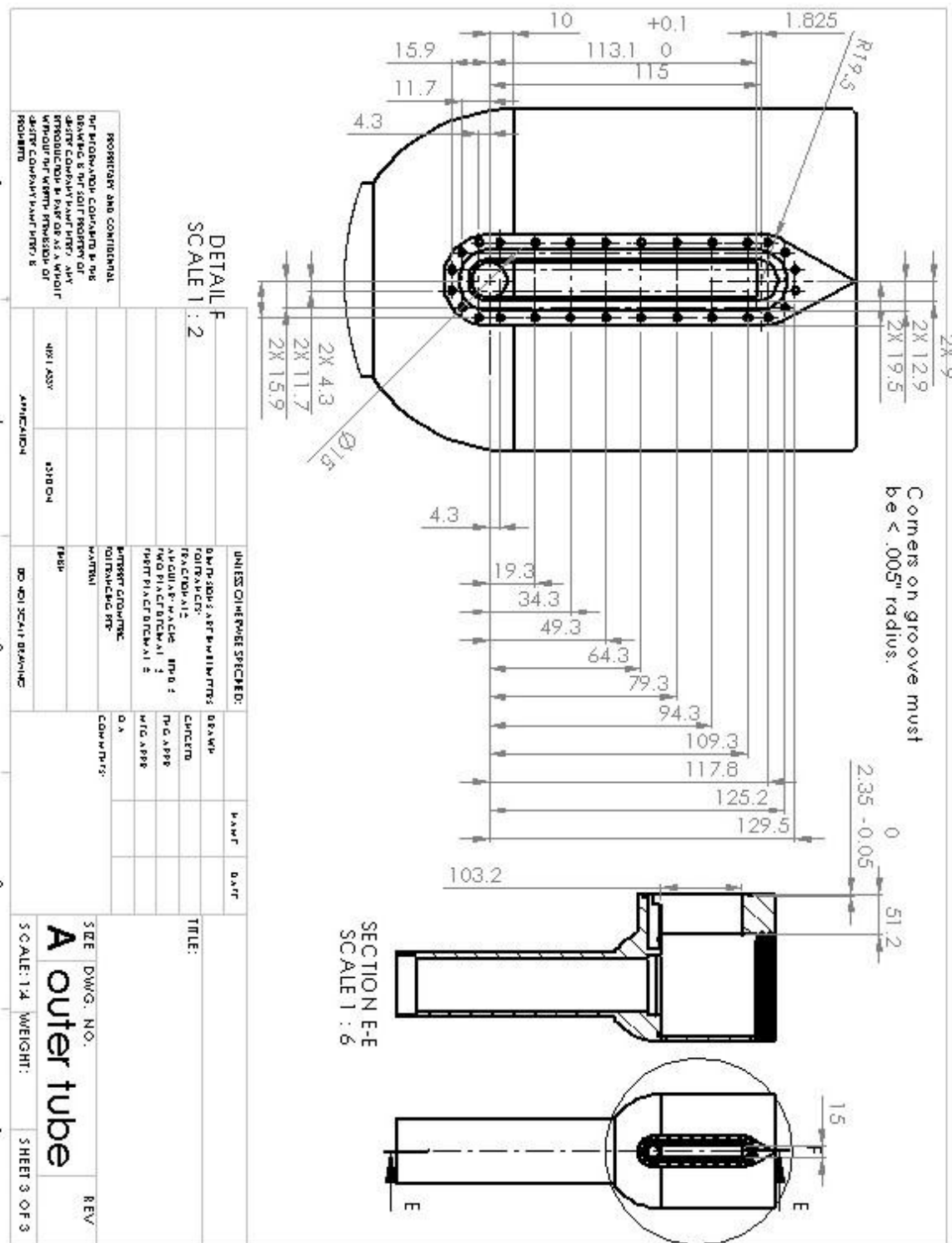


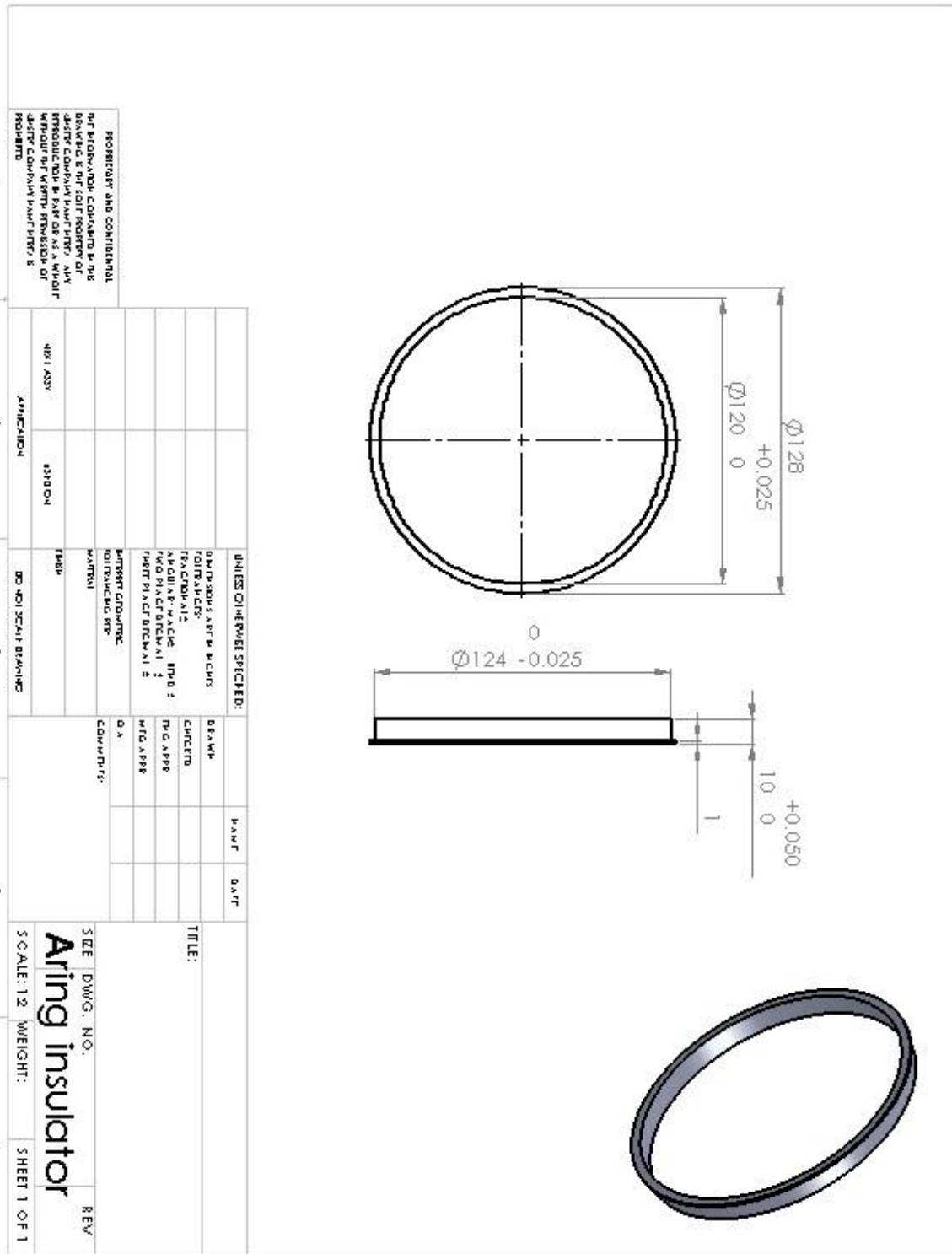


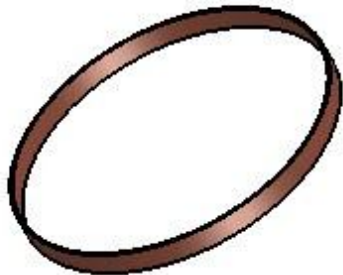
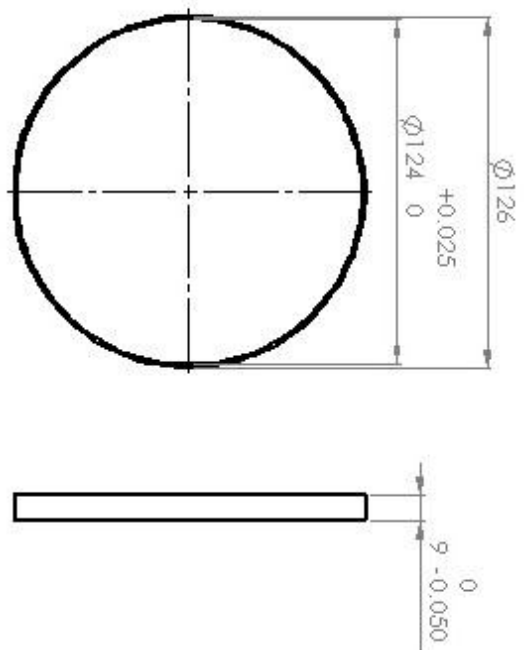






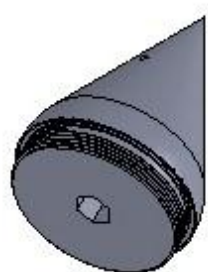
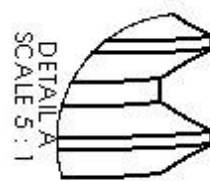
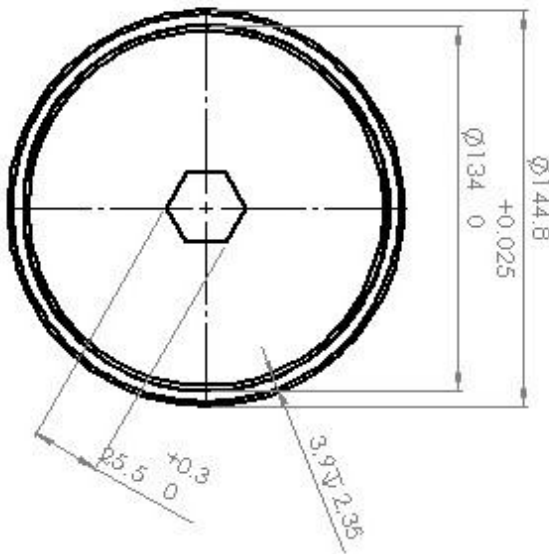




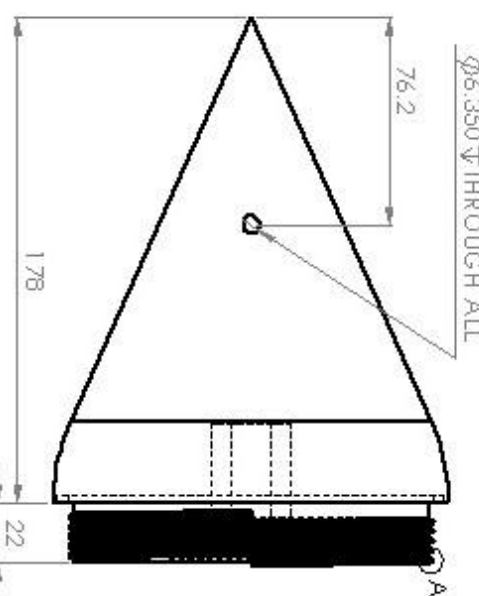


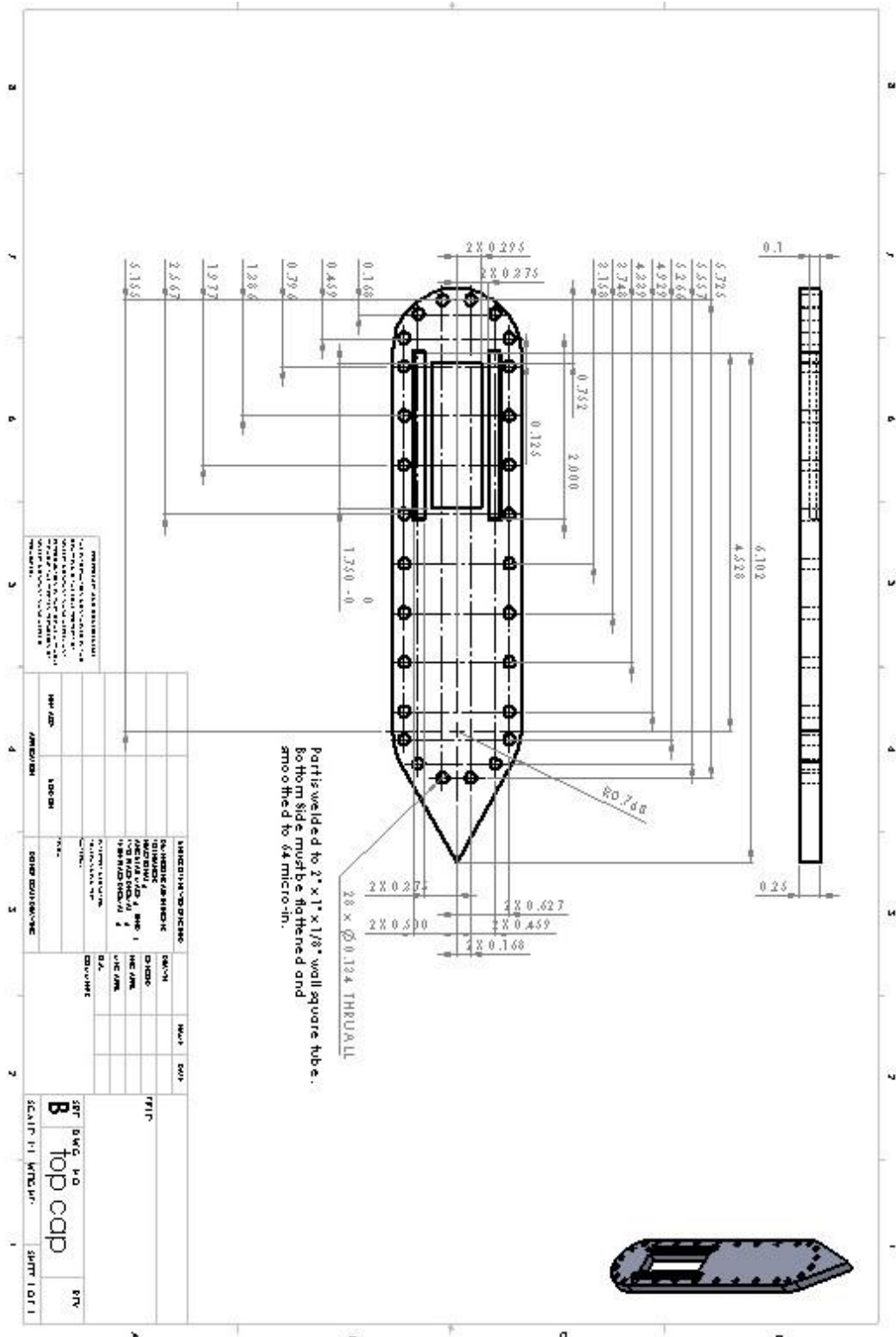
Bottom corners on groove must be rounded to <.005" radius.

Thread pattern is 5 turns of standard metric 3.5 mm thread pitch, 130 mm minimum diameter, 131.52 mm pitch diameter.



UNITS OF MEASURE SPECIFIED:		INCHES	MILLIMETERS	DEGREES
DIMENSIONS ARE IN INCHES				
CONTRACTS FACTURE = AND EXP. = NO. OF CONTRACTS = PART NUMBER =		CONTRACTS FACTURE = AND EXP. = NO. OF CONTRACTS = PART NUMBER =	CONTRACTS FACTURE = AND EXP. = NO. OF CONTRACTS = PART NUMBER =	CONTRACTS FACTURE = AND EXP. = NO. OF CONTRACTS = PART NUMBER =
PREFERRED DRAWING FORMAT		DIA.		
		CONTRACTS FACTURE = AND EXP. = NO. OF CONTRACTS = PART NUMBER =	CONTRACTS FACTURE = AND EXP. = NO. OF CONTRACTS = PART NUMBER =	CONTRACTS FACTURE = AND EXP. = NO. OF CONTRACTS = PART NUMBER =
INCH ASSY	INCH OR			
SPECIFICATIONS				
DO NOT SCALE DRAWING				
		SIZE	DWG. NO.	REV.
		A	tail cone	
SCALE 1:12 WEIGHT:		SHEET 1 OF 1		





Appendix D: Running the Machine.

Go to the following web address.

<http://web.mit.edu/mangle/www/CRP/>

Download drivers for the USB to Serial converter. Then download Copley CME2 and install it. This is all you need to talk to the controller with your computer.

Next, make sure everything in the box is turned off. Connect the computer via the usb cable. At this point, you may plug in the box if it's not already plugged in, turn the red knob in the upper right corner 90 degrees clockwise, and flip the single breaker to the left of the red knob up to on. Do not yet flip the double breaker between the red knob and the single breaker on. If you do, the motor will instantly spin up to $\sim 2\text{krpm}$, possibly injuring someone or breaking something. At this point, the green light on the 24V power supply to the left of the breaker will turn on, and the light on the amplifier (bottom left of the box) will glow red.

Establish communication with the controller by opening CME2. There's a connection wizard that will immediately come up. Just click through these things til it talks. At this point, it will download data from the amplifier. I'll do something separate that tells you how to save and reload profiles for motors, but we shouldn't need to with this series of testing.

You should now immediately press F12 to software disable the amplifier. **Make sure you see "Amp Software Disabled" in the box at the bottom of the main CME2 screen (second from the right) before proceeding.**

Now, flip the double breaker up to on. You should hear the fans in the box spin up, and the power light on the amplifier will flash green. You're now ready to run.

To run the machine, go to the commanded velocity block on the main screen of CME2. Click on it, and it will bring up a dialog box with a commanded RPM. Enter whatever speed your heart desires.

Next, click on the second icon from the left on the top toolbar. This brings up control panel. You might switch one of the boxes on the upper right to display commanded RPM. The top two should default to current and actual speed.

To make the motor run, click enable at the bottom left. To stop it, click disable or hit F12.

Appendix E: Motor Parameters.

KOLLUMORGEN MOTION TECHNOLOGIES GROUP										TE- 8301	
STANDARD ACCEPTANCE TEST PROCEDURE FOR BLDC MOTORS										Key: + V Sheet 5 of 6	
Written by:	Mike Schermer	Date:	6-20-87	Customer Part #:	TLU- 946712	Tester:JB	Date: 09/14/10	Spec:	CCW	Current	In A/m
Approved by:	Ms	Date:	7-7-87	Customer P.O.:	P0055603		Spec:	CCW	CCW	CCW	CCW
Serial Model #:	KBMS-25H02-B00	MOTOR TERMINAL	3-Prict	MOTOR TORQUE	ACTUAL	Spec	in RPM	in RPM	CCW	CCW	CCW
Serial No.	1332	Motor Term. Reg.	0 & Cog	12.700	Torque	in RPM	2	125.0 V	CCW	CCW	CCW
Serial No.	1332	Lead Length 23.0	10-30	12.700		in RPM	2	125.0 V	CCW	CCW	CCW
Serial No.	1332	3.340 to 4.000 Commes	10-30	12.700		in RPM	2	125.0 V	CCW	CCW	CCW
1035	/ / / /	A B C	3	CW	CCW	CCW	CCW	CCW	CCW	CCW	CCW
52943	/ / / /	3.610 3.610	3.610	19,300	19,300	19,300	19,300	19,300	19,300	19,300	19,300